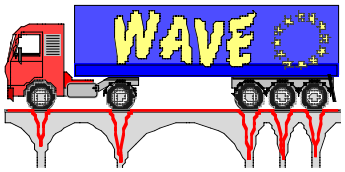

European **C**ommission

DG VII - Transport

4th Framework Programme

Transport

Weigh-in-motion of

Axles and

Vehicles for

Europe

RTD project, RO-96-SC, 403

Weigh-in-motion of Road Vehicles for Europe (WAVE)

Report of Work Package 1.1

Multiple sensor WIM

May 2001

CONTENTS

The Project ii
Origin of the Project ii
Objectives ii
Project Organisation and Means iii
Project Output v

Summary 1

1 Objectives 1

2 Organisation of the Work 2
2.1 Theoretical Studies 2
2.2 Experimental Work 2

3 Signal Reconstruction and Kalman Filtering (FR) 3
3.1 Introduction 3
3.2 The Developed Approach 4
3.3 Reconstruction and Estimation Procedure 7
3.4 Conclusion 10

4 The Maximum Likelihood Method (UK) 11
4.1 Overview of the Sample Mean Approach 11
4.2 The Maximum Likelihood Method 16
4.3 Analysis of the Estimation Error and Optimal Spacing 18
4.4 Simulation Results 22
4.5 Success Rate of the Weight Estimation Algorithm 27

5 Experimental Studies on MS-WIM Sites 32
5.1 Errors and Calibration 32
5.2 The MS-WIM Array at Trappes (FR) 33
5.3 The MS-WIM Array at Metz - Obrion (FR) 40
5.4 Data Collected with a Load Measuring Mat (UK) 45
5.5 The MS-WIM Array at Abingdon (UK) 49

6 Comparison of the New Algorithms Using the Trappes MS-WIM Array 62
6.1 Vehicle Sample 62
6.2 Computation Time 62
6.3 Outliers 62
6.4 Performance of Each Method 63
6.5 Influence of Calibration Method 64

7 Conclusions 66
7.1 Theory of MS–WIM 66
7.2 Tests in France 66
7.3 Tests in the UK 66
7.4 Comparison of WIM Algorithms 67

8 Recommendations and Future Research 68
8.1 Recommendations 68
8.2 Future Research 68

9 Implementation and Dissemination 69
9.1 Pre–Selection, Enforcement and Monitoring 69
9.2 Pavement Design and Maintenance 69

10 References 70

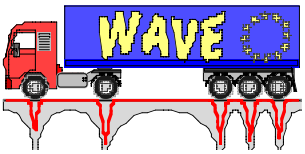

THE PROJECT

'WAVE' (**W**eigh-in-motion of **A**xles and **V**ehicles for **E**urope) is a research and development project of the fourth Framework Programme (Transport). Concerned with the weighing in motion of road vehicles, the project ended in June 1999 after two and a half years of steady work. Thanks to an integrated programme with a fruitful collaboration between the partners, and complementary contributions from the participating organisations, significant scientific and technical progress was made and very many results were achieved.

Origin of the Project

During the COST 323 action (WIM-LOAD, 1993-98), part of the activities of COST Transport, it emerged that further research on WIM was necessary to address the latest requirements of road managers and decision makers. In 1994, the 4th Framework Programme of the European Commission was presented, with a specific "Road Transport" programme. Part of the latter was entitled "Road infrastructure" and a task of this was "Monitoring of factors affecting pavements and structures to support existing and future harmonisation legislation in respect of axle and vehicle weights" (task 7-4/27).

To address this task, a proposal for a large research project, 'WAVE' (**W**eigh-in-motion of **A**xles and **V**ehicles for **E**urope) was submitted to the Commission by a consortium of 11 partners from 10 countries, following the first call in March 1995. A majority of the partners were already participants in the COST 323 action. After a positive review by the experts and a negotiation phase in Autumn 1995, the project began in September 1996, after a 6 month delay for administrative reasons.

Objectives

The objective of the 'WAVE' project was to effect a significant step forward for those responsible for road networks, through the following actions :

1.1 Improve the capacity of conventional WIM systems to accurately estimate static loads from measurements of dynamic impact forces applied by axles, through use of arrays of sensors whose combined results can allow for the dynamic interaction between vehicle and pavement.

1.2 Develop and improve the functioning and accuracy of bridge-based WIM systems through more sophisticated vehicle/bridge interaction modelling and data processing.

2 Develop common data structures, formats and quality assurance procedures to facilitate the exchange and comparison of WIM data throughout Europe, to increase confidence in such data and to provide reliable management information to decision makers.

3.1 Perform tests of WIM systems to assess their durability and performance in various climatic conditions, particularly in cold regions where pavements deform and are weaker during the thaw and sensors are susceptible to studded tyres and de-icing salt.

3.2 Develop standardised calibration methods and procedures by improving existing methods and extending their applicability to all European climates and types of WIM system.

4 Develop and implement a new WIM technology, based on an innovative fibre optic sensor which has considerable potential in terms of quality and the extent of information provided and its insensitivity to harsh climatic conditions.

This project constituted a strategic policy initiative to confirm the Europe's leadership in WIM. It led to the development of new technologies such as advanced multiple sensor and bridge WIM systems, a quality assurance procedure to be implemented in a pan-European database, data about the behaviour of WIM systems in harsh environments, an improvement in calibration procedures and the development of a new European optic-fibre WIM technology. That will help road and transport decision makers.

Project Organisation and Means

The consortium involved 6 Contractors and 5 Associate Contractors:

Coordinator: Laboratoire Central des Ponts et Chaussées - LCPC - France

Contractors

Cambridge University Engineering Department - CUED - United Kingdom
Trinity College Dublin - TCD - Ireland
Road and Hydraulic Engineering Division - DWW - The Netherlands
Alcatel Contracting - ALCO (9/96-5/98) / Alcatel CIT Saintes (6/98-6/99) - France
Swedish National Road Administration - SNRA - Sweden

Associated Contractors

Belgian Road Research Centre - BRRC - Belgium
Technische Universitaet Muenchen - TUM - Germany
Technical Research Centre of Finland - VTT - Finland
Swiss Federal Institute of Technology - ETH - Switzerland
National Building and Civil Engineering Institute - ZAG - Slovenia

All together, more than 15 senior scientists and engineers, 25 Ph.D. students, post-doctoral or young engineers or researchers, and many technicians were involved in WAVE. Some subcontractors were SME (Small or Medium Enterprises), manufacturers and/or vendors of WIM systems or services; they were therefore self-motivated and interested in the output and deliverables of the project.

The project was planned for 24 months, from September 1996. A 9 month extension was subsequently accepted by DGVII, which lead to a project completion date of June 1999.

The complete project was organised in 4 main research areas, each of which was divided into two or three parts to give a total of nine work packages (WPs). The WPs were sub-divided into tasks. Each task consisted of work with a specific deliverable or output to be used in another task. Each specific WP covered one of the main objectives of the project and a basic need in Europe. The four main research areas were consistent areas, but had relationships between them. Each WP worked towards providing more efficient and accurate WIM systems and more reliable traffic load data.

The detailed organisation of the WPs is described below:

WP1. Accurate Estimation Of Static Weights Using Wim Systems

WP1.1. Multiple Sensor WIM (MS-WIM) - *leader: CUED / co-leader: LROP/LCPC*

a. New and improved theories
b. Validation using experimental data
c. Tests of MS-WIM systems
d. Specifications and legal issues

WP 1.2. Bridge WIM systems (B-WIM) - *leader: TCD*

a. Increased Accuracy for Typical Bridges
b. Extension of B-WIM to Orthotropic Decks
c. Extension of B-WIM to Other Bridges
d. Dynamic Analysis for Typical Bridges
e. Calibration

WP2. Quality, Management And Exchange Of Wim Data - Leader: DWW

WP2.1. WIM data quality assurance

a. Analysis of existing quality systems
b. Site quality
c. System quality
d. Calibration procedures
e. Data quality

WP2.2. WIM data format and database structures

a. Submitted data format
b. Harmonisation procedure
c. Description of two database levels
d. Database management and maintenance

WP3. Consistency of Accuracy and Durability

WP3.1. Durability of WIM systems in cold climates - *leader: SNRA*

0. Preparatory work in advance of the project start
a. Reporting previous experience on the subject matter
b. Inviting WIM manufacturers to the test
c. Final decision on test site localisation
d. Site preparation
e. WIM installation
f. First summer test
g. Winter test
h. Second summer test
i. Random traffic test
j. Final report

WP3.2. Calibration of WIM systems - *leader: VTT*

a. State of the art report
b. Test of calibration devices and procedures
c. Specification of the calibration procedures

WP4. OPtical Fibre Wim Systems, Technology For The Future - Leader: LCPC

WP4.1. Sensor Design
- a. Feasibility
- b. Characterisation and testing
- c. Calibration
- d. Mathematical model (1)

WP4.2. Optoelectronic Head
- a. Design
- b. Multiple sensor head
- c. Long-term performance
- d. Prototype improvements

WP4.3. Data Acquisition and Processing Unit
- a. Data acquisition and treatment
- b. Mathematical model (2)
- c. Validation and Report

A total budget of 1.5 million Euros was allocated to the WAVE project, of which 0.75 million Euros was provided by the European Commission. The total time spent on the project was nearly 30,000 man-hours, i.e. 20 man-years. The personnel cost represents 69% of the total budget. A mid-term seminar was organised in September 1997 in Delft, The Netherlands (WAVE, 1997) and a Final Symposium in Paris (May 1999), in order to widely disseminate the results of the project. In addition, much of the results were presented at the Second European Conference on WIM organised through the COST 323 action. A Web site was initially built by LCPC and is now merged with the European WIM web site built by the COST 323 action and hosted by ZAG (http://www.zag.si/wim/). A CD-ROM was prepared (edited by the BRRC) to present all the reports and output of the project.

Several large testing facilities or bridge and road test sites were used in the project. Two road sections were instrumented with multiple-sensor arrays, in the UK and France, for testing MS-WIM systems. For the calibration of these arrays, instrumented lorries and pre-weighed lorries were used. Several bridges of different type were instrumented in France, Germany, Sweden, Slovenia and Ireland to develop and test B-WIM systems. For WP3.1 in Sweden, a road section of 0.5 km was instrumented with five WIM systems, and a static weighing area with a large weigh-bridge was used.

Project Output

New theories, models, algorithms, and procedures have been generated, prototypes built, and field tests performed. New prospects have been opened up for weighing using multiple sensors and instrumented bridges, an innovative technology has been developed using optical fibres and optronics, and there have been significant advances in the calibration of the systems and in the quality and management of weigh-in-motion data. Experiments on roads fitted with sensors and on instrumented bridges have yielded highly valuable quantitative information on the durability, performance, and precision of many types of weigh-in-motion system.

As happens in most active and innovative research projects, many questions have been answered and others asked, opening up new prospects. The scope of weigh-in-motion has been expanded to encompass new needs in the checking of vehicle weights, thanks to a substantial improvement of the levels of precision, and in the design and management of road infrastructure, thanks to new approaches to the instrumentation of roads and bridges.

In addition to performing the research and attaining the project's objectives, the consortium has attached special importance to dissemination of the knowledge and results acquired, both within the scientific community and to the users and industrial builders of the systems. The fallout from such a project is almost as much a matter of "making known" as of "know-how".

Overall results of the project are presented in the General Project Report, published by the LCPC. Detailed results of each WP are presented in each WP's report, which are published by the WP leader's organisations.

Report on the WP 1.1

This report was edited by D Cebon.

The main contributors were: L. Stergioulas, MD Macleod, M. Siffert, V. Dolcemascolo, P. Argoul, J. Sainte-Marie, B. Jacob.

Other Participants :

LROP :
- JP Eloi
- D Dominois
- C Le Verger

CETE de l'Est :
- D Stanczyk
- A Braun
- D Simon

UK Highways Agency
- G Bowskill

Transport Research Laboratory
- R Addis
- W Newton
- D Jacklin

Electronique Contrôle Mesure
DRE Lorraine
CRS 39 de l'autoroute A31
Golden River Traffic
Thames Valley Police
UK Vehicle Inspectorate

SUMMARY

This report describes work on Multiple–Sensor Weigh-in-Motion, undertaken in France by LCPC and in the UK by Cambridge University Engineering Department (CUED). The research involve independent development of two different theories for MS–WIM processing, and analysis of four different sets of experimental WIM data - two in France and two in the UK.

Overall it is concluded that MS–WIM arrays of 10 or more suitably–spaced sensors are capable of achieving accuracies of B+(7) (COST 323 assessment scale). This corresponds to errors of approximately 4% RMS in estimating the static loads. The main factor preventing MS–WIM systems from achieving better levels of accuracy was found to be random sensor errors, due to noise and calibration.

1 OBJECTIVES

High speed (HS) WIM systems are widely used throughout Europe for purposes such as statistical traffic load survey, traffic management and infrastructure design and maintenance. More than 350 WIM sites are currently in operation and various types of sensors are manufactured and used in Europe. Large scale tests, carried out over long time periods have shown accuracy limitations, due dynamic tyre forces induced by pavement roughness. There has been considerable activity recently in the development of WIM systems for accurate evaluation of the static axle loads of heavy vehicles travelling at normal highway speeds. In future, such systems could possibly be used for commercial and legal applications, such as overload enforcement.

A fundamental limitation of the performance of WIM systems is imposed by the dynamic tyre forces due to vehicle-pavement interaction. These dynamic forces have RMS amplitudes ranging from 10% to 30% of the static axle loads (Cebon, 1993). The dynamic forces depend on variety of factors such as the speed of the vehicle, the roughness of the road and the suspension characteristics.

The main objective of the MS-WIM (Multiple Sensor Weigh in Motion) work package (WP1), is to improve the estimation of static loads from the measurements of dynamic impact forces. Multiple-sensor WIM enables the effects dynamic tyre forces to be ‘smoothed out’, by processing the outputs of multiple WIM sensors (Glover, 1988; Cebon, 1990).

Appropriate selection of the sensor array design and data processing method plays a key role in minimising the effects of such errors. The aim of this work package, is to develop new procedures and methods for MS–WIM in order to improve the accuracy of weight estimates.

The most important factors which contribute to accurate estimation of static loads are respectively: accuracy and calibration of the sensors, site selection, an appropriate sensor array design and data processing methods. The work done in this package is concerned with the two last factors. Since cost is also an important issue for future implementation of MS-WIM systems, it is necessary to search for a design which balances the requirements of accuracy and the number of sensors needed.

This report presents results obtained from theoretical studies in France (LCPC), and in the UK (CUED) and experimental investigations performed on several MS-WIM test sites in France and the UK.

2 ORGANISATION OF THE WORK

2.1 Theoretical Studies

Two theoretical studies were undertaken on multiple sensor WIM: one in the UK (CUED) and in France (LCPC). The work involved development of analysis methods and algorithms for processing the outputs of MS–WIM sensors; as well as simulation studies to test the methods.

Two new methods for estimating the static weight from WIM measurements were developed:

(i) The first approach, developed by LCPC, is based on a simplified modelling of heavy vehicles and uses mathematical signal processing tools.

(ii) The second approach, developed by CUED, is based on Maximum Likelihood estimation. It fits one or two sine waves to the measured dynamic tyre forces to produce an unbiased estimate of the mean value.

These two methods and key theoretical results are presented in Chapters 3 and 4 of this report.

2.2 Experimental Work

Four different sets of experimental data were analysed for this study. Researchers at LCPC investigated two WIM arrays:

(i) An array near Trappes (FR), originally installed for the OECD/DIVINE project (Jacob, 1995). It was located in the slow lane of RN10. It had 24 piezoceramic sensors at non-uniform spacings, with a total instrumented length of 36m.

(ii) An array at Metz - Obrion (FR). This array was installed as part of WAVE. IT was located in the slow lane of the south-bound A31 motorway, 30km from Metz, and 20km from Nancy. It had 16 piezoceramic sensors at 1.6m spacings.

Researchers at CUED investigated two different systems:

(i) A load-measuring mat, containing 96 capacitative strip sensors, used previously for measurements of dynamic tyre forces in the USA (Cebon and Winkler, 1991a). The mat was tested under controlled conditions on a vehicle test track.

(ii) An array of 20 capacitative strip sensors installed at 1.1m spacings on the north-bound A34 trunk road near Abingdon (UK) as part of WAVE.

Chapter 5 of this report discusses the experimental work and results.

3 SIGNAL RECONSTRUCTION AND KALMAN FILTERING (FR)

3.1 Introduction

The force applied to an horizontal pavement by an axle of a stationary heavy vehicle equals the static load W^{stat} of the considered axle. But when the vehicle moves along the pavement, the applied fore Wi*(t)* at instant *t* of the i^{th} axle has a dynamic component so that :

$$W_i(t) = W_i^{stat} + f_i^{dyn}(t) \qquad (1)$$

Figure 1 below, representing the impact force variations of the second axle of a five axle instrumented truck, shows the importance of the dynamic component f_2^{dyn}. This recording has been obtained on the RN10 near Trappes (78) where the quality of the evenness is good for a French national road. The speed of the truck was 80 km/h.

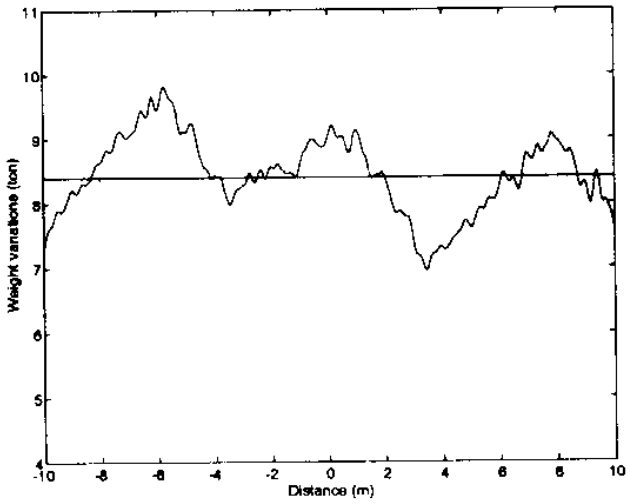

Fig. 1 Variations of the impact force $W_2(t)$ around the static load W_2^{stat}

Moreover, the amplitude of the variations of $W_i(t)$ presented in figure 1 implies that the quantity $f_i^{dyn}(t)$ representing the dynamic overloading could reach significant values (40 % of the static load). Because these overloadings are responsible for a great part of the damages caused to road structures (Corte 1998), researches on vehicle-pavement interaction and weigh-in-motion systems have been conducted for tenyears by the "Laboratoire Central des Ponts et Chaussées", (Jacob 1995).

For this purpose, two experimental sites have been installed in France, at Trappes near Paris (RN10) and near METZ (A31), (Siffert et al 1997). The sites consist in an array of piezo-electric sensors inserted in the pavement as described in figure 2-a. One experiment can be summarised as follows. A vehicle crosses the sensor array at normal speed V. Each sensor records the dynamic load of each axle. Thus, $W_i(t_j)$ represents the load of the i^{th} axle of the vehicle at the instant t_j when the axle runs over the j^{th} sensor. For all the sensors, a set of data is then collected (figure 2-b) ; the study of the dynamic interaction consists in the reconstruction and the analysis of the continuous signal $t \rightarrow W_i(t)$, the weigh-in motion problem is the estimation of W_i^{stat}.

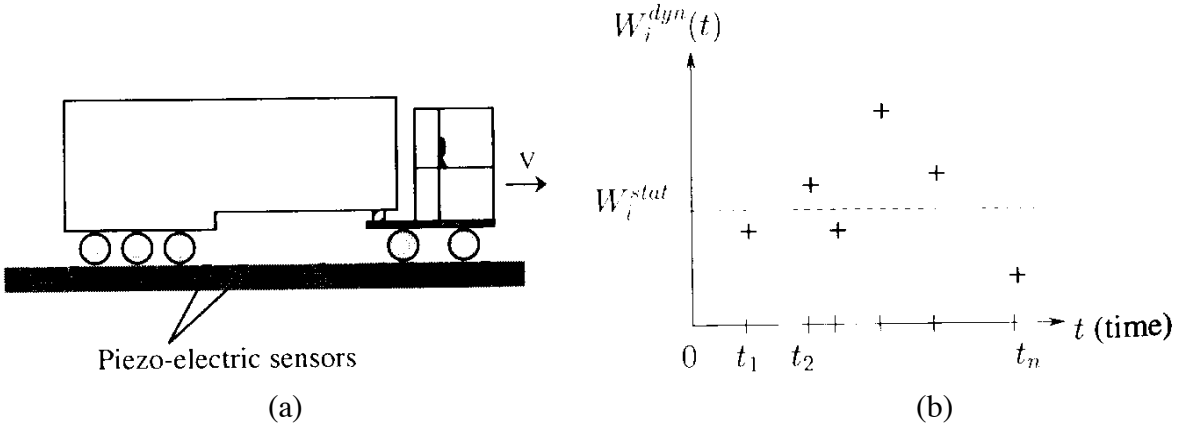

(a) (b)

Fig. 2 (a) A heavy vehicle crossing the sensor array
(b). Discrete measures of the impact force of the j^{th} axle provided by the array.

3.2 The Developed Approach

Our approach consists in three steps. First, a mechanical analysis of some simplified models of vehicles is performed. It allows to find a family of functions associated with each type of vehicle and with the evenness of the site. Then a reconstruction algorithm of the impact force $t \rightarrow W_i(t)$, is performed over this set of functions. And finally, an estimation procedure of the static load W^{stat} is proposed. We will mainly focus on the first and third steps, the second one has already been presented and validated (Sainte-Marie 1998).

3.2.1 Mechanical Modeling

If one assumes a heavy vehicle can be represented by an assembly of rigid bodies (tractor, trailer, axles), the virtual work principle allows to derive the equations of motion of the model under the form :

$$M\ddot{u} + A_e(x,t,u) = f(x,t) \tag{2}$$

where u denotes the state vector of the mecanicalsystem, M the mass matrix, x the situation of the vehicle along the pavement and f the contribution of the weight of the bodies but also of the evenness and its derivates. A represents the modeling of the suspensions and the differents links between the rigid bodies. An equivalent linearization of equations (2) arround the static load position of the heavy vehicle gives :

$$M\ddot{u} + A_e(x,t)u = f(x,t) \tag{3}$$

In order to illustrate the differences between (2) and (3), we give some examples of the impact forces simulations carried out, For a two dimensionnal five-axle truck below (figure 3-a), the responses of the tires (non-linear) and of the suspensions (hysteresis) have been recorded on a test truck (Cebon, 1992), we compare (figure 3-b) the variations of the impact forces obtained by numerical resolution of models (2) and (3) with a Runge-Kutta method of order 4-5. The programmation of the hysteretic behaviour of the suspensions has been achieved with the technique developed by Fancher (Fancher et al 1980). For these calculations, the evenness of the site, the aerodynamic effects and the tire-pavement friction are taken into account.

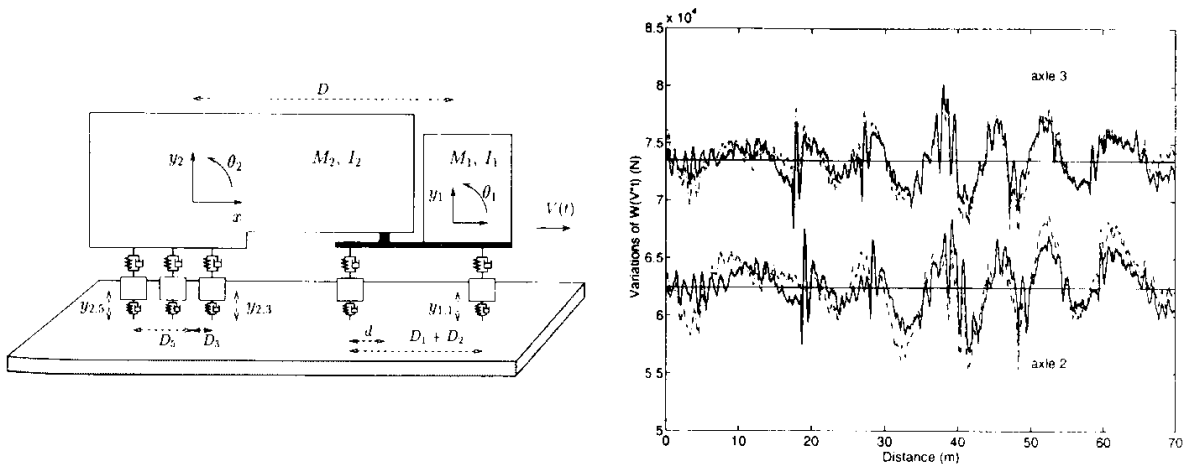

(a) (b)

Fig. 3 (a) two-dimensionnal model of a 5-axle truck
(b) variations of the impact forces $W_i(V*t)$ for the second and third axles, numerical resolution. (-) non linear caracteristics and (-.) equivalent linearization.

For other models of vehicles with two or three axles (Sainte-Marie 1999), we have obtained similar results proving that in normal conditions of speed, loading and evenness, the influence of the non linearities of suspensions and tires over the variations of the impact forces are relatively small.

Now, we compare (figure 4) the variations of the impact forces recorded with an instrumented truck circulating on the experimental site of Trappes with those simulated with a linear equivalent model of the considered truck.

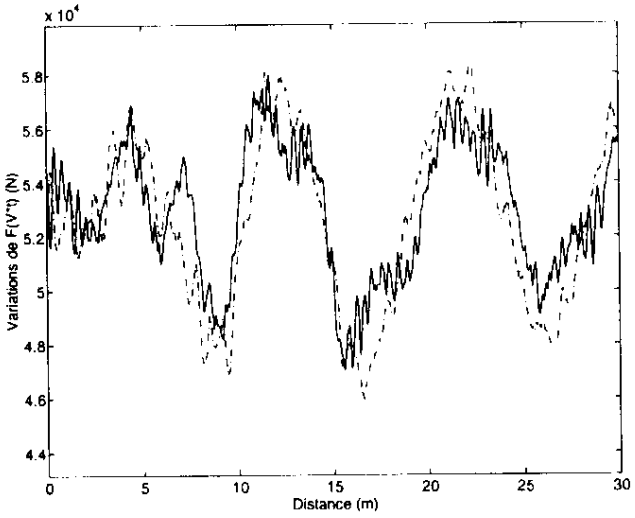

Fig. 4 Variations of the impact forces for the first axle of a five axle instrumented truck, (-) experimental measurement, (-.) numerical simulations.

These comparisons have been performed for several types of vehicles, several types of axles leading or driving with mechanical or air suspensions. For each situation, the obtained results prove that a two-dimensionnel linear model allows to have a good approximation of the experimentally measured impact forces. It is important to notice that the problems induces by axles groups (tandem or tridem) or by a linearization in limit conditions of loading are non completely solved until now.

3.2.2 Mechanical Analysis

From a truck model of the form $M\ddot{x} + A_e(x,t)u = f(x,t)$, we are now interesting in finding a family of functions over which the impact force variations of an axle $t \to W_i(t)$ could be broken up. As for a great number of evolution problems, we use for the resolution of equations (3) a Fourier method of diagnonalization. For more details about the results used and their proofs, one can refer to Sainte-Marie (1999). We make the following assumptions :

- the operator $Ae\ (x,\ t)$ is diagnoalizable with a discrete spectrum $\{\lambda(t)\}_{k\in I}$,
- the eigenmodes g_k are defined by $A(t)g_k = \lambda k(t)g_k$, the vectors g_k are independent of time t,
- for all eigenvalues $\lambda_k(t)$ of $A_e(x,\ t)$, there exists a constant $C > 0$ such that $|\lambda_k(t)| \leq C$ et $0 < Re\lambda_k(t) < C$ almost everywhere on the interval of simulation.

These assumptions are not restrictive for a truck model, the vibrations of a heavy vehicle are always damped and there is a finite number of eighenmodes so that the third condition is obviously fulfilled. With these assumptions, for a suitable choice of the initial conditions (e.g the static equilibrium of the vehicle), it is possible to develop the solution of (3) under the form:

$$u(x,t) = \sum_{k\in I}\left(\mu_k^0 + \int_0^t e^{\int_0^s \lambda_k(v)dv}\gamma_k(s)ds\right)e^{-\int_0^s \lambda_k(u)du} g_k(x) \tag{4}$$

with $\gamma_k(t) = \int M^{-1} f(x,\ t)g_k(x)dx$. If one can make the assumption that the vibrations of the model only depends on time t and not of the location x of the vehicle along the pavement, then expression (4) becomes :

$$u(t) = \sum_{k\in I}\alpha_k e^{-\int_0^t \lambda_k(u)du}\int_0^t e^{\int_0^s \lambda_k(v)dv} M^{-1}f(s)ds. \tag{5}$$

Let k_e and C denote respectively the equivalent stiffness and the viscous damping of the tire, the impact force for axle i is given by :

$$W_i(t) = k_e * \left(u_i(t) - r(t)\right) - C * \left(\dot{u}_i(t) - \dot{r}(t)\right) \tag{6}$$

where u_i is the compression of the tires of axle i and r denotes the variations of the evenness for the considered site. $M^{-1}f_i$, the i^{th} component of vector $M^{-1}f$ *corresponding to the* i^{th} component u_i of vector u can be written under the form $M^{-1}f_i = f_{ir} + f_{i,p}$, $f_{i,p}$ *(resp.* $f_{i,r}$*)* representing the contribution of the weight of the different bodies (resp. the variations of the evenness). Generally $f_{i,p}$ is a constant corresponding to the gravity constant g. Then, with both expression (5) and (6), if n = card I, one obtains the impact force $W_i(t)$ as a linear combination of the $2n + 3$ functions :

$$\begin{cases} h_1(t) = 1 \\ h_2(t) = r(t) \\ h_3(t) = \dot{r}(t) \\ h_k(\lambda_{k-3},t) = e^{-\int_0^t \lambda_k(v)dv}\int_0^t e^{\int_0^s \lambda_k(v)dv} ds \quad k \in \{4,....n+3\} \\ h_{k+n}(\lambda_{k-3},t) = e^{-\int_0^t \lambda_k(v)dv}\int_0^t e^{\int_0^s \lambda_k(v)dv} f_u(s)\,ds \quad k \in \{4,....n+3\} \end{cases}$$

In order to validate the mechanical analysis performed above, figure (5) presents a comparison of the impact forces obtained first, by numerical resolution of (3) (for the model presented in figure 3-a) and then by reconstruction of $W_2(t)$ over the family $\{h_k\}_{k=1}^{2n+3}$.

The reconstruction is carried out by the means of a sampling algorithm for band-limited signals with respect to a discrete transform: the algorithm called ACT (Adaptive weights Conjugate gradient Toeplitz method) was used and proved to be efficient and stable. This technique is valid for arrays with regular and irregular spacings between sensors (Sainte-Marie 1998).

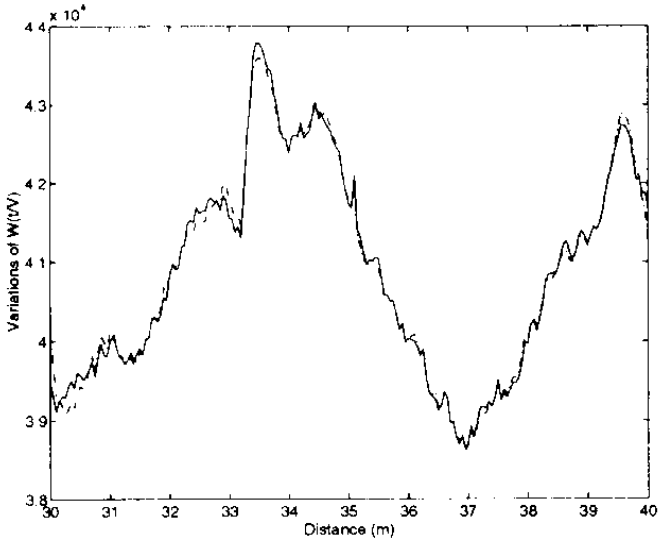

Fig. 5 Variations of the impact for the second axle of the linear equivalent model of a 5-axle truck, (–) numerical simulation, (-.) sampling over the $\{h_k\}_{k=1}^{2n+3}$ for $n = 5$ with $r = 17$ samples.

3.3 Reconstruction and Estimation Procedure

In the previous paragraph, we have seen that for the axle i of a heavy vehicle, one can write $W_i(t)$ under the form :

$$W_i(t) = \sum_{j=1}^{3} \beta_j^i \, h_j(t) + \sum_{j=4}^{n+3} \beta_j^i \, h_j(\lambda_{j-3}, t) + \sum_{j=n+4}^{2n+3} \beta_j^i \, h_j(\lambda_{j-n-3}, t).$$

In practice for a vehicle of the trafic flow, the parameters $\{\beta_j^i\}_{j=1}^{2n+3}$ and $\{\lambda_j(t)\}_{j=1}^{n}$ are un-known. But one can notice that $W_i(t) - \sum_{j=1}^{3} \beta_j^i \, h_j(t) - \sum_{j=4}^{n+3} \beta_j^i \, h_j(\lambda_{j-3}, t)$ is the solution of the problem :

$$\begin{cases} \ddot{f}_i + \left(M^{-1} A_e\right)_i f_i = f_{i,u} \\ f_i(0) = f_{i,0} \end{cases} \tag{7}$$

where $f_{i,u}$ depends only on the evenness caracteristics that are known, condition $f_i(0) = f_{i,0}$ indicates that at $t = 0$, the vehicle is supposed to be in static equilibrium. So we can develop a reconstruction procedure consisting in an estimation of coefficients $\{\beta_j^i\}$ by a sampling technique coupled with an estimation of the eigenvalues $\{\lambda_j(t)\}$ by a Kalman filtering procedure (Sainte Marie 1997). The reconstruction algorithm has the following form :

choice of $\{\beta_j^{i,0}\}_{j=1}^{2n+3}$ *et* $\{\lambda_j^0(t)\}_{j=1}^{n}$

For k FROM 1 TO q DO,

→ Estimation of $\left\{\lambda_j\right\}_{j=1}^{n}$ by Kalman filtering

→ Estimation of $\left\{\beta_j^i\right\}_{j=1}^{2n+3}$ by reconstruction

→ $\beta_1^{i,0} = \beta_1^i, \beta_2^{i,0} = \beta_2^i, ..., \beta_{n+3}^{i,0} = \beta_{n+3}^i$

→ $\lambda_1^0(t) = \lambda_1(t), \lambda_2^0(t) = \lambda_2(t), ..., \lambda_n^0(t) = \lambda_n(t)$

END FOR k.

The observation measures necessary for the use of the Kalman filter (7) are given by quantities

$$\left\{R_l^i\right\}_{l=i}^{r} = \left\{W_i(t_l) - \sum_{j=1}^{3} \beta_j^i \, h_j(t_l) - \sum_{j=4}^{n+3} \beta_j^i \, h_j(\lambda_{j-3}(t_l), t_l)\right\}_{l=1}^{r}.$$

In order to validate the reconstruction procedure, we record the measures of the impact forces of an instrumented truck, whose mechanical characteristics are unknown, when it axles run over a sensor array (see figure 2). So, we have at our disposal the following informations : the measures : $\left\{R_l^i\right\}_{l=i}^{r}$, the mean speed of the vehicle on the considered site, the number and spacing of axles then we apply the algorithm presented before. Figure (6) below is an example of a reconstruction carried out with the proposed procedure.

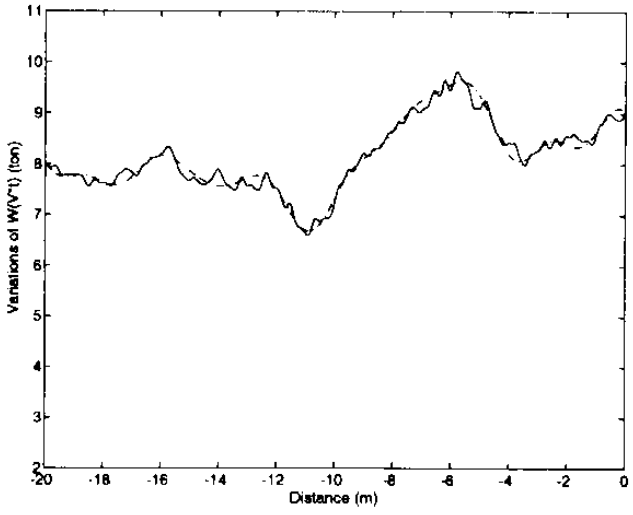

Fig. 6 Variations of the impact force for the second axle of a 5-axle truck for n = 4, (–) experimental measurement, (-.) reconstruction algorithm.

Now, we are going to use the reconstruction step to obtain a static load estimation of an axle based on a quadrature of the reconstructed signal $t \rightarrow W_i(t)$. Let f_1 and f_2 be respectively the two natural frequencies associated with rolling and bouncing vibrations, for each axle f_1 and f_2 are in fact estimated by the Kalman filtering. We define T by :

$$T = \frac{p}{f_1} \approx \frac{q}{f_2}$$

where p, q are integers so that $V * T$ has approximately the same length as the sensor array, V being the mean speed of the vehicle over the array. Then, the static load estimation is given by :

$$\left[W^{stat}\right] = \frac{1}{T}\int_T \left(W_i(t) - W_a(t)\right) dt$$

where W_a denotes the aerodynamic effects over the first two axles of each vehicles.

The accuracy of this static load estimation procedure has been tested with pre-weighed heavy vehicles from the traffic flow. The figures below present the results obtained for a set of 34 5-axle trucks (2-axle tractors and 3-axle trailors).

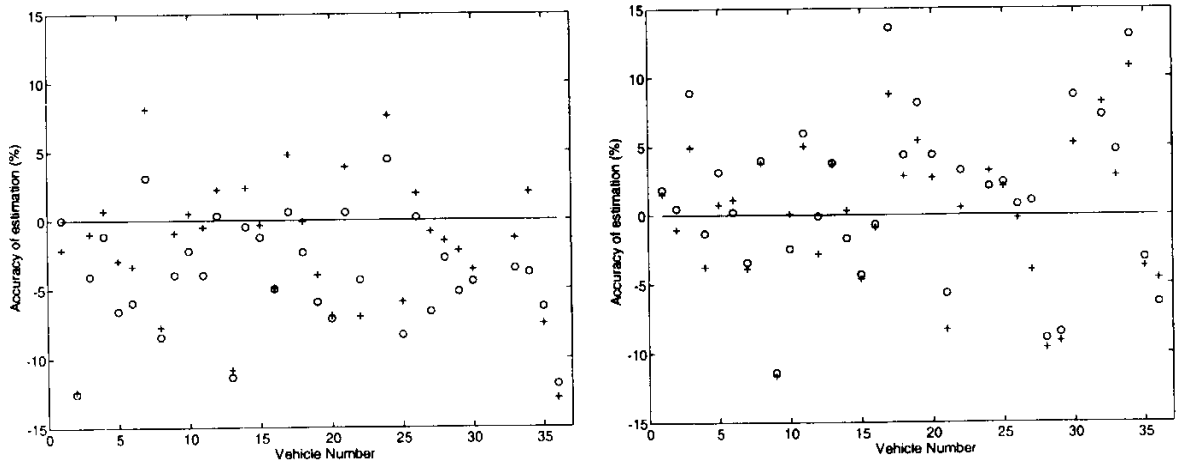

(a) (b)

Fig. 7 Accuracy of the estimation procedure with 6 sensors, for 34 vehicles of the traffic flow - 'o' simple mean estimation, '+' the developed technique.
(a) 1st axle and (b) 2nd axle

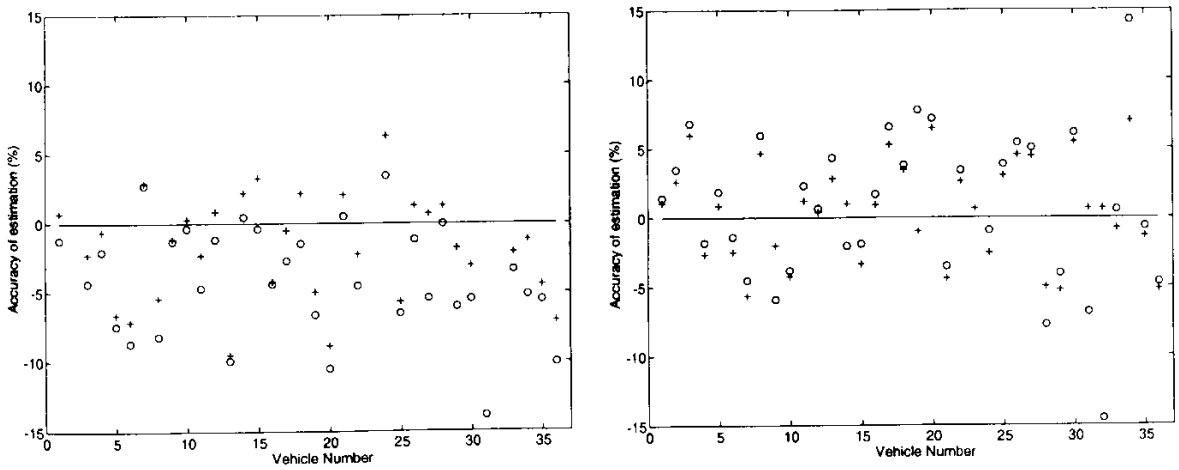

(a) (b)

Fig.8 Accuracy of the estimation procedure with 12 sensors, for 34 vehicles of the traffic flow - 'o' simple mean estimation, '+' the developed technique
(a) 1st axle and (b) 2nd axle

Table 1 below summarises the accuracy of the different estimations carried out for the set of 34 trucks. It also gives the accuracy classes according to European specifications (COST323 1997b). δ_m denotes the minimum confidence interval according to the considered tests conditions. In the same conditions with the same set of trucks, we have obtained in Sainte-Marie (1999) the accuracy class B+(7) with respectively δ_m = 9.2 and δ_m = 8.6 for 6 and 12 sensors.

	Vehicles of the traffic flow			
	6 sensors		12 sensors	
	Axle 1	axle 2	axle 1	axle 2
Number of trucks	34	34	34	34
Mean error (%)	-1.8	0.14	-2.25	0.66
Maximum error (%)	-12.9	10.8	-9?4	7.1
Stand. Dev.	4.9	5.21	3.55	3.72
COST323 specif.	B+(7) $\delta_m = 8,9$		A(5) $\delta_m = 6,3$	

Table 1 Accuracy of the MS-WIM for single axles, conditions R2

3.4 Conclusion

A procedure for the reconstruction of the impact force variations of an axle and the estimation of its static load has been developed. The technique uses a filtering technique coupled with a reconstruction step over the eigenmodes of some simplified vehicle models. It seems to be efficient and stable. It also allows to estimate the dynamic interaction between a vehicle and the road profile. Experimental data from one of the two MS-WIM sites in France were investigated using the SR method. The results are presented in Section 5.2.

4 THE MAXIMUM LIKELIHOOD METHOD (UK)

The second approach to multiple–sensor WIM was developed by CUED and is a probabilistic method based on Maximum Likelihood (ML) estimation. Before discussing the Maximum Likelihood approach it is necessary to review previous results from the Sample Mean method.

4.1 Overview of the Sample Mean Approach

4.1.1 The Sine Wave Model

Earlier studies of Multiple-Sensor Weigh-in-motion (MS-WIM) have been based on a *Sample Mean* (SM) calculation. In (Cebon, 1990), a simple WIM array design procedure was used to design low-cost systems with improved accuracy.

This work introduced the idea of modelling the dynamic force as a sum of sine waves, based on strong experimental evidence that the vast majority of contemporary heavy vehicle suspensions generate their dynamic tyre forces due to two distinct types of oscillation modes:

(a) low-frequency body pitch and bounce vibration modes at low frequencies f_1, ranging from 1.5 to 4.5 Hz, and

(b) axle-hop vibration at a high frequency f_2, ranging from 8 to 15 Hz.

The former vibration mode is present in the dynamic tyre forces of all heavy vehicles, whilst the latter is significant for only a small proportion of vehicles with lightly-damped bogie pitch modes, and some air suspensions. Two simple generic vehicle models were chosen as representatives of the two main classes of suspensions (Cebon, 1990; Cebon and Winkler, 1991a):

(a) The *quarter car model* (Figure 9a), represents about 80% of trucks in current use with air- or leaf-spring suspension, which generates their dynamic tyre forces primarily due to sprung mass motion. In this model, the tyre force spectrum can be reasonably approximated by a single sinusoid of low frequency.

(b) The *walking beam* model, representing about 20% of trucks with axle group suspensions has lightly-damped axle-hop modes, typically due to bogie pitch (Figure 9b). The walking beam model generates a tyre force spectrum which can be approximated by two sinusoidal components.

Typical power spectral density functions are shown in Figures 10a, b, for both of the generic vehicle models; using mass, suspension, and tyre parameters shown in figure 9.

When sensor signals are obtained from measurements on a WIM array, a ‘signal model’ can be used to approximate the measured dynamic force, and from its calculated parameters the static weight of the vehicle can be estimated. The success of the data processing will heavily depend on the correctness of the model.

From Figures 10a,b, it is apparent that suitable signal models consist of one or two sine waves - shown by upright arrows in the spectral densities (corresponding to the narrow-band peaks) plus a constant (the static weight). The vehicle models represented in the graphs by their power spectral densities can be viewed as “smeared” or “noisy” version of the idealised signal models (pure sinusoids). Additional sine waves could be included to account for other periodic effects (for example, tyre tread pattern, wheel out-of-round or other tyre non-uniformity effects (Cebon and Winkler, 1991a)).

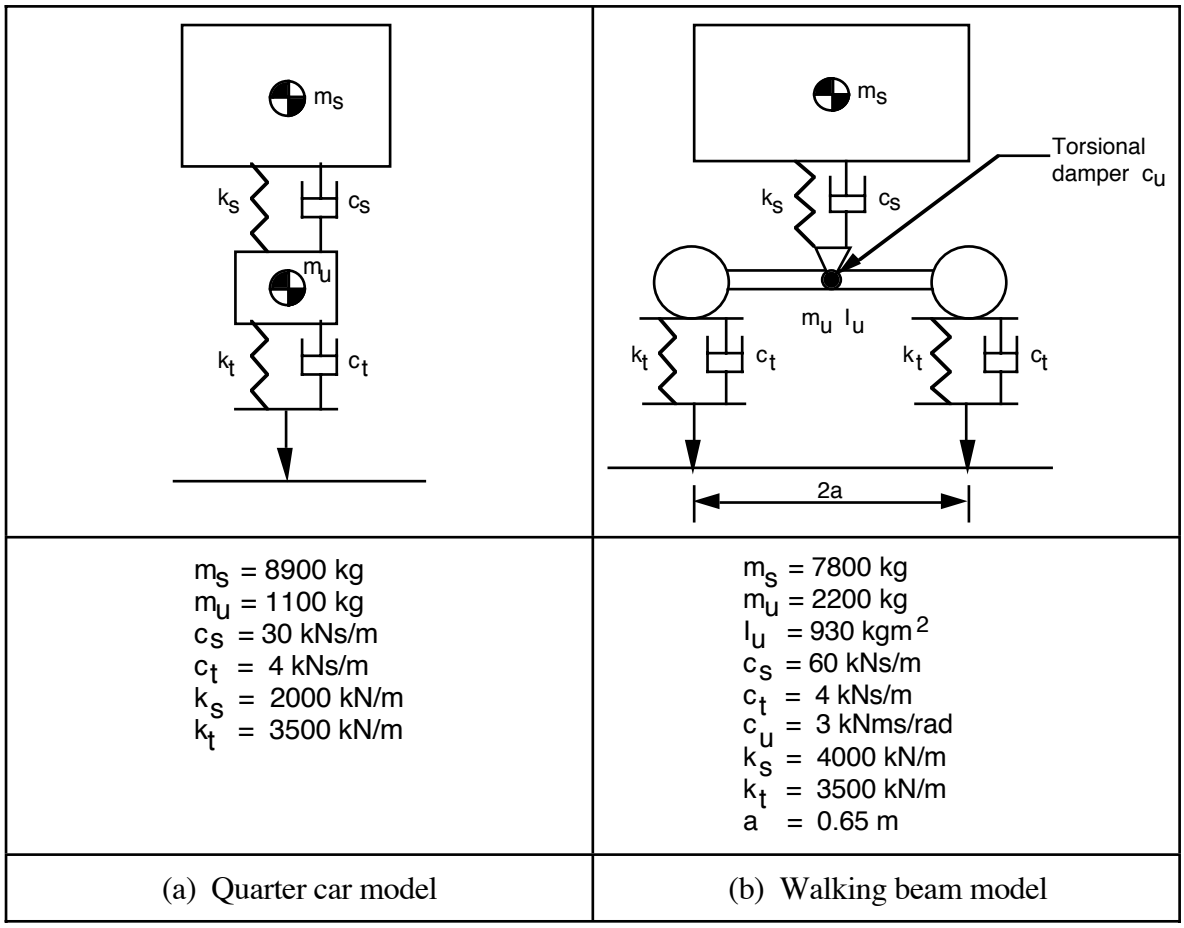

Fig. 9 Vehicle models. Details of the simulation technique can be found in (Cebon, 1990; Cebon, 1993).

A general model of M sine waves can be completely described by $3M+1$ parameters:

$$F(t) = F_o + \sum_{i=1}^{M} F_i \sin\left(2\pi f_i t + \phi_i\right) \tag{8}$$

where F_o is the mean level (which is assumed to be the static weight), F_i, f_i, ϕ_i are the amplitude, frequency, and phase of the i-th sine wave correspondingly. For simulation purposes, random uncorrelated noise $n(t)$ can be added to account for the errors in the signal model and the errors introduced in the measurement process.

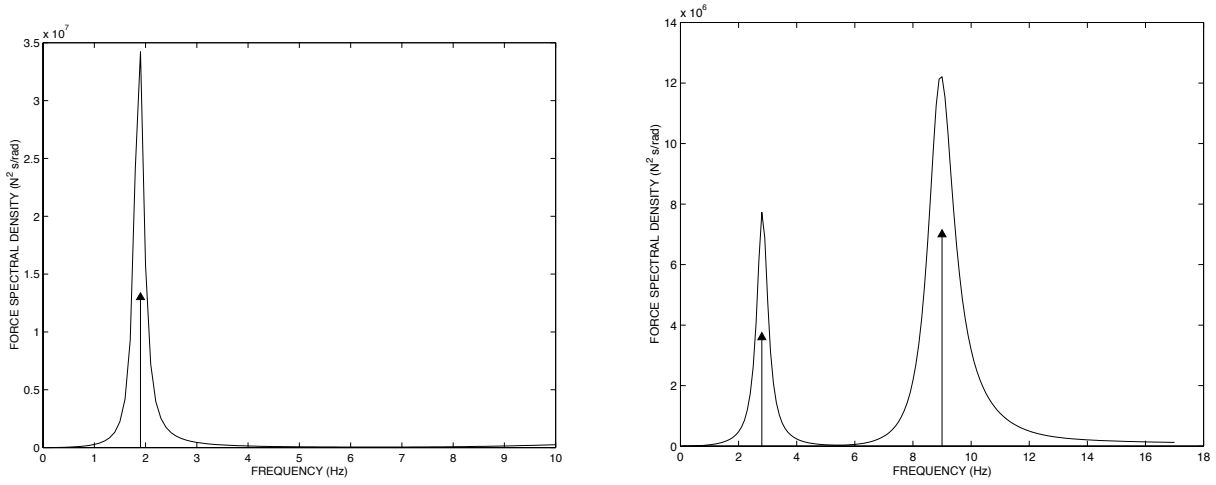

(a) (b)

Fig. 10 Dynamic tyre force spectral density generated by (a) the quarter car vehicle model and (b) the walking beam vehicle model.

4.1.2 The Sample Mean Approach

Cebon (1990) presented a detailed analysis of the errors generated by the Sample Mean approach for a single-sine wave model, using the notation shown in figure 10.

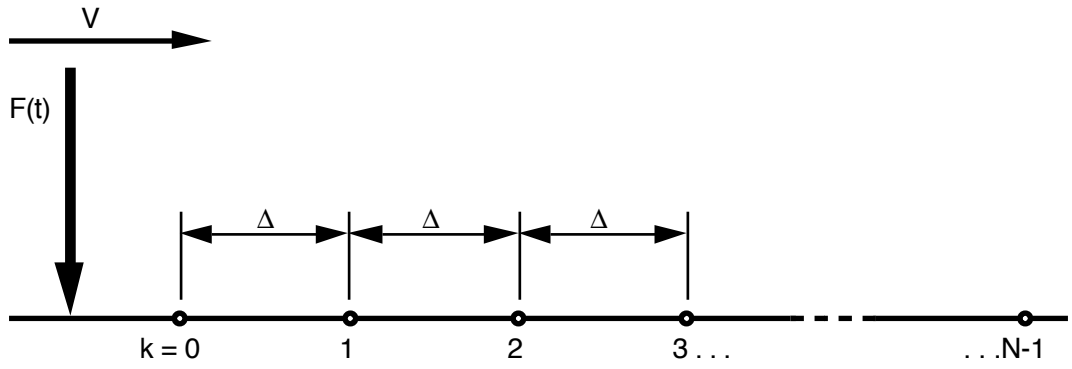

Fig. 11 Cross-section of an n-sensor WIM array, traversed by force F(t) at speed V.

The fact that the dynamic tyre force is limited to only one sine wave permits elimination of the vehicle-dependent parameters (speed V and resonant frequency f), by replacing the array spacing Δ by a convenient measure of non-dimensional spacing:

$$\delta = \Delta/(V/f) \tag{9}$$

For a single sine wave, the Sample Mean estimate $\overline{F}$ of the static weight from N sensor outputs F_k is then given by:

$$\overline{F} = \frac{1}{N}\sum_{k=1}^{N} F_k = F_o + \frac{F_1}{N}\sum_{k=0}^{N-1}\sin(2k\pi\delta + \phi) + n_k, \tag{10}$$

where n_k is the measurement error for the k-th sensor.

The relative (non-dimensional) error can be defined as

$$\varepsilon = \frac{\overline{F} - F_o}{F_1}\ , \tag{11}$$

Even for the idealised case that the WIM sensors are noise-free, i.e. $n_k = 0$, $k = 0, 1, 2, \ldots, N-1$; and the dynamic tyre force is given by an exact sinusoid, the mean error of the estimate is generally non-zero. This means that the Sample Mean estimator is *biased*. In this case, equation (10) gives

$$\varepsilon = \frac{1}{N}\sum_{k=0}^{N-1}\sin\left(2k\pi\delta + \phi\right) \ . \tag{12}$$

Assuming that ϕ is a random variable with a uniform distribution in the interval $[-\pi, \pi]$ and using standard statistical operations, the worst-case 'envelope' error ε_e can be derived (Cebon, 1990):

$$\varepsilon_e = \pm\left(\frac{1}{N} + \frac{2}{N^2}\sum_{k=1}^{N}(N-k)\cos\left(2k\pi\delta\right)\right)^{1/2} \ . \tag{13}$$

The root mean square (RMS) error is then given by

$$\varepsilon_{RMS} = \varepsilon_e / \sqrt{2} \ . \tag{14}$$

The variation of the envelope error ε_e with the non-dimensional spacing δ for various values of N is shown in Figure 12.

Three important features can be observed from figure 12 (Cebon, 1990):

1. The error is equal to ±1 for integer values of δ. These values correspond to the sample points (sensors) being spaced an integer number of dynamic force cycles apart.

2. The 'unit cell' pattern $(0 \le \delta < 1)$ repeats for each integer value of δ and is symmetric about $\delta = 0.5, 1.5, 2.5, \ldots$ This repetition is due to aliasing with a Nyquist spacing of $\delta = 0.5$. Therefore, the useful range of spacings for WIM design is $0 \le \delta < 1$.

3. There are $N-1$ zeros within each unit cell at values

$$\delta_k = k/N, \quad k \ne 0, 2N, 3N, \ldots \tag{15}$$

   In all cases, the region between the first and last zeros (from $\delta_1 = 1/N$ to $\delta_{N-1} = (N-1)/N$) has consistently small envelope errors. The width of this region increases with N.

These features can be used to derive a design spacing for the case of Sample Mean estimation. The WIM array should be designed to be accurate for the widest possible range of vehicle speeds and resonant frequencies. Generally the characteristic frequencies lie within a relatively narrow interval, whereas the vehicle speeds can vary with considerable spread. Therefore, a good design procedure is to ensure that the system performs accurately within a desired range of speeds $[V_{\min}, V_{\max}]$.

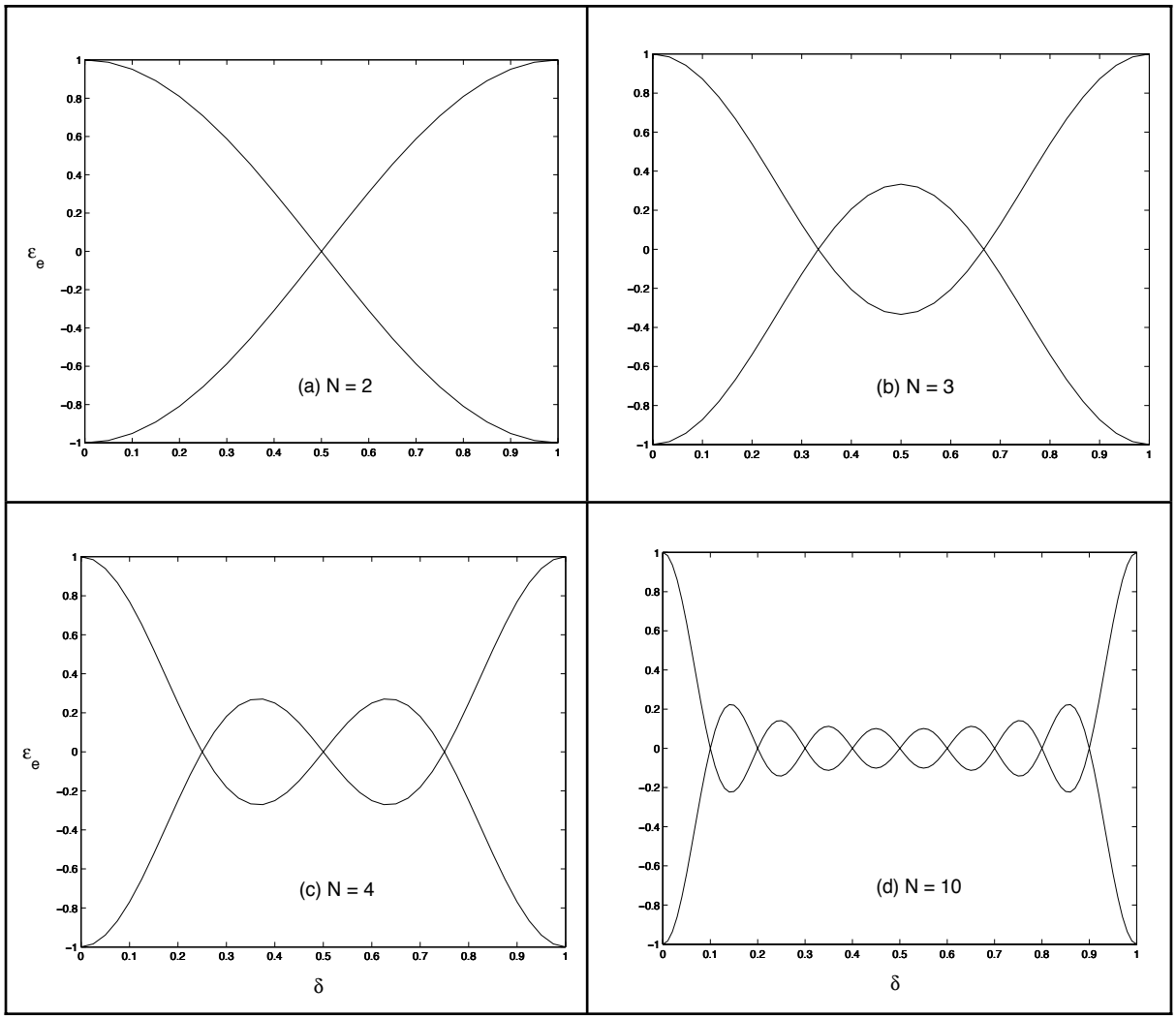

Fig. 12 Plots of envelope error ε_e plotted against non-dimensional sensor spacing δ.

For given values of Δ and average frequency $\bar{f}$, and using Equations (15) and (9), the zeros of the envelope error (in the first 'unit cell') occur at speeds

$$V_k = \frac{\bar{f}\, N \Delta}{k} \ . \tag{16}$$

where $k = 1, 2, 3, \ldots, N-1$ and the bar symbol indicates the mean value.

The region with small envelope error (Figure 12) is determined by the first and last zeros $(k = 1$ and $k = N-1)$. Thus the range of speeds for which the WIM system is reasonably accurate (operating range) is given by the maximum and minimum values:

$$V_{\max} = V_1 = \bar{f}\, N \Delta, \quad N > 1 \tag{17}$$

and

$$V_{\min} = V_{N-1} = \frac{\bar{f}\, N \Delta}{N-1}, \quad N > 1 \ . \tag{18}$$

Combining Equations (17) and (18), a simple formula for the design spacing Δ_{d_1} at the average vehicle speed $\bar{V}$ can be derived (Cebon, 1990):

$$\Delta_{d_1} = \frac{(N-1)\left(V_{\min} + V_{\max}\right)}{\bar{f}\, N^2} = \frac{2(N-1)\bar{V}}{\bar{f}\, N^2} \ . \tag{19}$$

This assumes that the probability distribution of speeds is symmetric, so that

$$\overline{V} = \frac{V_{\min} + V_{\max}}{2}.$$

The design procedure simply involves choosing the number of sensors N , and calculating the sensor spacing using Equation (19) for the assumed average speed. In many cases, the choice of the number of sensors is limited (for example, due to cost) and therefore non-negotiable during design.

Cebon (1990) concluded that considerable improvement in WIM accuracy could be obtained by using arrays of 3 sensors, spaced according to Equation (19). Experimental results (Cebon and Winkler, 1991a) showed a close agreement with theoretical predictions. Use of 3 or more sensors achieves improved 'robustness' to variations of vehicle speed and suspension characteristics.

A major drawback of the method is its inability to weigh accurately vehicles of the 'walking-beam' type, i.e. with two dominant frequency components (Figure 10b).

In the following sections, an extension of this work leading to a new method of WIM data processing based on the *Maximum Likelihood (ML)* estimator is presented. The problem of determining the design that optimises the performance of the data processing algorithms for one or two sine wave inputs is also addressed.

For the purposes of MS-WIM design, regular spacing has been chosen. As it will be shown, regular spacing is vulnerable due to aliasing, but this can certainly be avoided. On the other hand, regularly-spaced WIM can be studied systematically.

4.2 The Maximum Likelihood Method

The algorithm presented here is based on the well-known *Maximum Likelihood (ML)* method, which can exploit prior information and give the most probable set of parameter estimates, consistent with the sensor measurements. Compared to the Sample Mean, the Maximum Likelihood estimator has negligible bias (for sufficiently high signal-to-noise ratio) and only the RMS errors are important. Being essentially *unbiased*, it therefore has potential for smaller errors.

The algorithm fits the signal model parameters by finding those parameter values $\left(F_o, F_1, f_1, \phi_1, \ldots\right)$ that maximise the associated *Likelihood function* (Kay, 1988). For a given signal model, suitable knowledge of vehicle dynamics can be used as prior information for constraining the optimisation process. In the following analysis, **bold** letters are used to describe a vector, and the hat symbol ^ denotes the ML estimate.

If the dynamic force is exactly represented in the time domain by the continuous signal model $F(t)$, given by Equation (8), a MS-WIM system will sample the signal $F(t)$ with some error, resulting in a vector of noisy measurements $\mathbf{Y} = \left[Y_0, Y_1, \ldots, Y_{N-1}\right]$ (the sample Y_i taken at time t_i). The errors (due to model-induced error, sensor noise, quantisation noise etc.) can be approximated by independent samples of a zero-mean white Gaussian process of standard deviation σ_n . For a system of N sensors, the Maximum Likelihood method can be employed to fit a M-sine wave signal model with 3M+1 parameters to the N observed data points $\left(t_i, Y_i\right), i = 0, 1, 2, \ldots, N-1$. The Maximum Likelihood algorithm will predict new "ML" values $\hat{F}\left(t_i\right)$ for each point. The algorithm will only work if the number of sensors is greater the number of unknown parameters $\left(N \geq 3M+1\right)$.

If $\mathbf{X} = \left[F\left(t_0\right), F\left(t_1\right), \ldots, F\left(t_{N-1}\right)\right]$ is the noise-free signal vector corresponding to the parameter vector $\mathbf{A} = \left[F_0, F_1, f_1, \phi_1, \ldots, F_M, f_M, \phi_M\right]$, the Likelihood function $L\left(\mathbf{Y}; \mathbf{A}\right)$ is the natural logarithm of the conditional probability $P(\boldsymbol{Y} \mid \boldsymbol{X})$ that the measured data set ($\mathbf{Y}$) is the correct one, within accuracy ΔF for any individual sample, given the parameter vector $\mathbf{A}$. This probability is given by the product of the individual probabilities p_i for each sample point:

$$L(\mathbf{Y};\mathbf{A}) = \ln P(\mathbf{Y}/\mathbf{X}) = \ln\left(\prod_{i=0}^{N-1} p_i\right) = \ln\left[\prod_{i=0}^{N-1} \exp\left(-\frac{[Y_i - X_i]^2}{2\sigma_n^2}\right)\Delta F\right]. \quad (20)$$

ΔF is constant, and can be treated as an unknown scale factor, which is irrelevant to the subsequent analysis. Maximising $L(\mathbf{Y};\mathbf{A})$ is thus equivalent to minimising the mean square error which is given by the quantity:

$$l(\mathbf{Y};\mathbf{A}) = \sum_{i=0}^{N-1} (Y_i - X_i)^2 = \sum_{i=0}^{N-1} W_i^2, \quad (21)$$

where $\mathbf{W}$ is the noise vector $(W_i = Y_i - X_i)$, and the new estimated values for each point will be

$$\hat{X}_i = \hat{F}(t_i) = \hat{F}_o + \sum_{i=1}^{M} \hat{F}_i \sin(2\pi \hat{f}_i t_i + \hat{\phi}_i).$$

The problem is thus equivalent to non-linear *Least Squares* (LS). The value of $\mathbf{A}$ which maximises the Likelihood function will provide the static weight estimate $(\hat{F}_o = \hat{A}_1)$.

For multiple sine waves, the minimisation of Equation 21 is computationally intensive. In cases where the number of samples is much greater than the number of parameters, the ML estimates can be obtained by the periodogram method (Macleod, 1998) after a small number of iterations. Unfortunately, this is not the case for Multiple-Sensor WIM, because the number of sensors is limited and not significantly greater than the number of the model parameters. A sequential estimation algorithm is therefore proposed. The algorithm addresses the related linear LS problem (reduced to 2M+1 parameters), in which the frequencies f_i are assumed constant. In this case, the linear model can be explicitly written as

$$F(t) = F_o + \sum_{i=1}^{M}\left[F_i \sin(\phi_i)\cos(2\pi f_i t) + F_i \cos(\phi_i)\sin(2\pi f_i t)\right], \quad (22)$$

The new vector of unknown parameters is

$$b = \left[F_o, F_1 \sin(\phi_1), F_1 \cos(\phi_1), F_2 \sin(\phi_2), F_2 \cos(\phi_2), \ldots\right],$$

and the *normal equations* (Van Trees, 1968) are

$$\left(\boldsymbol{G}^T \cdot \boldsymbol{G}\right)\hat{\boldsymbol{b}} = \boldsymbol{G}^T \cdot \boldsymbol{Y}, \quad (23)$$

where $\mathbf{G}$ is the design matrix of the least-squares fit:

$$\mathbf{G} = \begin{pmatrix} 1 & \cos(2\pi f_1 t_0) & \sin(2\pi f_1 t_0) & \ldots & \cos(2\pi f_M t_0) & \sin(2\pi f_M t_0) \\ 1 & \cos(2\pi f_1 t_1) & \sin(2\pi f_1 t_1) & \ldots & \cos(2\pi f_M t_1) & \sin(2\pi f_M t_1) \\ 1 & \cos(2\pi f_1 t_2) & \sin(2\pi f_1 t_2) & \ldots & \cos(2\pi f_M t_2) & \sin(2\pi f_M t_2) \\ \cdot & \cdot & \cdot & & \cdot & \cdot \\ \cdot & \cdot & \cdot & & \cdot & \cdot \\ \cdot & \cdot & \cdot & & \cdot & \cdot \\ 1 & \cos(2\pi f_1 t_{N-1}) & \sin(2\pi f_1 t_{N-1}) & \ldots & \cos(2\pi f_M t_{N-1}) & \sin(2\pi f_M t_{N-1}) \end{pmatrix}.$$

A fine search of the linear least-squares result over a reasonable range of frequencies provides an accurate estimate $\boldsymbol{b_o}$ (at nearly optimal frequency values). It has been found that an adequately small step of the search routine always guarantees convergence to the global optimum.

The method can be used for both regular or irregular sensor arrays and behaves well in the presence of sensor noise. The minimum number of sensors required for the solution of the Maximum Likelihood calculation is equal to the number of signal model parameters, i.e. 3M+1.

The algorithm imports the noisy sensor data and the parameter 'priors' and outputs the estimate of the static load. The calculation is robust, always convergent, and adequately fast for real-time implementation.

Depending on the application, modifications of this method can be employed. For example, in cases where speed of calculation is more important than accuracy, it may be more effective to perform a preliminary coarse search over frequencies, using the proposed linear LS algorithm; the linear LS estimate $\boldsymbol{b_o}$ can then be used as a good starting value for a constrained non-linear LS maximisation of the likelihood function. Prior information on the feasible range of static loads (F_o), dynamic force amplitudes (F_1, F_2), velocities (V) , and the frequencies (f_1, f_2) can be used to constrain the optimisation.

4.3 Analysis of the Estimation Error and Optimal Spacing

4.3.1 Sample Mean Performance for a Single Tone

In the case of Sample Mean estimation for a quarter-car vehicle model, the variation of relative error versus spacing for a regularly spaced, N-sensor WIM array is generally described by a graph similar to absolute value of the errors shown in Figure 12 (Cebon, 1990). The design spacing can easily be calculated by the simple formula of Equation (19).

The Sample Mean result is always biased (Equation (10)), and in the presence of zero-mean white Gaussian noise of variance σ_n^2 , the estimation error will be given by

$$\varepsilon_e = \frac{\sum_{i=0}^{N-1} F(t)}{N} - F_o \tag{24}$$

with a standard deviation of $\sigma_n / \sqrt{N}$.

4.3.2 ML performance: Cramer-Rao Bounds

The lower bounds on the variance of the ML estimator are equivalent to the theoretical or *Cramer-Rao Bounds* (CRB's) for an unbiased estimator (Rife and Boorstyn, 1974; Rife and Boorstyn, 1976).

The unbiased CRB's are the diagonal elements of the inverse of the *Fisher information matrix* **J**, which has elements

$$J_{lm} = -\mathrm{E}\left\{ \frac{\partial^2}{\partial A_l \, \partial A_m} \ln L(\boldsymbol{Y;A}) \right\} \tag{25}$$

where **Y** is the vector of the unknown parameters, $L(\mathbf{Y;A})$ is the Likelihood function, and $\mathrm{E}\{\sum$ denotes expectation with respect to the sample vector **Y**.

The variances of the parameter estimates satisfy the inequality:

$$\mathrm{var}\left\{ A_l \right\} \geq J_{ll}^{-1} \tag{26}$$

where the notation J_{ll}^{-1} denotes the *l*-th diagonal element of $\mathbf{J}^{-1}$.

ML Performance for a Single Tone

For the case of a single-sine wave signal model, and assuming zero-mean white Gaussian noise of variance σ_n^2 , the Fisher information matrix is easily derived from Equation (25):

$$J_{lm} = \frac{1}{\sigma_n^2} \sum_{i=0}^{N-1} \frac{\partial^2 X_i}{\partial A_l \partial A_m} \tag{27}$$

The RMS error of the static weight estimator will thus be

$$\mathrm{var}\left\{\hat{F}_o\right\} = \mathrm{var}\left\{\hat{A}_1\right\} \geq J_{ll}^{-1} = \frac{\sigma_n^2}{N} \tag{28}$$

The ML estimator approximately meets the Cramer-Rao lower bounds, i.e. $\mathrm{var}\left\{\hat{F}_o\right\} \approx \sigma_n^2 / N$ (Rife and Boorstyn, 1974). For the ideal case of noise-free sensors sampling a perfect sine wave with a sufficient number of points and no aliasing, the ML error is exactly *zero*.

It is useful to examine the performance of the ML estimator against the performance of the SM estimator for noisy sine waves. A useful measure of the system performance is the Error Coefficient of Variation (ECOV) ρ , defined by (Cebon, 1990):

$$\rho = \frac{\sigma_e}{F_o} \tag{29}$$

where the standard deviation $\sigma_e = \sqrt{\mathrm{var}\{\hat{F}_o\}}$ corresponds to the RMS estimation error. For the case of single sensor systems $(N = 1)$, the ECOV is equal to the 'Dynamic Load Coefficient' (DLC), which characterises the dynamic tyre force (Sweatman, 1983; Cebon, 1990).

A number of numerical experiments were undertaken to examine the performance of the ML estimator. The test signals consisted of either one or two sine waves with added noise; or the simulation models shown in figure 9, using the spectral density of a 'Very Good' road (Robson, 1979) as input (See Table 2).

Figure 13 shows the ECOV as a function of non-dimensional spacing δ for both estimation methods, for the conditions of Test 1 (Table 2: 10 sensors, noisy sine-wave input). The point $\delta = 0.5$ corresponds to the Nyquist sampling rate with $\delta = 0.5V/f$. It can be seen that the CRB's rise dramatically near zero sensor spacing (at $\delta = 0$) or where aliasing to zero spacing occurs (at $\delta = 1$). Therefore, a crucial requirement in the design of the WIM array is to ensure that aliasing to zero spacing is avoided for a wide range of operating conditions. If this requirement is met, the algorithm will perform within its accurate operating region, i.e. the 'plateau' region (solid line) of Figure 13. It can be seen that the rapid increase of the CRB's starts around $\delta = 1/10$. In general, for N sensors this threshold occurs at $\delta = 1/N$ (the first zero in Equation (15) and Figure 12d). Therefore, the ML algorithm requires that the sensor array should be longer than one cycle of the lowest frequency component. The rise in the CRB's near $\delta = 1$ occurs at $\delta \approx 9/10$, i.e. $(N-1)/N$ – the last zero in the unit cell in Equation (15) and Figure 12d.

Test	'Measurement' system	Test Signal
1	10 sensors (N = 10) Sensor noise: $\sigma_n = 0.04F_0$	Single sine wave of amplitude $F_1 = 0.2F_0$
2	As for Test 1	two sine waves $\bar{f}_1 = 2.5Hz, \quad \bar{f}_2 = 10Hz.$ $\bar{V} = 20m/s,$ Dynamic force amplitudes: $F_1 = F_2 = 0.2F_0$
3	4 sensors (N = 4) Δ_{d1} as per Eq. 19. Single-tone fit - ML1 Priors: $\bar{V} = 20\text{m/s}; \quad f_1 = 1.5 \pm 4\text{Hz}.$	$F_0 = 100\text{kN}$ $F_1 = 8\text{kN}$ $f_1 = 1.9\text{Hz}$ V = 20m/s
4	As for Test 3, with varying σ_n (N = 4) and with varying N ($\sigma_n = 0$). Single-tone fit - ML1 Priors: as for Test 3	Quarter car (Figure 9a), V = 20m/s 'Very Good' pavement (Robson, 1979)
5	As for Test 3, with varying σ_n (N = 10, Δ_{d2} as per Eq. 33.) and varying N ($\sigma_n = 0$). Two-tone fit - ML2 Priors: As for Test 3 wit $f_2 = 815$ Hz	Walking beam (Figure 9b), V = 20m/s 'Very Good' pavement (Robson, 1979)

Table 2 Numerical experiments performed to test the Maximum Likelihood algorithm.

Furthermore, the previous analysis suggests that the error of the biased SM estimate worsens as the dynamic force F_1 increases, whilst ML performance remains unaffected.

Another important aspect of the Maximum Likelihood approach is that it is robust to variations in vehicle speed and resonant frequencies within its operational limits. The simulation results presented in the following section will verify the above theoretical analysis.

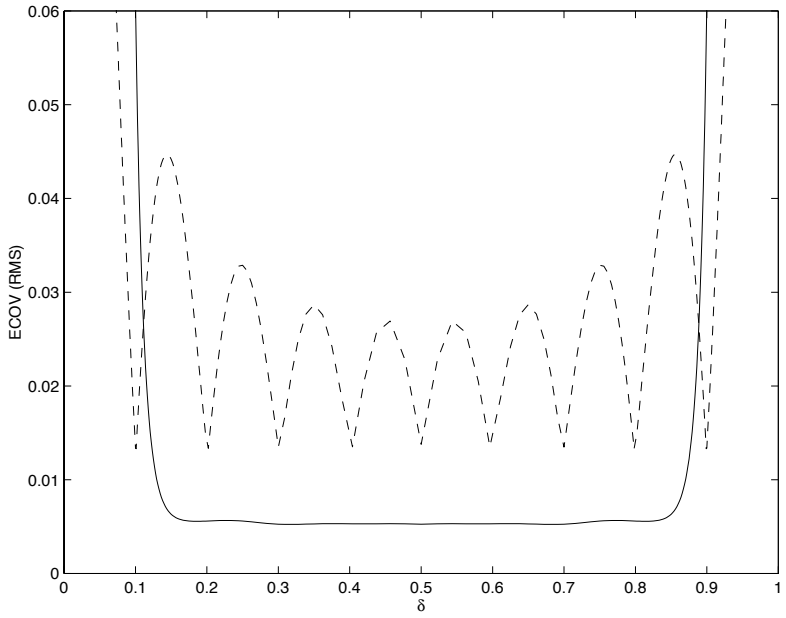

Fig. 13 Variation of the Error Coefficient of Variation ρ with non-dimensional spacing δ for Test 1 (see Table 2). ———— Cramer-Rao bounds, – – – – SM estimation.

ML Performance for Two Tones – Design Considerations

Investigating the Cramer-Rao Bounds for the case of a single tone, offers useful insight for the two-tone case (e.g. for dynamic tyre force spectra like that shown in Figure 11b). It is known (Macleod, 1998) that the CRB's for two sufficiently separated tones approach the corresponding single-tone CRB's.

The suitable spacings in this case can be derived from the requirement of sampling both frequency components correctly. The range of available spacing depends exclusively on the extrema of the ratio V/f. Assume that the parameters V, f_1 and f_2 have known Gaussian distributions, with mean values and standard deviations: $\overline{V}, \sigma_V, \bar{f}_1, \sigma_{f_1}, \bar{f}_2, \sigma_{f_2}$. From the single-tone analysis (Figure 13) it is concluded that the correct sampling intervals for both frequencies must satisfy the inequality:

$$\frac{1}{N} < \delta < \frac{N-1}{N} \tag{30}$$

Applying $\delta = \Delta f / V$ to the above, approximate lower and upper values of Δ (depending on low frequency f_1 and high frequency f_2 respectively) can be derived:

$$\Delta > \frac{1}{N}\frac{\overline{V}}{\bar{f}_1} = \Delta_1, \tag{31}$$

and

$$\Delta < \frac{N-1}{N}\frac{\overline{V}}{\bar{f}_2} = \Delta_2. \tag{32}$$

Figure 14 shows typical CRB's as a function of spacing for the two separate sine-wave components in Test 2 (Table 2).

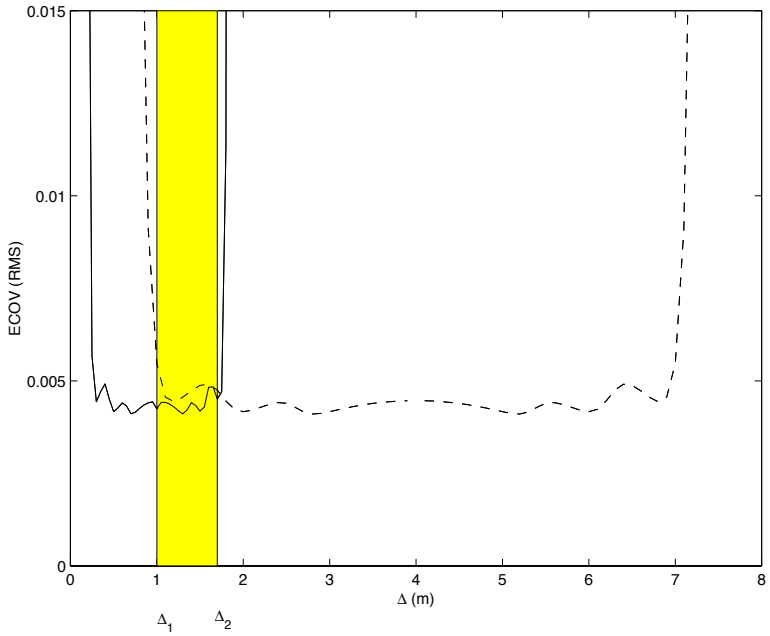

Fig. 14 Variation of the Error Coefficient of Variation (derived from the corresponding CRB's) with sensor spacing for Test 2 (see Table 2).
– – – – – low frequency f_1, ———— high frequency f_2,
Shaded area: the operating region between Δ_1 and Δ_2.

From Figure 14 it can be seen that a good design strategy would be to set the 'design' sensor spacing Δ_d to the average of Δ_1 and Δ_2 :

$$\Delta_{d_2} = \frac{\Delta_1 + \Delta_2}{2} = \frac{\bar{V}}{2N}\left(\frac{1}{\bar{f}_1} + \frac{N-1}{\bar{f}_2}\right). \tag{33}$$

The estimation algorithm will fail if there is no overlap between the 'plateau' regions for the two frequency components. Therefore it must always be $\Delta_2 \geq \Delta_1$. The operational limit of the algorithm occurs at $\Delta_2 = \Delta_1$, which, using Equations (31) and (32) is $N = f_2/f_1 + 1$. This determines the limit on *minimum possible* number of sensors:

$$N \geq \text{Smaller of}\left(\frac{f_2}{f_1} + 1;\quad 3M + 1\right). \tag{34}$$

It is clear that the ratio of frequencies f_2/f_1 is very important. A system designed for a low ratio f_2/f_1 will need less sensors (and therefore cost less) than systems designed for higher rations f_2/f_1. In practice, this ratio will be set by the types of vehicles using the road - in particular, their suspensions and tyre types and the masses of their axles and bodies (see Cebon, 1999).

4.4 Simulation Results

Simulation studies in the time domain were undertaken for the quarter-car model and the walking beam model. The test conditions are listed as Tests 3-5 in Table 2.

4.4.1 Sine Wave-Plus-Noise Model

For figure 15, the test signals had the general form of a pure sine wave (with mean value F_o) plus Gaussian noise. The parameter values are those for Test 3 in Table 2. Monte Carlo simulation was used to generate an accurate estimate of the ECOV. Figure 15 shows the ECOV plotted against the standard deviation of noise σ_n for a 4-sensor system, calculated using 500 Monte Carlo runs. Both Sample Mean and Maximum Likelihood results are shown.

It can be seen that for low noise levels $(\sigma_n < 0.04F_o)$, the Maximum Likelihood method with one tone ('ML1') reduces the ECOV significantly compared to the Sample Mean. In agreement with the theoretical results, the Maximum Likelihood error is close to zero at $\sigma_n = 0$ (Eq. 28). (The accuracy of the calculation depends on the frequency increment used in the search algorithm.) The minimum error for the Sample Mean (at $\sigma_n = 0$) is due to bias. As expected, for higher noise levels, the performance of both methods (SM and ML) become similar.

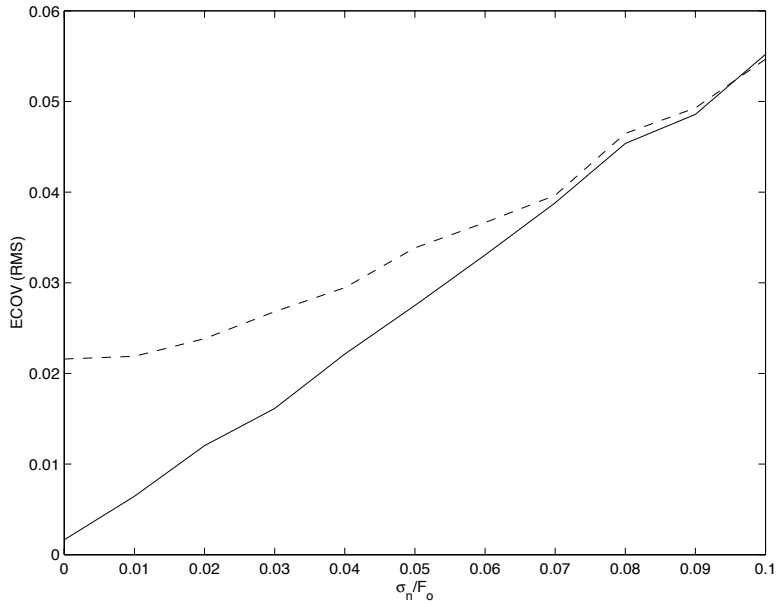

Fig. 15 Sine wave-plus-noise simulation: Variation of the Error Coefficient of Variation with noise level, represented as a fraction of F_0 for Test 3 (see Table 2).
– – – – – Sample Mean, ———— Maximum Likelihood (ML1).

4.4.2 Quarter-Car Model

In the following examples, the test signals were generated by time-domain simulation of a quarter-car vehicle model on a 'random' road profile.

The simulation was performed for the quarter car model (figure 9a) travelling at 20m/s on a 'Very Good'- type pavement (see (Robson, 1979)). The dynamic force was 'measured' by a WIM system described by the parameters of Test 4 (Table 2). The ECOV was evaluated from 500 Monte Carlo runs using both estimation methods (SM and ML1).

Figure 16 shows the variation of the ECOV with the standard deviation of sensor noise for $N = 4$, and is comparable to Figure 15. The ML result is better than the SM result, particularly for $\sigma_n \leq 0.05F_o$. The gap between the two approaches is reduced because the input signal is not a pure sine wave. For $\sigma_n = 0$, the ML1 error is due to 'modelling' error in the ML1 algorithm.

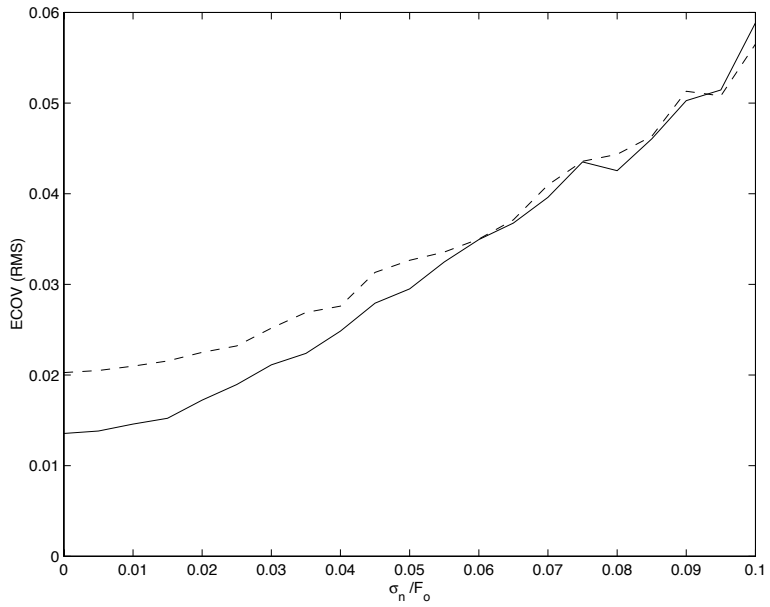

Fig. 16 Quarter-car simulation: The Error Coefficient of Variation for different levels of noise: Test 4 (see Table 2). – – – – – Sample Mean, ———— Maximum Likelihood (ML1).

In Figure 17, the ECOV is plotted against the number of sensors, for Test 4. The ML result can be calculated only for $N > 4$, whereas the SM result is plotted for all values of N. For $N = 1$, the SM curve gives the dynamic Load Coefficient (approximately equal to 0.075). The ML1 approach requires less sensors for given accuracy, leading to potential cost reductions.

Figure 18 shows the variation of the ECOV with sensor spacing for cases of perfect (noise-free) and noisy sensors with $\sigma_n = 0.04 F_o$. These ECOV results are directly comparable to previous experimental results (Glover and Newton, 1989; Cebon and Winkler, 1991a).

In both noiseless and noisy cases, the Maximum Likelihood error is generally smaller, producing a relatively smooth 'plateau' region over a wide range of spacings, however the relative benefits of ML are significantly less in the noisy case. This suggests that the performance of the ML1 method is not affected significantly by frequency and speed variations over a wide range of spacings for 4 sensors. On the other hand, the performance of the Sample Mean is more sensitive to variations of the resonant frequency and the vehicle speed. Indeed, Figure 18 follows and oscillating pattern similar to the result for a simple sine-wave in Figures 12 and 13.

The design spacing Δ_{d1}, from Equation (19), is also shown on Figure 18, as a dashed vertical line. It is clear that this is a good choice of spacing in this case, since it falls within the general 'plateau' region of the curves.

Variation with velocity gives a similar result to Figure 18 due to the effect of non–dimensional spacing (Equation (9)). It appears that the ML1 algorithm is slightly more robust to variations of vehicle speed than the SM approach.

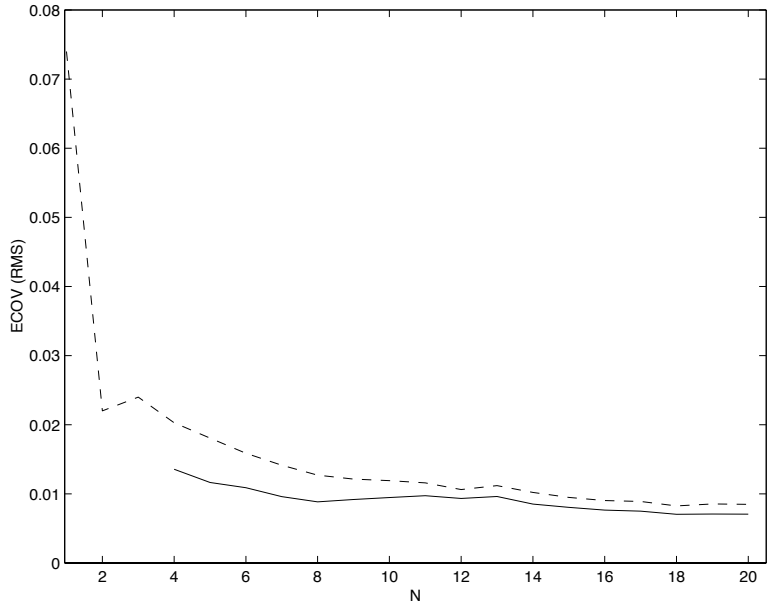

Fig. 17 Quarter-car simulation: Variation of the Error Coefficient of Variation with the number of sensors: $\sigma_n = 0$, Test 4 (see Table 2).
– – – – – Sample Mean, ———— Maximum Likelihood (ML1).

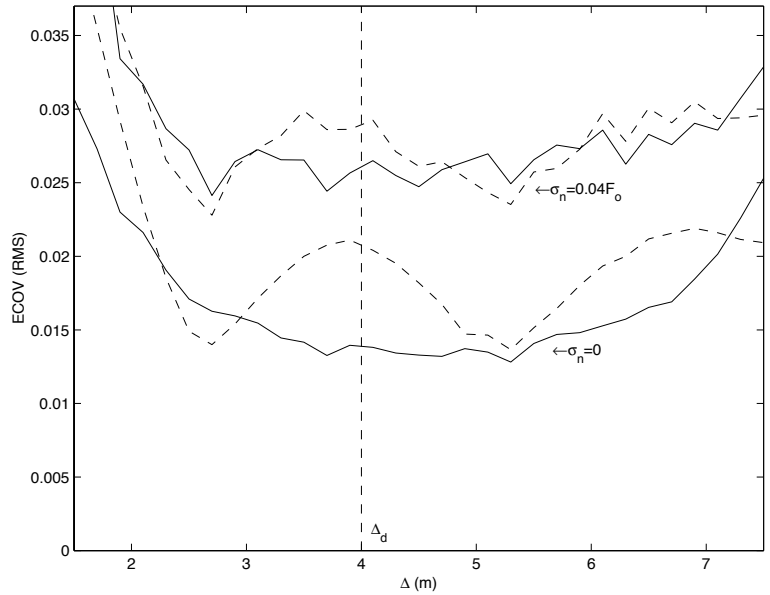

Fig. 18 Quarter-car simulation: Variation of the Error Coefficient of Variation with sensor spacing for $N = 4$, Test 4 (see Table 2).
– – – – – Sample Mean, ———— Maximum Likelihood (ML1).

4.4.3 Walking-Beam Model

In Test 5, signals were generated by time-domain simulation of a walking-beam vehicle model (figure 9b) on the same ('Very good'-type) road profile used in the previous section (Table 2).

The truck in this case had the parameters in Figure 9b and was 'measured' by a 10-sensor WIM system. The ECOV was again evaluated from 500 Monte Carlo runs using both estimation methods (SM and Maximum Likelihood with a 2-tone fit 'ML2').

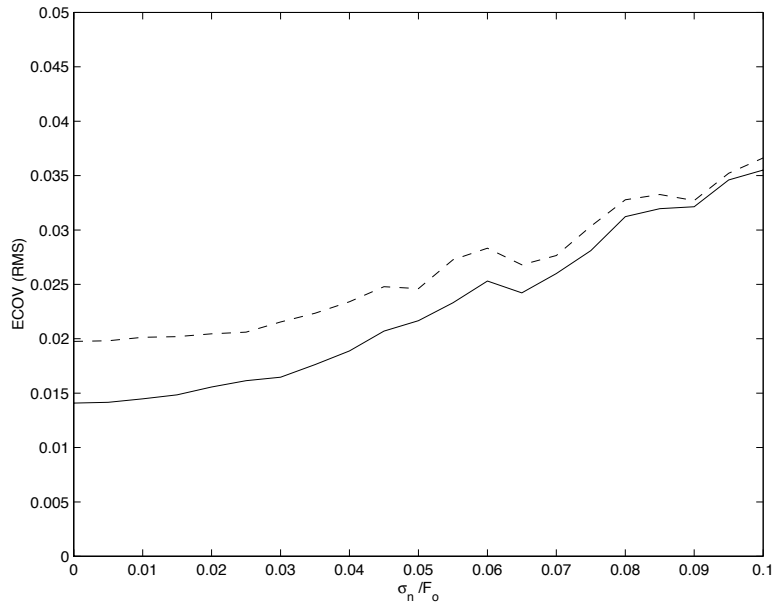

Fig. 19 Walking-beam simulation: Variation of the Error Coefficient of Variation with noise level: Test 5 (see Table 2).
– – – – – Sample Mean, ———— Maximum Likelihood (ML2).

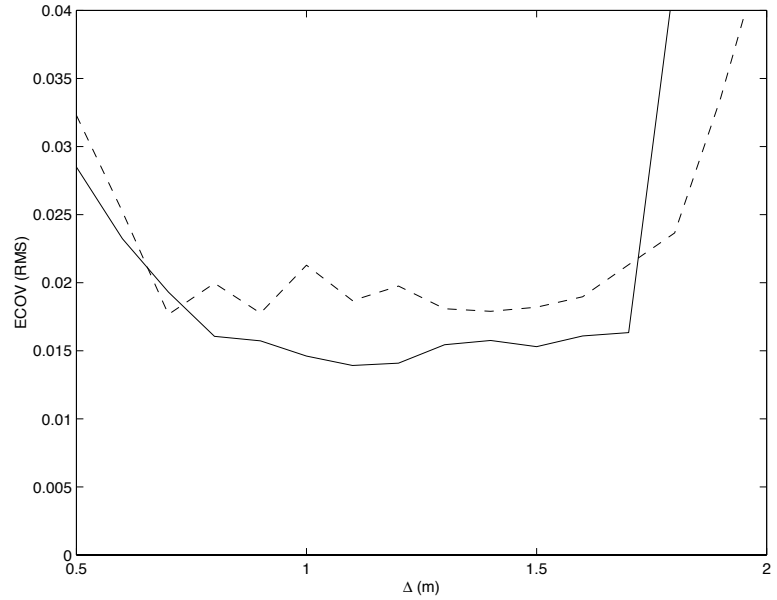

Fig. 20 Walking-beam simulation: Variation of the Error Coefficient of Variation with sensor spacing: Test 5 (see Table 2).
– – – – – Sample Mean, _____ Maximum Likelihood (ML2).

Figure 19 shows the variation of the ECOV with the standard deviation of sensor noise, and is comparable to figure 16. The relative improvement of the ML2 result is even greater in this case than in the quarter-car case. At $\sigma_n = 0$, the ML2 error is totally due to modelling error. It is also seen that for low noise levels $\sigma_n < 0.07F_o$, the Maximum Likelihood approach performs significantly better than the SM.

In Figure 20, the ECOV is plotted for various sensor spacings for the case of perfect (noise-free) sensors. As in the quarter-car case, the ML curve forms a smooth plateau over a wide range of spacings. The design spacing $\Delta_{d_2} = 1.3$m (Equation (33)), lies in the middle of the plateau region.

The ML2 algorithm is relatively insensitive to variations of the vehicle speed and the resonant frequencies in this case also, although its error rises sharply at spacings greater than 1.7m. It is apparent that the success of the ML2 approach relies heavily on the spacing falling within the 'plateau' region.

4.5 Success Rate of the Weight Estimation Algorithm

The success of the data processing algorithms is dependent on having correct sensor spacing. This section investigates the success rate of these algorithms and addresses important WIM-design issues. The analysis is general and can be applied for any WIM estimation method that requires efficient sampling, since the shape of the error curve calculated by the Cramer-Rao bounds is believed to be universal. Its aim is to calculate the success rate of the estimation algorithm for a known system (known parameters: array spacing Δ, number of sensors N, sensor noise σ_n).The analysis can also be used for the inverse problem, and produce the optimal design given the desired success rate.

Assume the two-sine wave model and relevant definitions of Section 4.3.2. The unknown parameter is the ratio V/f. Using the results of Section 4.3.2, the probability that a vehicle is measured successfully is the probability that the sensor spacing fits into the relevant 'plateau' regions of the error curves, and is given by:

$$P_S(N;\Delta) = P\left\{\left(\frac{V}{f_1} < N\Delta\right) \wedge \left(\frac{V}{f_2} > \frac{N}{N-1}\Delta\right)\right\}, \tag{35}$$

where $\Delta = \Delta_{d_2}$ is the spacing as given by Equation (33), and $\wedge$ denotes the logical AND. Alternatively this probability can be expressed as the complement of the probability of failure $P_F(N;\Delta)$, i.e. the probability that a measurement lies outside the operating region of the algorithm:

$$P_s(N;\Delta) = 1 - P_F(N;\Delta)\ . \tag{36}$$

Assuming the worst-case scenario with totally independent frequency distributions,

$$P_F(N;\Delta) = P\left\{\left(\frac{V}{f_1} > N\Delta\right) \vee \left(\frac{V}{f_2} < \frac{N}{N-1}\Delta\right)\right\} = P\left\{\frac{V}{f_1} > N\Delta\right\} + P\left\{\frac{V}{f_2} < \frac{N}{N-1}\Delta\right\}, \tag{37}$$

where $\vee$ denotes the logical OR. The two terms in Equation (37) can be calculated in similar ways.

4.5.1 Calculation of the Probability of Failure

To determine the probability of failure $P_F(N;\Delta)$ (Equation (37)), it is necessary to calculate the probability that the ratio V/f of the two independent Gaussian variables (f,V) is less (or greater) than a given threshold Λ.

Let $Q_1(\Lambda)$ be the probability that the ratio V/f of the two independent Gaussian variables (f,V) is *less* than a given threshold Λ:

$$Q_1(\Lambda) = P\left\{\frac{V}{f} > \Lambda\right\}\ . \tag{38}$$

Let the corresponding Gaussian probability density functions (pdf's) be

$$P(f) = \frac{1}{\sqrt{2\pi}\sigma_f}\exp\left[-\frac{(f-\bar{f})^2}{2\sigma_f^2}\right] \tag{39}$$

and

$$P(V) = \frac{1}{\sqrt{2\pi}\sigma_V} \exp\left[-\frac{(V-\bar{V})^2}{2\sigma_V^2} \right]. \tag{40}$$

The pdf's are mutually independent and the joint (2-D) probability distribution will be

$$P(f,V) = \frac{1}{2\pi\sigma_f\sigma_V} \exp\left[-\frac{(f-\bar{f})^2}{2\sigma_f^2} - \frac{(V-\bar{V})^2}{2\sigma_V^2} \right], \tag{41}$$

where $\bar{f}$ is the mean frequency, $\bar{V}$ is the mean velocity, and σ_f, σ_V are the corresponding standard deviations. The probability that $V/f < \Lambda$ can be found by integrating the pdf $P(f \mid V < \Lambda f)$. The domain of integration is effectively a 'wedge' defined by the f-axis and the line $V = \Lambda f$.

The calculation for the probability of failure $P_F(N;\Delta)$ is shown in Figure 21 (the parameters were those of Test 2 (Table 2) including $\sigma_V = 2\text{m/s}$. The two shaded areas indicate the domains of integration. The figure includes both distributions $\left(P(f_1,V)\right.$ and $\left.P(f_2,V)\right)$ for the sake of clarity, while it is clear that they are mutually independent and need to be calculated separately.

The volume under the lower wedge is given by

$$\begin{aligned} Q_1(\Lambda) &= \iint_R P(f,V)\,df\,dV \\ &= \int_0^\infty df \int_0^{\Lambda f} \frac{1}{2\pi\sigma_f\sigma_V} \exp\left[-\frac{(f-\bar{f})^2}{2\sigma_f^2} - \frac{(V-\bar{V})^2}{2\sigma_V^2} \right] dV \end{aligned} \tag{42}$$

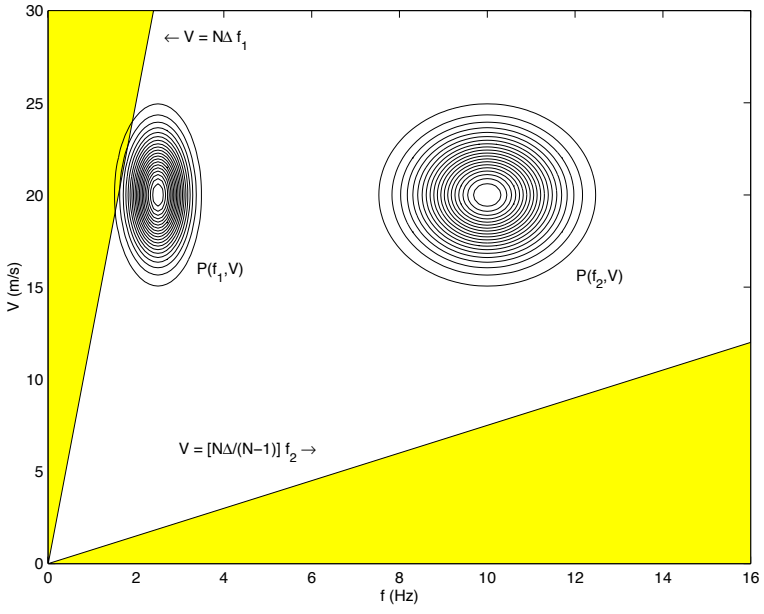

Fig. 21 Calculation of the probability of failure.

The inner integration gives

$$Q_1(\Lambda) = \frac{1}{2\sqrt{2\pi}\sigma_f} \Phi\left(\frac{\bar{V}}{\sqrt{2}\sigma_V} \right) I_1 + \frac{1}{2\sqrt{2\pi}\sigma_f} I_2 \ , \tag{43}$$

where $\Phi(u)$ is the Error Function

$$\Phi(u) = \frac{2}{\sqrt{\pi}} \int_0^{\infty} \exp\left(-x^2\right) dx \ , \tag{44}$$

and the integrals I_1 and I_2 are defined by

$$I_1 = \int_0^{\infty} \exp\left[-\frac{\left(f - \bar{f}\right)^2}{2\sigma_f^2} \right] df \ , \tag{45}$$

and

$$I_2 = \int_0^{\infty} \exp\left[-\frac{\left(f - \bar{f}\right)^2}{2\sigma_f^2} \right] \Phi\left(\frac{\Lambda f - \overline{V}}{\sqrt{2}\sigma_V} \right) df \ . \tag{46}$$

The integral I_1 is a standard integral and can be easily calculated:

$$I_1 = \frac{\sqrt{2\pi}\sigma_f}{2} \Phi\left(\frac{\bar{f}}{\sqrt{2}\sigma_f} \right) + \frac{\sqrt{2\pi}\sigma_f}{2}. \tag{47}$$

Equations (43) and (47) give

$$Q_1(\Lambda) = \frac{1}{4}\left[1 + \Phi\left(\frac{\bar{f}}{\sqrt{2}\sigma_f} \right) \right] \Phi\left(\frac{\overline{V}}{\sqrt{2}\sigma_V} \right) + \frac{1}{2\sqrt{2\pi}\sigma_f} I_2 . \tag{48}$$

The integral I_2 (Equation (46)) can only be calculated numerically.

The probability $Q_2(\Lambda)$ that the ratio V/f of the two independent Gaussian variables (f,V) is *greater* than a given threshold Λ can similarly be calculated:

$$Q_2(\Lambda) = \frac{1}{4}\left[1 + \Phi\left(\frac{\overline{V}}{\sqrt{2}\sigma_V} \right) \right] \Phi\left(\frac{\bar{f}}{\sqrt{2}\sigma_f} \right) + \frac{1}{2\sqrt{2\pi}\sigma_V} I_3, \tag{49}$$

where

$$I_3 = \int_0^{\infty} \exp\left[-\frac{\left(f - \bar{f}\right)^2}{2\sigma_f^2} \right] \Phi\left(\frac{\Lambda f - \overline{V}}{\sqrt{2}\sigma_V} \right) df \ , \tag{50}$$

which, similarly to I_2, can only be calculated numerically.

4.5.2 Design Methodology

Using the above results, the probability of failure $P_F(N;\Delta)$ is given by

$$P_F(N;\Delta) = Q_2(N\Delta) + Q_1\left(\frac{N}{N-1}\Delta \right), \tag{51}$$

and the success rate can easily be derived using Equation (36).

Using the parameters of Test 2 (Table 2), Figure 22 shows the success rate $P_S\left(N;\Delta_d\right)$ as a function of the number of sensors for different spreads of the velocity distribution σ_V with constant frequency spreads: $\sigma_{f_1} = 0.4\text{Hz}, \sigma_{f_2} = 1\text{Hz}$. For each case the spacing was set to Δ_{d_2} as calculated by Equation (33). For a given success rate the minimum number of sensors can be derived (which in any case must be greater than both $f_1/f_2 + 1$ and the number of model parameters $3M + 1$). As can be verified in the graph, at the limit $N = f_2/f_1 + 1 = 5$, the success rate falls to zero as required by Equation (34). It should be noted that if the spread of velocities is

small (for $\sigma_V < 0.2\overline{V}$ in the graph), the success rate follows a steeper descent and the exact limit $N = 5$ cannot be reached.

It is apparent that the spread of velocities (σ_V) is an important parameter, which has a significant effect on the minimum number of sensors. On the other hand, this is not the case with the mean velocity $\overline{V}$. Analysing similar success-rate graphs for difference values of mean velocity, showed that the mean velocity does not affect the success rate significantly, producing almost identical results for a broad range of speeds. This indicates that mean velocity is not as important for determining the *number* of sensors as the velocity variance σ_V or the frequency ratio f_2/f_1, which are the controlling factors.

A new design procedure for MS-WIM arrays can be extracted from the analysis above. It includes a number of steps:

1. Set requirements (vehicle types, minimum success rate, sensor noise).
2. Collect or estimate prior information:
   - Velocity pdf: $\overline{V}$, σ_V (from a traffic survey)
   - Low frequency pdf: $\bar{f}_1, \sigma_{f_1}$
   - High frequency pdf: $\bar{f}_2, \sigma_{f_2}$

   Define extreme values where applicable. Note that the reasonable values of $\bar{f}_1$ and $\bar{f}_2$ can be obtained from the literature (Cebon, 1993).
3. Calculate the design spacing Δ_{d_2} from equation (33).
4. Plot the graph of $P_F(N;\Delta_d)$ (calculated as described above) against number of sensors (eg Figure 22); and use it to determine the number of sensors N required to achieve the desired success rate.
5. Repeat steps 3 and 4 as necessary.

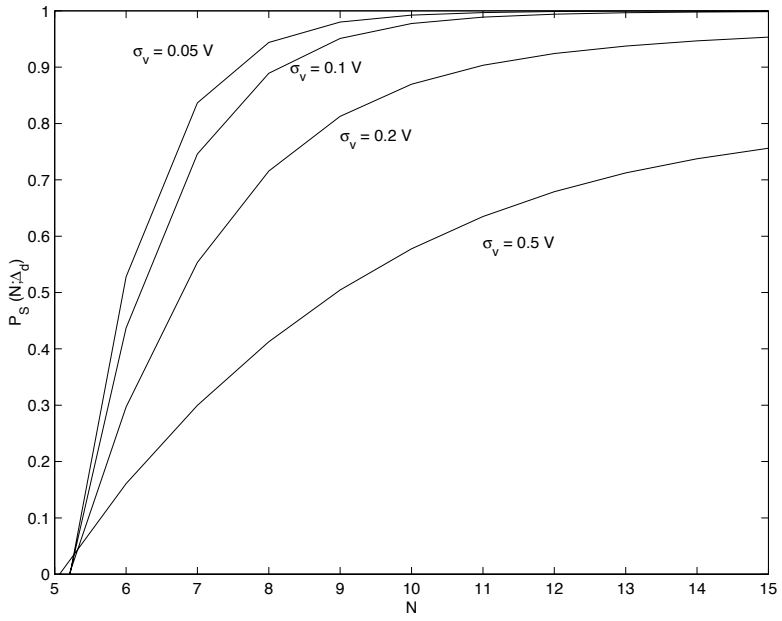

Fig. 22 The success rate $P_s(N,\Delta_d)$ as a function of the number of sensors for different values of σ_V.

4.5.3 Practical Considerations

(i) Due to the generality of the first and last zeros of the envelope function (equation 15 and figure 13) the sensor array design procedure developed here is believed to be applicable for *any* weight estimation algorithm, using uniformly–spaced sensors.

(ii) The main practical problems with existing WIM sensors are measurement errors caused by sensor noise, defects in the installation, tyre tread effects, inadequate calibration, etc (see Chapter 8 of (Cebon, 1999) for details). Typical noise levels for good sensors are of the order $\sigma_n/F_0 \geq 4\%$ RMS (Cebon and Winkler, 1991a). From figures 15, 16, 18 and 19 it can be seen that at this level of noise, Maximum Likelihood estimation is not that much more accurate than the Sample Mean. It is clear, therefore, that in order to obtain the maximum benefit from the data analysis methods developed in this chapter, it will be necessary for more accurate WIM sensor hardware to be developed.

5 EXPERIMENTAL STUDIES ON MS-WIM SITES

Experiments were performed on two MS-WIM sites in France (Trappes and Metz); one MS-WIM site in Abingdon (UK); and using data previously collected in the USA by researchers from CUED and University of Michigan, with a load-measuring mat.

This chapter describes each of the experiments and presents its key conclusions. First the methods of calibrating the arrays and characterising their accuracy are described.

5.1 Errors and Calibration

5.1.1 Characterisation of Measurement Accuracy

Mean Error

The measures of experimental WIM system performance, are defined as follows. The *relative error* x_i for test run i is defined as (COST 323, 1997b):

$$x_i = \frac{W_{d_i} - W_{s_i}}{W_{s_i}}. \tag{52}$$

where W_{d_i} and W_{s_i} are the estimated (in–motion) and the reference (static) weights respectively. These weights may refer to individual axles, groups of axles, gross weights, or any other different sub–populations.

The mean value of the relative error is:

$$\bar{x} = \frac{1}{n}\sum_{i=1}^{n}\frac{W_{d_i} - W_{s_i}}{W_{s_i}}, \tag{53}$$

where n is the number of estimates of x_i in the ensemble (eg the number of passes of the calibration vehicle over the array).

Error Coefficient of Variation

The standard deviation of the relative error (which is denoted above as the 'Error Coefficient of Variation' – ECOV) s, is defined by:

$$s^2 = \frac{1}{n}\sum_{i=1}^{n}\left(\frac{W_{d_i} - W_{s_i}}{W_{s_i}}\right)^2, \tag{54}$$

COST 323 Specification

The COST 323 working group developed a draft specification for representing the statistics of WIM system performance. The accuracy of the system is defined by an ‘accuracy class’ (A, B, C, D, E), along with a weight ‘tolerance (%)’ (confidence interval) in parenthesis. For example A(5) means class A with a 5% confidence interval for the individual WIM measurements. The confidence interval depends on the accuracy class, the type of measurement (eg single axle, group of axles, etc) and the number of runs in the data set. See (COST 323, 1997b) for details. These classifications are used to analyse the experimental data described below.

5.1.2 Calibration Methods

Careful calibration is critical for WIM accuracy. There are two main calibration methods for WIM arrays (see discussion in (Cebon, 1999)). Both involve driving one or more calibration vehicles over the site and comparing the sensor outputs W_{d_i} with reference loads W_{s_i}. The reference

loads may be either: (i) *static* loads (measured on a static weigh-scale) of various axles; or (ii) *dynamic* tyre forces measured by an instrumented axle (Cebon, 1999). In this latter case, care must be taken to synchronise the measurements taken on-board the instrumented vehicle with the data collected on the WIM array.

The calibration coefficient C, is defined by

$$W_d' = C.W_d \tag{55}$$

where W_d' is the calibrated weight and W_d the uncalibrated measured weight. The Calibration coefficient may be derived by various formulae given in (COST 323, 1997b), depending on the method of calibration. The method used here consisted of minimising the mean square error between the sensor measurement and the reference loads, using a linear regression through the origin. Calibration factor C was calculated from:

$$C = \frac{\sum_i n_i W_{s_i}^2}{\sum_{i,k} W_{s_i} W_{d_{ik}}} \tag{56}$$

where n_i is the total number of runs of the i^{th} test vehicle, and k is the run number. The details of the calibration method for each set of tests are provided below.

5.2 The MS-WIM Array at Trappes (FR)

5.2.1 Description

An MS-WIM array (see figure 23) was installed on the slow lane of the national road RN10 near Trappes in May 1994 for the OECD/DIVINE project (Jacob, 1995). The test site was chosen because its pavement and traffic conditions are representative of European highways. The mean traffic speed of the vehicles passing on the RN10 is 80 km/h.

The pavement and road conditions fulfil the requirement of a class II (good) WIM site, according to the COST 323 specification (COST 323, 1997b). The international roughness index (IRI) value was 1.71, and the APL (Analyseur de Profil en Long) ratings were 7, 7 and 6 in the long, medium and short wavelength ranges. The characteristic surface deflection was less than 0.15 mm and the maximum rut depth was 6 mm.

The array consisted of 24 piezo-ceramic strip sensors (‘bars’), each 3.20 m in length, and 7 magnetic loops. The bars were placed at non uniform spacings: 7 sensors 0.375 m apart; 4 sensors 1.125 m apart and 13 sensors 2.25 m apart. The total length of the array was 36 m. Three WIM processing boxes SAFT2000 (manufactured by the company LEEM) were connected to the sensors.

Fig. 23 General view of the Trappes MS-WIM array and the RN10 site

5.2.2 Calibration

Pre-Weighed Vehicles

A pre-calibration was carried out immediately after the sensor installation using two pre-weighed lorries. This was done to establish initial calibration factors for each sensor.

The vehicles were:

(i) a 2 axle rigid lorry Deflectometer (trademark Berliet), denoted T2, with static axle loads of 60 and 130 kN;

(ii) a 5 axle articulated lorry with a 2 axle tractor and a semi-trailer with a triaxle axle (trademark Scania), denoted T2R3.

Each pre-weighed vehicle made 12 passes at three speeds (40, 60, 80 km/h).

Instrumented Vehicles

A full calibration was also performed with a Canadian instrumented truck provided by the National Research Council of Canada (CNRC). The response of each sensor was recorded simultaneously with the dynamic tyre forces, which were logged by on-board instrumentation. This established the a more accurate set of calibration coefficients C_{ij} for sensor j and run i.

In November 1995, a further calibration was performed with an instrumented trailer provided by IKH (Hannover).

This was done in order to update the initial calibration factors, measured with the instrumented CNRC truck, so as to remove any possible drift with time. A re-calibration with the two test lorries (T2 and T2R3) was carried out in June 1996, and the calibration coefficients C_{2j} derived were compared to the same coefficients C_{1j} derived from the pre-calibration of May 1994. The final calibration coefficients were obtained by:

$$C_{fj} = C_{ij} \, . \, C_{2j} / C_{1j}. \qquad (57)$$

5.2.3 Test Program

The test program was designed according to the COST323 WIM specifications (COST323, 1997b).

Both of the test vehicles performed approximately 10 runs at three speed levels (50, 65 and 80 km/h), at one load for T2 and three different loads (empty, half-loaded and full) for T2R3. If all these runs are considered together, the test can be described as 'limited reproducibility' conditions (R1), according to the European specification COST 323 (COST323, 1997b).

Approximately 100 lorries, representative of the whole traffic flow, were stopped on a weighing area 5 km upstream to the test site, and weighed statically on an approved enforcement scale. Each of these lorries passed the MS-WIM system at normal traffic speed. This sample provided results in 'full reproducibility' conditions (R2) (COST323, 1997b). Moreover, this trial was carried out in 'environmental repeatability' conditions, because of the short test duration and the constant climatic conditions.

By the end of the project, the number vehicles logged on the Trappes MS WIM was as follow:

- 15805 lorries from the traffic, among them 4508 as part of the WAVE project
- 368 pre-weighted vehicles, among them 100 as part of the WAVE project
- 722 runs of test vehicles, among them 90 as part of the WAVE project

5.2.4 Results

On the Trappes MS-WIM site a major part of the experiment was concerned the analysis of the accuracy of the individual sensors and the accuracy obtained with several combinations of sub-arrays.

After the final calibration, the statistics of the relative errors for the gross weights were computed with the sample of pre-weighed lorries taken from the traffic flow, for each of the 16 uniformly spaced (2.25 m) sensors. The accuracy assessment was done following the procedure described in Section 5.1.1 (COST 323, 1997b). The results are summarised in Table 3. Sensors N°18, 21 and 23 showed a slightly higher standard deviation than the others while the N°22 had a larger bias. Therefore these four sensors are the least accurate in the WIM array, and are all in accuracy class D+(20). The remaining sensors are in classes C(15) or B(10), but two in class D+(20).

Sensor N°	Mean (%)	St. dev (%)	n	δ	δ_{min}	Accuracy class
1	-2.27	6.09	86	15.0	13.0	C(15)
7	0.14	7.19	86	15.0	14.5	C(15)
9	0.24	6.32	87	15.0	12.8	C(15)
11	-0.60	3.79	86	10.0	7.8	B(10)
12	0.91	4.88	87	10.0	10.0	B(10)
13	-1.09	7.47	85	20.0	15.3	D+(20)
14	-1.29	7.35	86	15.0	15.1	C(15)/D+(20)
15	-2.80	7.10	86	20	15.3	D+(20)
16	-0.26	4.99	85	10.0	10.1	B(10)/C(10)
17	-0.36	5.71	86	15.0	11.6	C(15)
18	-1.01	8.01	85	20.0	16.3	D+(20)
19	1.76	6.15	51	15.0	12.9	C(15)
20	1.58	4.81	86	10.0	10.2	B(10/C(10)
21	1.86	8.23	86	20.0	17.0	D+(20)
22	3.32	7.20	86	20.0	15.8	D+(20)
23	-1.10	8.07	83	20.0	16.4	D+(20)

Table 3 Statistics of the relative errors (gross weight) and accuracy classes of each sensor

Definition of the sub-arrays

The static axle load estimated by a WIM system is based on a set of sampled values of the dynamic tyre forces applied to the road surface by a vehicle. The following points should be considered in deciding the best spacing of sampling points (sensors) for MS–WIM (see Jacob and Dolcemascolo, 1997):

(i) some 'spatial repeatability' affects the impact forces at any location along the pavement, which results in up to 15 to 20% of the observed difference between the static load and the dynamic forces at any point along the pavement;

(ii) periodic variations in the axle (wheel) impact forces result from the dynamic motions of the vehicles induced by pavement roughness and also from wheel imbalance.

The criteria for a good estimator of the static loads are that it should minimise the bias and variance of the estimated loads. A reasonable estimator is the Sample Mean, provided the dynamic tyre forces are measured over a sufficiently long sensor array. According to the two points noted above, the sensors should be placed at a *uniform spacing* to avoid any bias due to spatial repeatability; and the length of the array should be longer than the longest wavelength generated by vehicle motion. Therefore, only the uniformly spaced sensors at 2.25 m were considered: N°1, 7, 9, and 11 to 23 (16 sensors in total).

In order to investigate the influence of the sensor number and spacing on the accuracy, 14 sub-arrays (MSA) were considered. These are listed in Table 4:

(i) the longest MSA1 contained all the 16 above mentioned sensors, at 2.25 m spacings;

(ii) the second array MSA2 contained 13 sensors after removal of the last three (N° 21 to 23) which were found to be of lower accuracy;

(iii) MSA3a-d were arrays with 7 sensors at 2.25 m uniform spacing, placed at the beginning, in the middle and at the end of the arrays MSA1 and MSA2;

(iv) MSA4a-c were arrays with 5 sensors at 2.25 m uniform spacing, placed at the beginning, in the middle and at the end of the array MSA2;

(v) MSA5 was the longest array, with 8 sensors spaced at 4.5 m;

(vi) MSA6 consisted of 7 sensors spaced at 4.5 m, derived from the MSA5 by elimination of the sensor N°22;

(vii) MSA7a-c had 5 sensors at 4.5 m uniform spacing, placed at the beginning, in the middle and at the end of the array MSA5.

The theoretical 'design' spacings Δ_{d1} from equation 19 are also shown (in parentheses) in the third column of Table 4. The minimum spacing of 2.25 m in this array is somewhat different to the design spacing given by equation 19, which for $\bar{f}$ = 1.8 Hz (air suspension), $\overline{V}$ = 22.2 m/s (80 km/h), and N=16 is Δ_{d1} = 1.45 m. However, the MS-array on RN10 was initially designed for investigating 'spatial repeatability' as part of the OECD/DIVINE project (Jacob, 1995; Jacob and Dolcemascolo, 1997). This explains why some other spacings were chosen.

For each sub-array, the individual static axle loads were estimated using the sample mean of the measurements on the sensors considered, while the 'group of axle loads' and 'gross weights' were obtained by the appropriately summing these axle loads.

Accuracy of the sub-arrays

The accuracy verification was made for each sub-array using 84 pre-weighed lorries sampled from the traffic flow, which passed on the MS-WIM system. (Some of the 100 pre-weighed lorries by-passed the system, by travelling on the fast lane, or left the RN10 before the WIM site.) Using independent samples for the calibration and accuracy check, allows an in-service verification.

The results of the accuracy check, including statistics of the relative errors, are given in Table 5 for estimation of the *gross weight*. The tolerance δ of the accepted accuracy class and the value of δ_{min} such as the level of confidence of the interval $[-\delta_{min}, \delta_{min}]$ exactly meets the specified value π_0 of the European specification (COST 323, 1997b) are also given. Table 6 contains only the accepted accuracy class and the value of $\delta_{\min}$, for five different criteria (gross vehicle weight, axle group, single axle, axle of group, and all of these taken together).

The main findings are:

(i) The differences between the various sub-arrays are relatively small. For the *gross weights* (Table 5), the δ_{min} values are all between 6.6% and 7.7%, except for one at 8.7%. For the other criteria (Table 4), the differences between the smallest and largest δ_{min} do not exceed 2% for the *axle group* and *single axle*, and mostly 3% for the *axle of group*. (MSA4b, which is of lower accuracy is an exception.)

Sub-array	N_b sensors	Spacing (m)[1]	Array Length (m)	Sensors considered (N°)	Location (m)
MSA1	16	2.25 (1.45)	33.75	1, 7, 9, 11 to 23	0 - 33.75
MSA2	13	2.25 (1.75)	27	1, 7, 9, 11 to 20	0 - 27
MSA3a	7	2.25 (3.0)	13.5	1, 7, 9, 11 to 14	0 - 13.5
MSA3b	7	2.25 (3.0)	13.5	12 to 18	9 - 22.5
MSA3c	7	2.25 (3.0)	13.5	14 to 20	13.5 - 27
MSA3d	7	2.25 (3.0)	13.5	17 to 23	20.25 - 33.75
MSA4a	5	2.25 (3.95)	9	1, 7, 9, 11, 12	0 - 9
MSA4b	5	2.25 (3.95)	9	12 to 16	9 - 18
MSA4c	5	2.25 (3.95)	9	16 to 20	18 - 27
MSA5	8	4.50 (2.7)	31.5	1,9,12,14,16,18,20,22	0 - 31.5
MSA6	7	4.50 (3.0)	27	1, 9, 12, 14, 16, 18, 20	0 - 27
MSA7a	5	4.50 (3.95)	18	1, 9, 12, 14, 16	0 - 18
MSA7b	5	4.50 (3.95)	18	9, 12, 14, 16, 18	4.5 - 22.5
MSA7c	5	4.50 (3.95)	18	14, 16, 18, 20, 22	13.5 - 31.5

Note 1 The first figure is the spacing used in the experiment, the second in parenthesis ( ) is theoretical 'design' spacing Δ_{d1} from equation (19).

Table 4 Definition of the sub-arrays of sensors investigated on the RN10 site.

(ii) The length of the sub-array is of great importance for the gross weight accuracy. The longest arrays (over 27 m) are the most accurate, in class B+(7). This length must exceed, as far as possible, the longest wavelength of the dynamic tyre force signal, in order that the averaging procedure smoothes the bias resulting from the spatial repeatability for individual vehicles.

(iii) The effect of the longitudinal location of the sub-array is low. This means that the influence of 'statistical spatial repeatability' (Jacob and Dolcemascolo, 1997) is not significant for a well calibrated MS-WIM system.

(iv) Almost all the sub-systems meet the requirements of accuracy class B(10) for the four criteria, while MSA2 is in class B+(7) for three criteria. A few more sub-systems (MSA1, MSA4c, MSA5 and MSA6) are in class B+(7) for two criteria. MSA4b is the less accurate, class C(15), since it contains 3 low accuracy sensors (sensor class D+(20)) out of 5. Therefore, on such a class II site, it appears that with 5 to 7 sensors individually in class C(15), on average, a MS-WIM system in class B(10) can be achieved. With 13 sensors, class B+(7) can almost be achieved.

(v) The best compromise between the number of sensors (cost) and accuracy seems to be for sub-array MSA4c, which has 5 sensors at 2.25 m spacing. However the sensor spacing is less than the theoretical value of Δ_{d1} computed by equation (19) which is about 4 m. It should be noticed that robustness is not ensured with such a small number of sensors and short spacing: for all the 5-sensor arrays with a spacing of 2.25 m, the mean and standard deviation of δ_{min} are respectively 7.43 and 1.25, with values between 6.7 and 8.7. Such arrays are too short (9 m) compared to the wavelength of the impact force signal, which exceeds 12 m.

For the set of sub-arrays (MSA7a to MSA7c), the spacing is 4.5 m while the theoretical spacing is about 4 m; in this case the values of δ_{min} were less scattered (with mean and standard deviation of 7.46 and 0.2, and values between 7.3 and 7.7). Thus the recommended compromise would be either 5 sensors at 4 m (close to MS7a-c) or 7 sensors at 3 m; the design of these both sub-arrays is consistent, with instrumented lengths of 20 - 21m.

(vi) The performance of the averaging method is limited by the individual performance of each sensor. Instead of increasing the number of sensors, it would likely be better to improve their performances, by a better calibration or improving the signal processing methods.

Sub-array	N_b sensors	Length (m)	m (%)	σ (%)	n	δ (%)	δ_{min} (%)	Class
MSA1	16	33.75	0.22	3.26	84	7	6.6	B+(7)
MSA2	13	27	-0.19	3.27	84	7	6.6	B+(7)
MSA3a	7	13.5	-0.18	3.61	84	10	7.3	B(10)
MSA3b	7	13.5	-0.51	3.77	84	10	7.7	B(10)
MSA3c	7	13.5	-0.29	3.55	83	7	7.2	B(10)
MSA3d	7	13.5	1.13	3.47	83	10	7.3	B(10)
MSA4a	5	9	0.10	3.66	84	10	7.4	B(10)
MSA4b	5	9	-0.63	4.29	84	10	8.7	B(10)
MSA4c	5	9	0.35	3.06	83	7	6.2	B+(7)
MSA5	8	31.5	0.54	3.31	84	7	6.8	B+(7)
MSA6	7	27	0.07	3.50	84	7	7.1	B+(7)/B(10)
MSA7a	5	18	-0.16	3.64	84	10	7.4	B(10)
MSA7b	5	18	0.09	3.81	84	10	7.7	B(10)
MSA7c	5	18	0.83	3.51	83	10	7.3	B(10)

Table 5 Statistics of the relative errors and accuracy of the sub-arrays for measurements of *Gross Vehicle Weight*

Sub-array	Gross weight	Axle group	Single axle	Axle of group	All criteria
MSA1	6.6 - B+(7)	11.6 - B(10)	10.0 - B+(7)	14.5 - B(10)	B(10)
MSA2	6.6 - B+(7)	10.9 - B(10)	10.0 - B+(7)	13.6 - B+(7)	B+(7)/B(10)
MSA3a	7.3 - B(10)	12.1 - B(10)	10.7 - B+(7)	14.6 - B(10)	B(10)
MSA3b	7.7 - B(10)	12.6 - B(10)	11.3 - B(10)	15.0 - B(10)	B(10)
MSA3c	7.2 - B(10)	11.9 - B(10)	11.0 - B+(7)	15.1 - B(10)	B(10)
MSA3d	7.3 - B(10)	13.7 - C(15)	10.9 - B+(7)	17.4 - B(10)	B(10)/C(15)
MSA4a	7.4 - B(10)	11.7 - B(10)	11.1 - B+(7)/B(10)	14.3 - B(10)	B(10)
MSA4b	8.7 - B(10)	14.9 - C(15)	11.6 - B(10)	17.4 - B(10)	C(15)
MSA4c	6.2 - B+(7)	10.6 - B(10)	11.1 - B+(7)/B(10)	14.6 - B(10)	B(10)
MSA5	6.8 - B+(7)	11.5 - B(10)	10.8 - B+(7)	14.6 - B(10)	B(10)
MSA6	7.1 - B+(7)/B(10)	11.6 - B(10)	11.0 - B+(7)	14.5 - B(10)	B(10)
MSA7a	7.4 - B(10)	12.1 - B(10)	11.1 - B+(7)/B(10)	15.0 - B(10)	B(10)
MSA7b	7.7 - B(10)	12.6 - B(10)	11.5 - B(10)	15.7 - B(10)	B(10)
MSA7c	7.3 - B(10)	12.7 - B(10)	11.8 - B(10)	16.6 - B(10)	B(10)

Table 6 Accuracy of each sub-array for all criteria, assessed by δ_{min} and the COST323 classes.

5.3 The MS-WIM Array at Metz - Obrion (FR)

5.3.1 Characteristics of the Site

The test site at Obrion is situated on the motorway A31, in the south-bound direction (Luxembourg-Nancy), on the slow lane (see figure 24). The general features of the site are:

(i) Heavily trafficked carriageway with 2 x 2 lanes, and 40 000 vehicles/day, of which 20% are heavy vehicles.

(ii) The site is situated 30 km from the CETE de l'Est (Metz) and 20 km from Nancy, on a straight section (2km) of the road; entrances and exits from the motorway allow for test vehicles to loop around the site every 10 minutes.

(iii) A lay-by which is located 7 km before the site (Lesmenils site) permits measurement of the static weights of vehicles sampled from the traffic.

(iv) A temporary shelter is installed on an embanked area to house and protect the systems (it is connected to telephone and electrical networks).

(v) The pavement is a mixed structure including 20 cm of bounded gravel with slag 0/31 (1972), 20 cm of bounded gravel with slag 0/20 (1972), 10 cm of bituminous concrete (1972), 7 cm of bituminous concrete 0/14 (1979) and finally 4 cm of bituminous concrete 0/14 (1987).

(vi) the site is classified as a class I (excellent site) in the European specification for weigh-in-motion (COST 323, 1997b). The characteristic deflection was measured with a 130kN axle. See Table 7 for details.

(vii) The WIM system consists of 18 piezoceramic strip sensors (only 16 are connected) spaced by 1.6m, linked to a Hestia data logger supplied by ECM company.

Fig. 24 General view of the MS-WIM test site at Metz (Obrion)

Criterion	Radius of curve (m)	Longl. slope	Transv. slope	Rut depth	Deflection (10^{-2} mm)	Surface Roughness APL(SW-MW-LW)/IRI
Obrion site	> 1000	< 1%	3%	4 mm	5	9-9-10 / 0.79
Tol. class I	> 1000	< 2%	< 3%	≤ 4 mm	< 15	≥ 9 / < 1.3

Table 7 Characteristics of the pavement of the Obrion site (A31) in 1996, compared with the specification for a Class I site from (COST 323, 1997b).

5.3.2 Calibration

On the A31 MS-WIM test site, calibration measurements were carried out during June 1998 with an instrumented lorry provided by the VTT. This truck was a 3 axle rigid lorry with tandem drive axles. It was instrumented to measure the dynamic tyre forces generated by some of the axles. Analysis of the dynamic tyre force measurements was performed by LROP and VTT. LROP was responsible for spectral analysis; calculation of the calibration coefficient of each piezo sensor; and investigation of spatial repeatability. VTT analysed the statistics of the dynamic tyre forces (as a function of load, speed, bump, etc).

The calibration of each sensor of the MS WIM array is described in the WP2.1 report.

5.3.3 Test program

The experiments with the instrumented vehicle took place on 9–12 June 1998.

The vehicle made 42 passes over the site at 3 speeds and 3 loads. Because the surface profile of the site was very smooth, an artificial bump was also installed on the pavement and 12 passes were done with this bump.

The load configurations are shown in Table 8 and the number of passes by configuration of load/speed is given in Table 9

	Axle 1(kN)	Axle 2 (kN)	Axle 3 (kN)	GW (kN)
Fully loaded	58.8	86.2	72.2	217.2

Half loaded	57.8	60.3	48.8	166.9
Empty	51.2	35.8	25.5	112.5

Table 8 Load configurations of the VTT truck used to calibrate the MS WIM array

Date	Load / Speed[1]
9-06-1998	Half loaded with bump / 4 – 4 – 2 - 0
10-06-1998	Half loaded/ 0 – 5 – 0 – 5 ; Empty/ 0 – 5 – 0 – 5
11-06-1998	Full/ 0 – 6 – 0 – 5; Full with bump/ 4 – 5 – 4 – 0
12-06-1998	Fully loaded/ 0 – 4 – 0 – 4

Table 9 Test runs performed with the instrumented VTT truck.
[1] The passes were at 40, 60, 70 and 90 km/h.

The deflectograph vehicle (T2) described in Section 5.2.2 also made 12 passes over the MSWIM array on 8 June 1998 and at various times over the following year.

Pre-Weighed Vehicles

A number of pre-weighed vehicles, selected from the traffic flow, were also measured on the site. However the calculations shown in this report used only data from passes of the VTT truck. This data was used for the calibration of each sensor of the Multi sensor WIM array and for the investigation of the performance of the MS–WIM algorithms.

By the end of the project, the number of vehicles recorded on the Metz (Obrion) MS WIM was as follow:

(i) 243 pre-weighed vehicles;

(ii) 93 runs of test vehicles (VTT truck and deflectograph vehicle T2).

5.3.4 Design of the MS WIM Array

Sixteen sensors were used on the site because previous research (Jacob and Dolcemascolo, 1998) showed that it is possible to reach an accuracy of 1% of the static weight with an MS WIM array consisting of 13 or 15 sensors. (Two of the sensors in the initial installation were not used.)

The mean traffic speed on the site was 25 m/s (90 km/h). The mean bounce motion frequency of vehicles was estimated to be f = 1.8 Hz, because of the predominance of air suspensions. The sensor spacing was selected using equation 19 and was Δ_{d1} = 1.6m.

5.3.5 Performance of Each Sensor

Each sensor was calibrated using dynamic tyre forces measured with the VTT truck (see WP2.1), and then its performance was evaluated using the same data. The results are shown in Table 10.

Sensor N°	Mean (%)	St. dev (%)	n	δ	δ_{min}	Accuracy class
-1	1.72	8.04	31	25	20	D(25)
0	-1.77	6.84	31	20	17.2	D+(20)

1	-3.49	7.64	31	25	20.1	D(25)
2	3.26	9.42	31	25	24.1	D(25)
3	5.09	8.26	31	25	22.8	D(25)
4	0.97	6.18	31	20	15.3	D+(20)
5	-1.96	4.10	31	15	10.8	C(15)
6	-1.87	5.42	31	15	13.8	C(15)
7	-4.50	13.05	31	35	33.3	E(35)
8	1.82	8.59	31	25	21.4	D(25)
9	1.54	5.74	31	15	14.4	C(15)
10	-2.87	9.24	31	25	23.4	D(25)
11	5.47	10.2	31	30	27.4	E(30)
12	7.47	12.1	31	35	33.3	E(35)
15	-6.14	8.78	31	25	24.8	D(25)
16	5.49	9.71	31	30	26.3	E(30)

Table 10 Statistics of the relative errors (gross weight) and accuracy classes of each sensor.

However, after a couple of months of measurements, the individual accuracy of the sensors (shown in Table 10) (between C(15) and E(35)) was not in accordance with the expected performance of sensors installed on a Class I site. Some experiment were performed, to investigate the errors: the electronic WIM stations were tested and also the pavement deflection was measured; then a few sensors were replaced; no explanation were found after these investigations. Some further analyses were performed at the end of the project, with the participation of the manufacturer (ECM). Finally it was proved that the errors resulted from a combination of two causes:

- the lorries on this heavily trafficked motorway were travelling close to the right emergency lane, i.e. close to the right margin of the slow traffic lane, because of the high vehicle density on the left passing lane;
- the WIM bars were either too short or centred in the traffic lane, and thus a significant proportion of the right wheels were passing outside or partially outside them.

That resulted in some large errors in the WIM measurements of some vehicles, which induced a wrong self-calibration of the whole WIM system. The manufacturer (ECM) was finally asked to replace all the initial sensors, in order to account for the site traffic conditions.

Definition of the sub arrays

Table 11 defines the sub arrays that were used for the comparison of the Sample Mean and Signal Reconstruction algorithms. The following factors were considered when defining the sub arrays:

(i) Sensor 7 was observed to have a large bias and error standard deviation. This sensor was not used in any of the sub arrays.

(ii) Each sub array was chosen to be as long as possible.

(iii) The signal reconstruction method required all the sub arrays to have an odd number of sensors.

(iv) Three sub arrays were chosen with 3, 5 and 7 uniformly spaced sensors to enable comparison of their performance using the Sample Mean and the Signal Reconstruction algorithms.

(v) It was not possible to design sub arrays with 9, 11 and 13 sensors with uniform spacing so for these sub array the spacings were not constant.

Sub-array	N_b sensors	Spacing (m)[1]	Length (m)	Sensors considered (N°)	Location (m)
MSSR1	13	NU (2.0)	20.8	-1 to 6 and 8 to 12	0 - 20.8
MSSR2	11	NU (2.1)	17.6	-1 to 6 and 8 to 10	0 – 17.6
MSSR3	9	NU (2.7)	14.4	2 to 6 and 8 to 11	4.8 – 19.2
MSSR4	7	1.60 (3.4)	9.60	-1 to 5	0 – 9.6
MSSR5	5	4.80 (4.4)	19.2	-1, 2, 5, 8 and 11	0 – 19.2
MSSR6	3	4.80 (6.1)	9.60	-1, 2, 5	9.6

Table 11 Definition of the studied sub-arrays – Metz (Obrion) site
1: Note: NU = Non Uniform; number in parenthesis ( ) is the theoretical spacing Δ_{d1} from equation (19).

Performance of the Sample Mean method

The performance of the Sample Mean method is shown in Tables 11 and 12. The results were generally disappointing. No sub-array achieved better than Class C(15) for any of the criteria. This can be attributed to:

(i) The low accuracy of the individual sensor measurements listed in Table 10.

(ii) The fact that the spacings of the sensors in the sub arrays were mostly significantly different to the theoretical design values Δ_{d1}, calculated using equation 19 (shown in parentheses in the third column of Table 11). The exceptions were the arrays with 3 and 5 sensors (MSSR5 and MSSR6), however these arrays are expected to be the least accurate.

Sub-array	N_b sensors	Length (m)	m (%)	σ (%)	n	δ (%)	δ_{min} (%)	Class
MSSR1	13	20.8	1.18	5.17	31	15	12.9	C(15)
MSSR2	11	17.6	0.22	4.53	31	15	11.1	C(15)
MSSR3	9	14.4	1.27	5.09	31	15	12.8	C(15)
MSSR4	7	9.60	0.54	5.11	31	15	12.6	C(15)
MSSR5	5	19.2	2.06	5.92	31	20	15.1	D+(20)
MSSR6	3	9.60	1.01	5.33	31	15	13.2	C(15)

Table 12 Statistics of the relative errors for gross weight, and accuracy of the sub-arrays using the Sample Mean – Metz (Obrion) site. (Sub-arrays defined in Table 11.)

Sub-array	Gross weight	Axle group	Single axle	Axle of group	All criteria
MSSR1	12.9 –C(15)	16.5 – C(15)	17.1 – C(15)	33.9 - D(25)	D(25)
MSSR2	11.1 – C(15)	14.3 – C(15)	17.2 – C(15)	31.0 - D(25)	D(25)
MSSR3	12.8 – C(15)	16.9 – C(15)	19.5 – C(15)	34.5 – D(25)	D(25)
MSSR4	12.6 – C(15)	17.2 – C(15)	18.7 – C(15)	32.2 – D(25)	D(25)
MSSR5	15.1 – D+(20)	20.1 – D+(20)	19.2 – C(15)	38.9 – E(30)	E(30)
MSSR6	13.2 – C(15)	18.0 – C(15)	20.7 – D+(20)	36.0 – E(30)	E(30)

Table 13 Accuracy of each sub-array for all criteria using the Sample Mean – Metz (Obrion) site

Because the performance of each sub array with the Sample Mean was not in accordance with that expected on such a site, it was decided *not* to apply any new MS–WIM algorithms on data from the array at Metz (Obrion).

5.4 Data Collected with a Load Measuring Mat (UK)

5.4.1 Description

Data collected previously with a wheel load measuring mat (Cebon and Winkler, 1991a) was re–analysed to investigate the accuracy of the Maximum Likelihood method. The mat incorporated 1.2m long capacitative strip sensors which were encapsulated in stiff polyurethane tiles of dimensions 1.2m x 1.2m x 13mm thick. Each tile had three sensors, laid transverse to the wheel path at a spacing of 0.4 m between sensors. The mat had 32 tiles, (a total of 96 sensors), which were mounted end-to-end on the road surface, to provide an instrumented test section of length 38.4 m along one wheel track. The polyurethane mat tiles were attached to the road with a sheet of double-sided adhesive tape and 12 masonry anchors per tile, screwed into the road surface. Golden River 'Marksman 600' data loggers were connected in a serial data network, from which data was uploaded by a personal computer.

5.4.2 Test Program

The field tests were performed in 1989 on the Navistar test track in Fort Wayne, Indiana, USA. Calibration was performed in various ways, including instrumented axles, and the static axle loads of a slowly-moving air-suspended vehicle (see (Cebon and Winkler, 1991b)).

Six different tractor/semi-trailer vehicles were provided by Navistar for testing on the mat. The vehicles had a variety of suspensions that were selected to be reasonably representative of the US truck fleet. Each vehicle was weighed to measure the static load of each axle. Each vehicle was driven over the mat at nominal speeds of 8, 16, 32, 48, 64 and 80 km/h in both directions around the track. Six repetitions were performed for most test conditions, giving a total of 460 test runs during four days of testing.

Detailed information concerning the performance of the sensors can be found in (Cebon and Winkler, 1991a). The important results are summarised here:

(i) The average coefficient of variation of the sensor calibration factors, measured at three points along the length of each bare sensor, was found to be 3.2%.

(ii) No systematic dependence of sensor calibration with temperature was measurable for mat surface temperatures of 15 to 40°C.

(iii) No systematic dependence of sensor output with vehicle speed could be detected and no evidence was found of fore-aft weight transfer affecting the mean loads for higher speeds.

(iv) The average 'baseline' sensor error for measured instantaneous loads (which is the fundamental limit on the accuracy of WIM measurements) was found to be less than 4% RMS. This can be attributed to noise and small calibration errors.

5.4.3 Analysis Method

The data recorded for the six articulated vehicles were processed to determine the static weight measurement error as a function of the WIM array design parameters (N and Δ), for each axle of each vehicle at the six nominal testing speeds. Due to space limitations, results for one axle of one vehicle, and one test condition only are presented here (axle 5 of vehicle 'S4', tested at 24 m/s (85km/h) - see (Cebon and Winkler, 1991a)[1]). The results for the other axles and vehicles were found to be qualitatively similar.

The WIM sensor data for each vehicle run was analysed to generate as many different static load estimates as possible. The method is shown in figure 25, where sensors in one wheel path are used to perform several three-sensor SM calculations, each with sensor spacings of Δ = 1.6m. The results for every possible array design configuration on each vehicle test pass were averaged together to smooth-out statistical variations - (for example, it is possible to calculated 190 different 2-sensor averages with Δ = 0.4m, from one axle pass of an axle over the 96-sensor mat)[2].

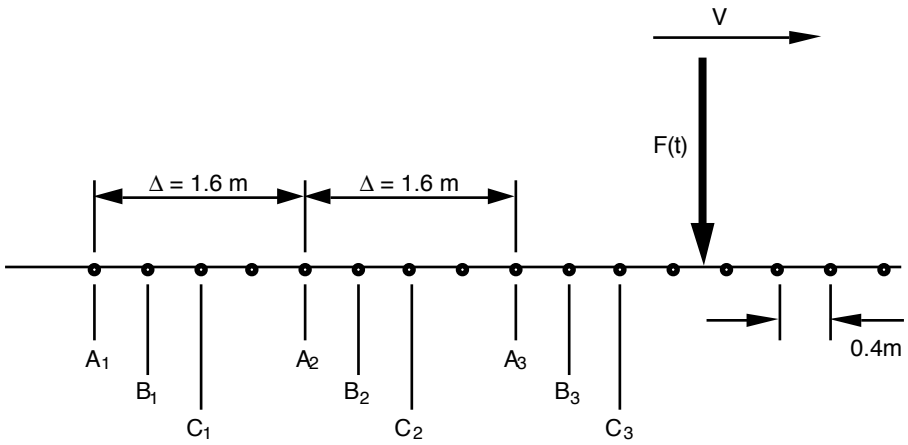

$$\overline{F}_A = \frac{f_{A_1} + f_{A_2} + f_{A_3}}{3} = \frac{1}{n}\sum_{k=1}^{n} f_{A_k}, \quad \overline{F}_B = \frac{1}{n}\sum_{k=1}^{n} f_{B_k}, \quad \overline{F}_C = \frac{1}{n}\sum_{k=1}^{n} f_{C_k}$$

Fig. 25 Scheme for generating multiple-sensor sub-arrays.

5.4.4 Results

Two graphs of RMS Error vs Δ are provided in figure 26. Figure 26a shows the results for the Sample Mean (SM) calculation, while figure 26b shows the results for a Maximum Likelihood fit with one-tone ('ML1'). The error of 11.5% at zero spacing on both graphs is the RMS dynamic tyre force normalised by the static load (otherwise known as the Dynamic Load Coefficient - DLC (Sweatman, 1983)). This would be the RMS error due to dynamic tyre forces that would be

---

[1] This vehicle had a 6x4 tractor and 2-axle trailer, with tandem leaf spring suspensions on both the tractor drive and trailer axles.

[2] Note that for the purposes of assessing the performance of the arrays using the COST 323 criteria (COST323, 1997c), the number of data points was taken to be the number of vehicle passes (mostly 12 per vehicle/speed condition), *not* the total number of sensor combinations, since multiple WIM estimates calculated from various combinations of the same set of sensor measurement for a vehicle run are not independent. This approach gives a 'pessimistic' (upper bound) view of the system accuracy.

observed on a single-sensor WIM system (see (Cebon and Winkler, 1991a)). A single-sensor system would therefore achieve accuracy Class E.

The general shape of the curves in figure 26 follow the theoretical predictions (eg figure 18). For either algorithm (SM or ML1), the MS–WIM systems with 5 or 7 sensors achieve class B(10) for spacings of 2.5 to 5m. Systems with 8 or 9 sensors can reach class B+(7) under some conditions. This corresponds to an RMS measurement error of less than 4%, which compares with an average error of approximately 2.7% in figure 18 (for the noisy sensors).

In general it can be seen that the results for the Sample Mean (SM) (figure 26a) and ML1 algorithm (figure 26b) are similar. In fact, ML1 performs slightly *worse* than SM for many conditions. The main reason is that the baseline sensor noise level, (measured to be 4% - see section 5.4.2), is sufficient to degrade the performance of the ML1 algorithm. (This result was predicted by the simulation study – see figure 18).

Figure 27 shows the results of the SM method and a two-tone Maximum Likelihood fit (ML2), for arrays with 9 to 15 sensors. Again SM is seen to be more accurate than ML2

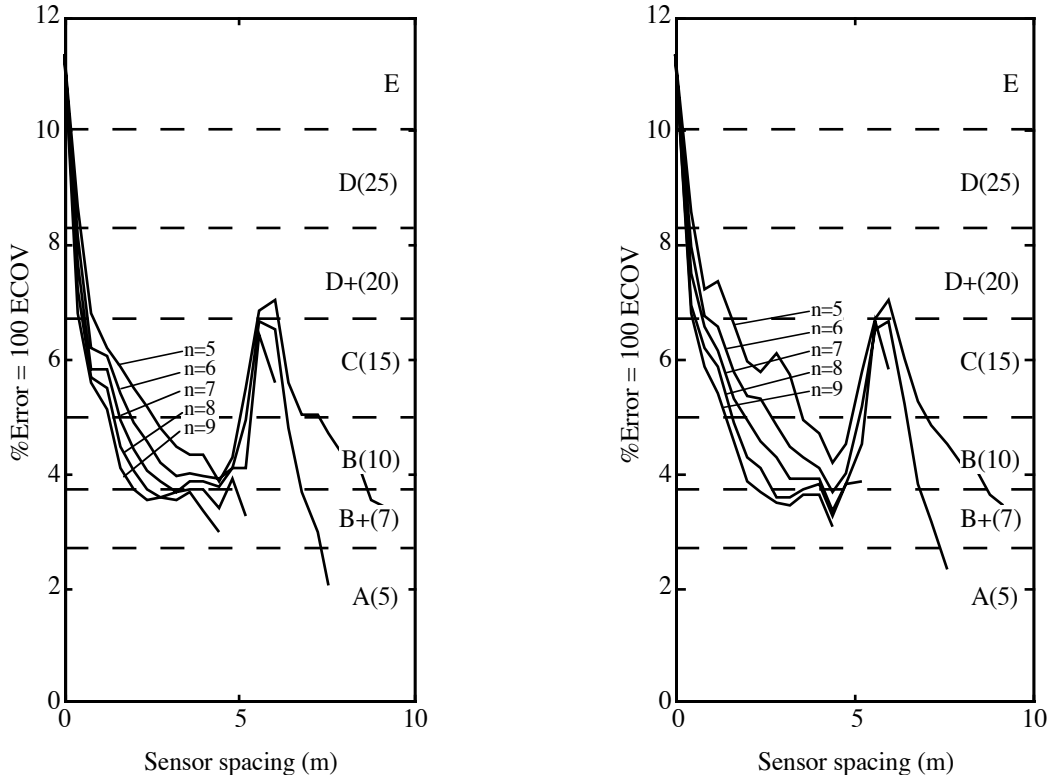

(a) Sample Mean (b) ML1 (one–tone fit)

Fig. 26 Vehicle S4, axle 5, speed 24 m/s.

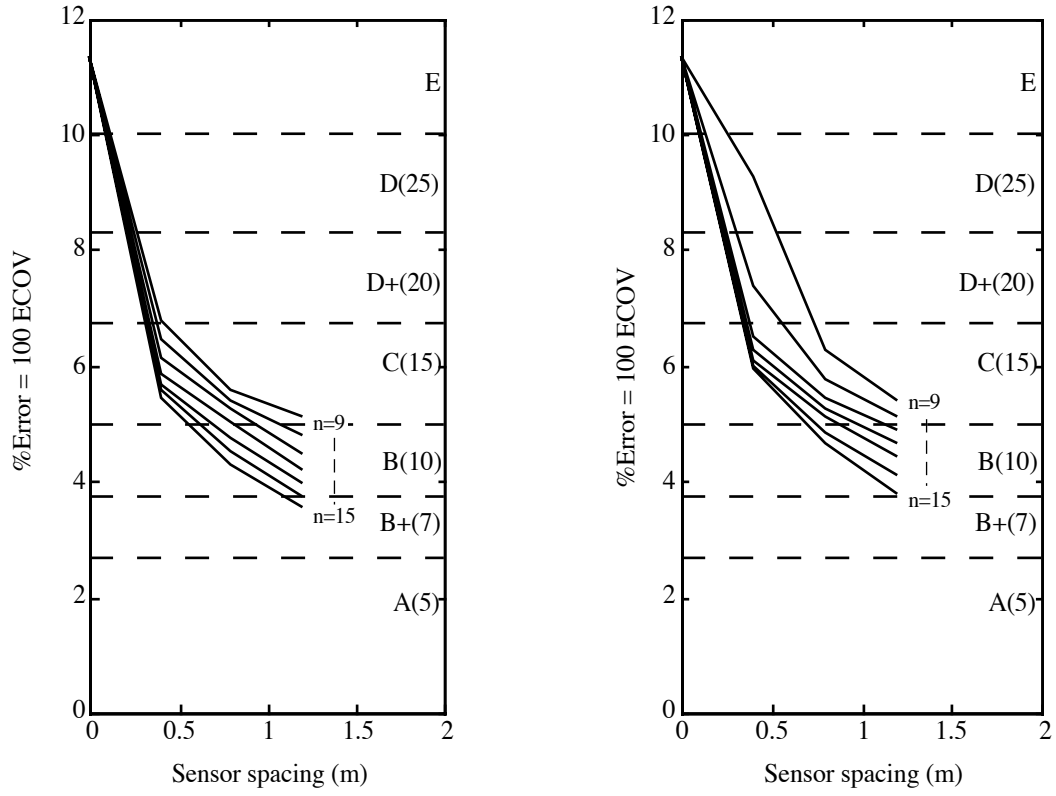

(a) Sample Mean (b) ML2 (two–tone fit)

Fig. 27 Vehicle S4, axle 5, Speed 24 m/s.

No estimates were performed for spacings greater than 1.2 m using the ML2 algorithm. This is because the frequency range over which the algorithm searches is outside that which can be estimated by the ML fitting process without greatly increasing the errors. This effect is shown by the Cramer–Rao bounds in figure 13, which rise rapidly for spacings outside the central 'plateau' region of the graph, because the estimation problem becomes ill–conditioned.

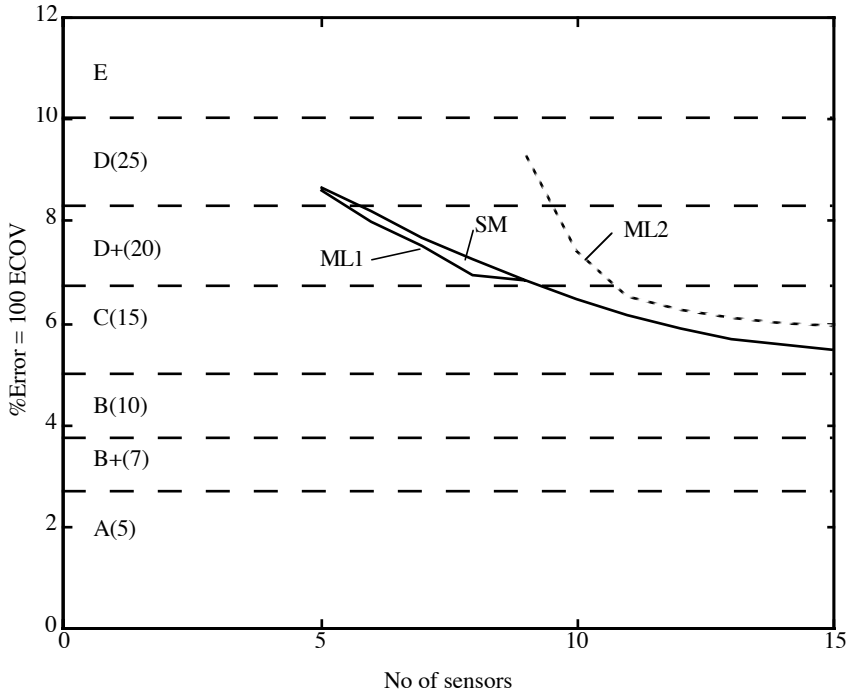

Fig. 28 Vehicle S4 axle 5 Speed 24 m/s. Sensor spacing = 0.4m

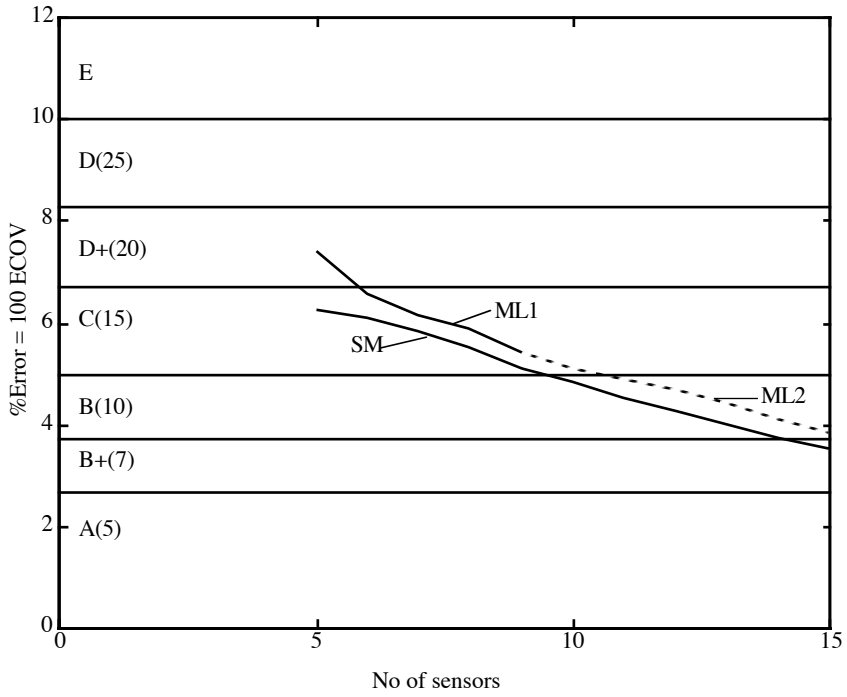

Fig. 29 Vehicle S4 axle 5 Speed 24 m/s. Sensor spacing = 1.2m

Figures 28 and 29 show some of the same data as in figures 26 and 27, this time with the errors plotted as a function of the number of sensors, for the three different processing methods. For $\Delta = 0.4$m (figure 28), ML1 is slightly better than SM (5–9 sensors). Conversely, ML2 is always worse than SM, particularly for 9 or 10 sensors. In these cases the ML algorithm becomes inaccurate (divergence of the Cramer Rao bounds - figure 7). For $\Delta = 1.2$m (figure 28), ML1 and ML2 are similar to, but always worse than SM. The reasons are those described above - primarily sensor noise.

5.5 The MS-WIM Array at Abingdon (UK)

5.5.1 Description

Site

A site on the North-bound carriageway of the A34 trunk road near Abingdon, Oxfordshire, UK, was chosen for the experimental component of WP1.1 performed in the UK. The location was at the downstream end of a 'lay-by' between junctions A4130 and A415. A weigh station, run by the Vehicle Inspectorate, is located at junction A415. The road surface was asphalt, with some evidence of minor wheel–path rutting.

Array Design

The parameters assumed for the experimental array design were as follows:

V = 20m/s (72 km/h); $f_1 = 2.5$ Hz, $f_2 = 12$ Hz; N = 10.

From equation 33, the design spacing was calculated to be 1.1m. Using the method in Section 4.5, it was estimated that with this spacing, it should be possible to measure the axle loads of most vehicles travelling in a speed range of 18m/s to 22m/s (64-80km/h).

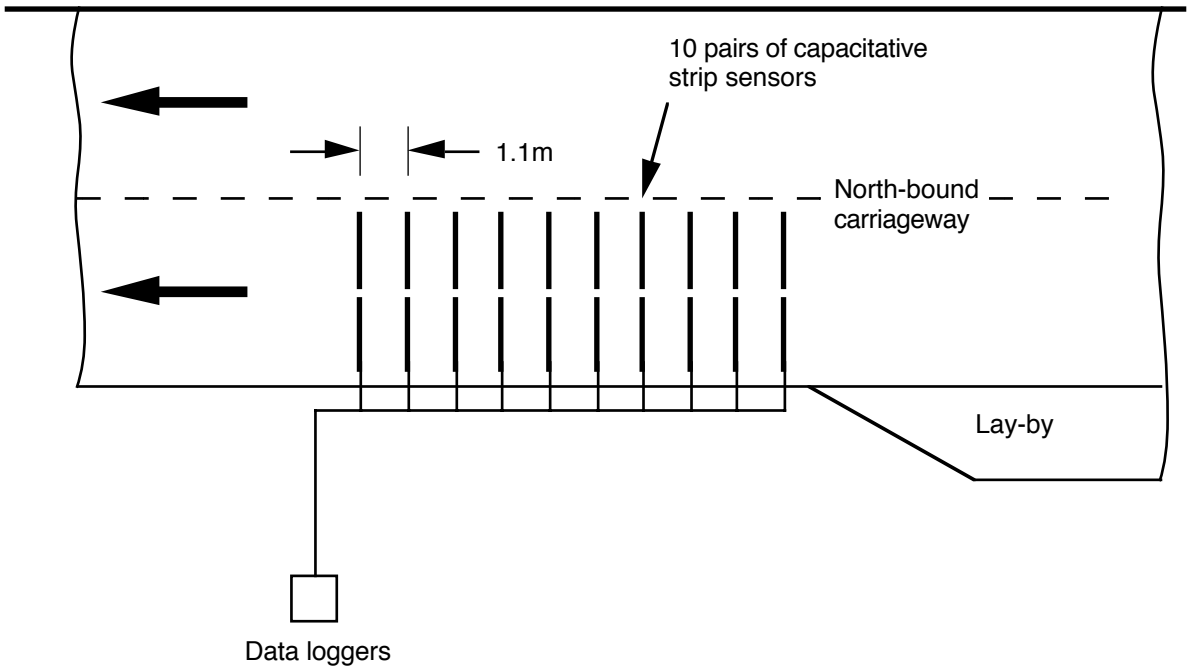

Fig. 30 Schematic layout of the WIM site on the A34 trunk road near Abingdon, Oxfordshire.

The experimental array is shown schematically in figure 30. It contained ten pairs of capacitative strip sensors (Cole and Cebon, 1989), from Golden River Traffic, located in the nearside traffic lane. Each sensor was long enough to span half of the traffic lane. The outputs of the sensors were recorded by two Golden River M660 data loggers.

5.5.2 Installation

Procedure

The sensors were installed by Golden River and their sub–contractors using their proprietary method. All installation was performed at night to minimise disruption to the traffic. The installation involved the following main steps:

(i) Cutting slots in the road surface across the traffic lane;

(ii) Gluing the sensors (contained in aluminium and rubber carriers) into the slots, and filling the cavity around the carriers with potting compound;

(iii) Running the sensor cables through the 'V-grooves' to the side of the road, then via underground ducting to the instrumentation cabinet;

(iv) Grinding the sensor–carrier flush with the road surface ;

Surface Rutting

During the grinding process [(iv) above], it was found that some sections of the traffic lane were more heavily rutted than observed in the initial site survey - with approximately 8 to 10mm deep ruts. This meant that even after the 'grindable' part of the sensor carrier was completely removed (about 6mm), the top of the carrier was proud of the road surface in the wheel path, by up to 2 mm. Approximately half of the sensors suffered from this problem. From previous work this was known to be a significant source of inaccuracy for WIM measurements (Cebon, 1999).

As a consequence it was decided to fill the space between the sensors with a thin layer of adhesive-based resurfacing compound, so as to bring the surface as near as possible to flush with the sensors. A compound known as Colas 'Retrack' was chosen and approved by the Highways Agency. Installation of this compound involved preparing the surface, trowelling–on the adhesive in the spaces between the sensors, covering the adhesive with fine chippings and allowing the

adhesive to cure. This provided a very durable running surface. (See (Stergioulas and Cebon, 1999) for details.)

Unfortunately the problem was not entirely solved, and noticeable surface roughness with a 1.1m wavelength remained on the site after the treatment. This excited the dynamics of passing vehicles, and undoubtedly decreased the accuracy of sensor measurements on the array. The final installation is shown in figure 31.

Fig. 31 Completed MS–WIM installation on the A34.

5.5.3 Calibration

Instrumented Vehicle

Calibration was performed using a 4-axle tractor semi-trailer vehicle, provided by the Transport Research Laboratory (TRL). It had a two axle tractor and tandem trailer. The nominal gross vehicle mass was 32.5 tonnes. The air-suspended tractor drive axle was instrumented with strain gauges and accelerometers to measure the dynamic tyre forces using the method described in (Cebon, 1993). An infra-red transceiver carried by the vehicle reflected its beam off targets at the edge of the road, so that a synchronisation signal could be recorded on the on–board data record when the vehicle passed the targets. The static load of all axles was measured on the Vehicle Inspectorate weigh–bridge prior to the calibration tests.

Procedure

The calibration runs took place during two days in October 1998. One set of calibration runs was performed at a low speed of nominally 8 km/h and a second was performed at a high speed of nominally 80 km/h. In each set, the two dynamic tyre forces generated by the drive axle of the calibration vehicle were recorded by the on–board data logger as the vehicle crossed the sensor array. These forces were compared with the measurements recorded by the WIM sensors in order to perform the calibration.

The object of the low speed runs was to minimise the dynamics of the calibration vehicle, so that the WIM measurements could be compared with the static loads measured on the weigh–bridge. The high speed runs were performed at a representative highway speed. In these tests it was considered to be essential to use measured dynamic tyre forces in the calibration.

Calibration Results

On analysis of the calibration data it was found that there was an unexpected difference of approximately 10% in the mean calibration factors for the high and low speed tests. As a consequence, it was found necessary to use the calibration factors from the high speed tests in subsequent analyses.

Figure 32 shows dynamic tyre force data from the calibration vehicle and measurements by the nearside WIM sensors, for one of the high speed calibration runs. Vertical lines indicate the positions of the WIM sensors. Points marked '*' indicate the dynamic tyre force applied to each WIM sensor (measured on the vehicle); while points marked 'o' indicate calibrated WIM sensor measurements. Differences between the vertical positions of these points indicate the magnitude of the measurement error for each sensor on this test run.

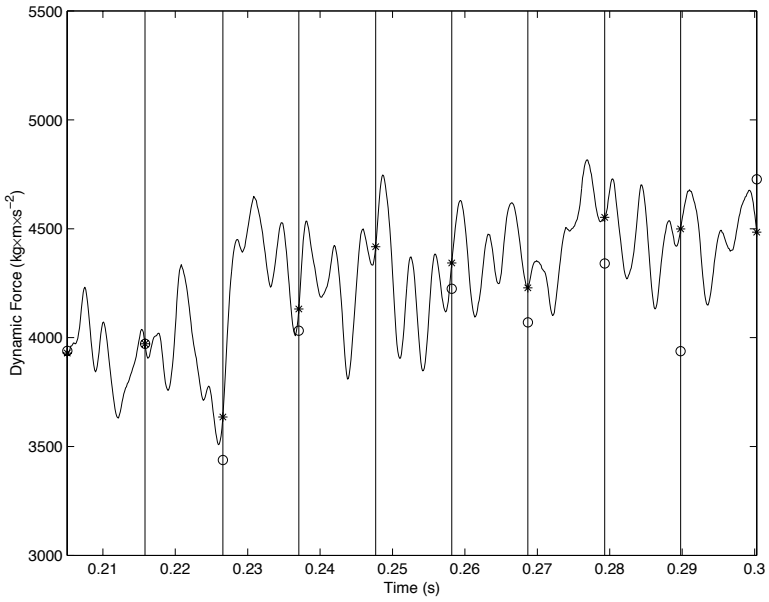

Fig. 32 Dynamic Tyre Forces recorded for calibration Run 10, Nearside sensors. Vertical lines indicate the positions of the WIM sensors. ———— = Dynamic tyre force; '*' = Dynamic tyre force applied to each WIM sensor; 'o' = WIM sensor output.

Note that the instrumentation system for measuring dynamic tyre forces is not expected to be perfectly accurate. In an error analysis performed by Cole (Cole, 1990), the RMS errors for this type of system were estimated to be approximately 1.5%. This is consistent with estimates of 3–5% peak errors by Mitchell and Gyenes (Mitchell and Gyenes, 1989). In practice, larger measurement errors might be expected in these tests because:

(i) There was considerable surface roughness over the site, which excited additional high frequency dynamic tyre forces (see figure 32). As a consequence, any small errors in the timing of the synchronisation pulses (generated by the infra-red transceiver) generated significant force errors.

(ii) The value of mass and roll moment of inertia of the wheel and axle components outboard of the strain gauges (used in the signal reduction procedure (Cebon, 1993)) were not known exactly, and had to be estimated.

As a consequence, the errors in dynamic load measured by the calibration vehicle are estimated to be approximately 3% RMS: double the values obtained previously under more favourable conditions.

Note that the calibration procedure eliminated any mean error (bias) between the sensor measurements and the dynamic tyre forces.

Figure 33 compares the forces measured by WIM sensor 2 (typical) with the instantaneous dynamic tyre forces measured by the calibration axle, for 14 runs of the calibration vehicle. Perfect measurements would lie along a diagonal line of slope 1.0. There is some scatter on both axes, due to the random nature of the dynamic tyre forces, WIM sensor measurement errors, and errors in the vehicle instrumentation. Note that the mean error is zero, as expected.

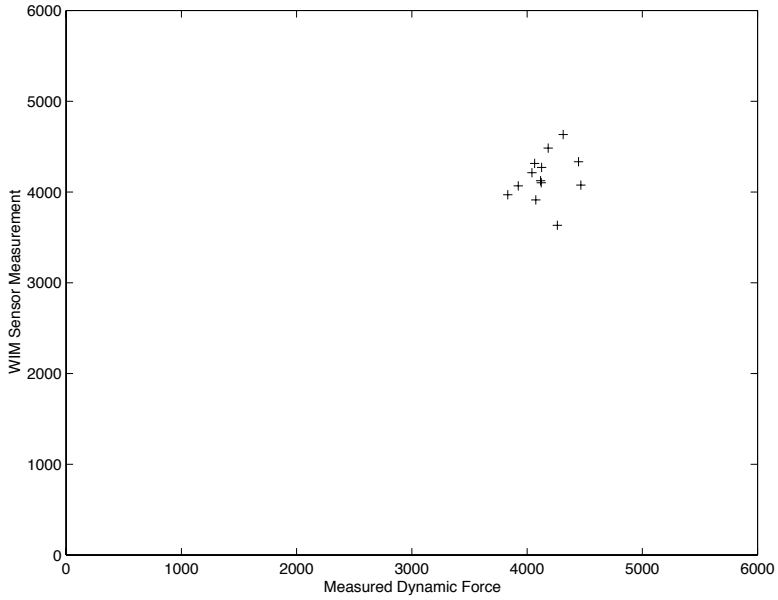

Fig. 33 Comparison of WIM sensor measurements with measured dynamic forces, for Sensor 2.

The RMS differences between the sensor measurements and dynamic tyre forces for all of the sensors are compared in figure 34. (Note that sensors 9 and 14 failed early in the testing programme, and so no data was available from them.) The average RMS error for all 18 functioning sensors was 9.26%.

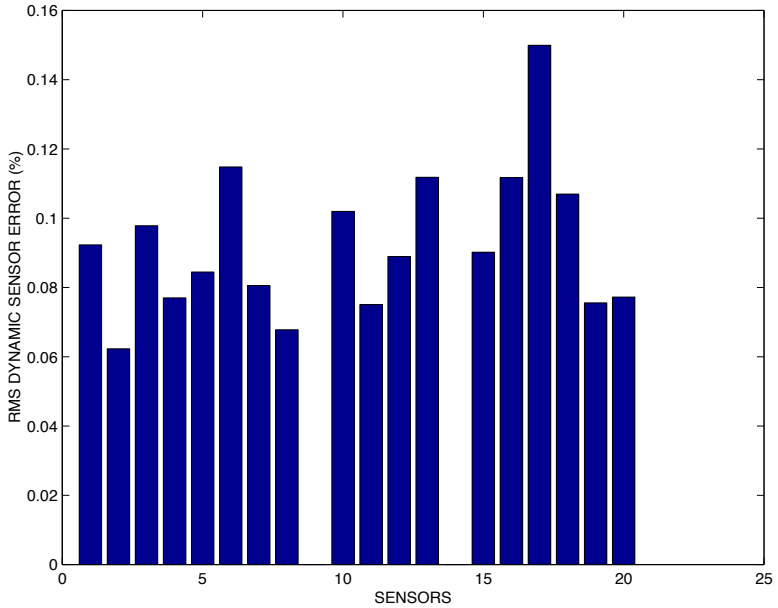

Fig. 34 RMS sensor errors. Average error for all sensors = 9.26%

Assuming that the errors generated by the vehicle instrumentation and the WIM sensors are uncorrelated, and that the vehicle instrumentation generated an RMS error of 3%, the average RMS WIM sensor error can be estimated to be:

$$\sigma_s = \sqrt{\sigma_T^2 - \sigma_V^2} \approx \sqrt{9.26^2 - 3^2} = 8.8\%.$$

This can be compared with a value of approximate 4% RMS determined in previous measurements using the same type of capacitative strip sensors in the polymer 'load measuring mat' described in section 5.4. The additional errors are likely to be the result of the differences in mounting arrangements for the two sets of tests, and particularly the wheel-path rutting. After the surface treatment described above, it was apparent that some sensors were set slightly *below* the level of the level of the re–surfacing material. This means that some tyres might have 'bridged' the sensors, thereby generating significant measurement errors.

5.5.4 Analysis of Calibration Vehicle Runs

The data collected for the calibration vehicle on its 14 runs over the site provides a consistent set of test results which can be analysed to investigate system performance. Although the calibration was performed with the tractor drive axle (axle 2), the other three axles on the vehicle provide independent repeatable data which is useful for statistical analysis. The test conditions can best be characterised as 'full repeatability' (r1) (COST 323, 1997b).

Sensor Spacing

The WIM sensor data for each vehicle run was analysed to generate as many different static load estimates as possible, using the SM estimation approach. The method was the same as that described in section 5.4.3 and shown in figure 25.

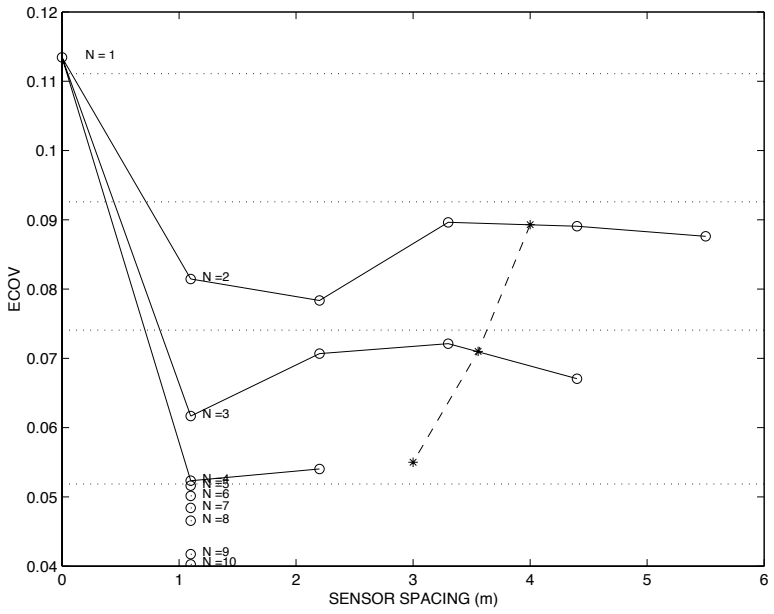

Fig. 36 WIM estimation errors as a function of sensor spacing Δ, for varying numbers of sensors in the array N, using the Sample Mean (SM) method. *Axle 3 of the calibration vehicle* (first trailer axle). Design spacings Δ_{d_1} (equation 19) are denoted by '*'.

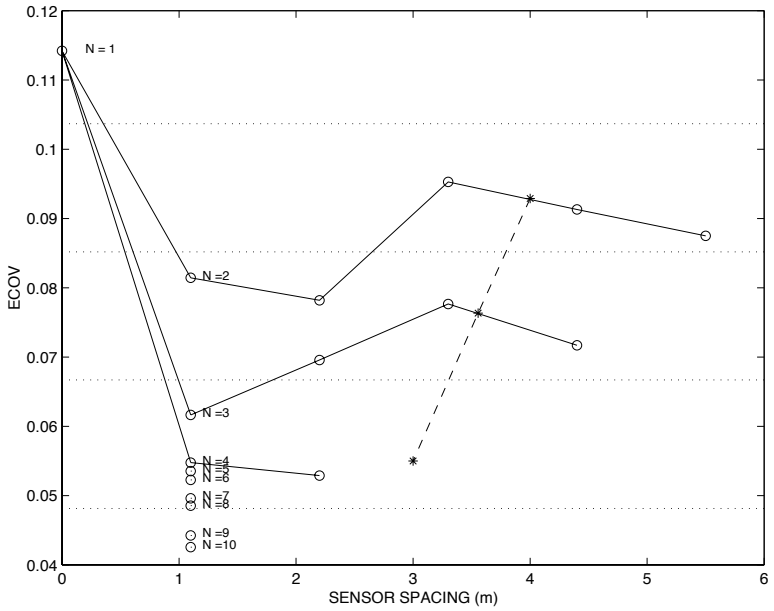

Fig. 36 WIM estimation errors as a function of sensor spacing Δ, for varying numbers of sensors in the array N, using the Sample Mean (SM) method. *Axles 3 and 4 of the calibration vehicle* (both trailer axles). Design spacings Δ_{d_1} (equation 19) are denoted by '*'.

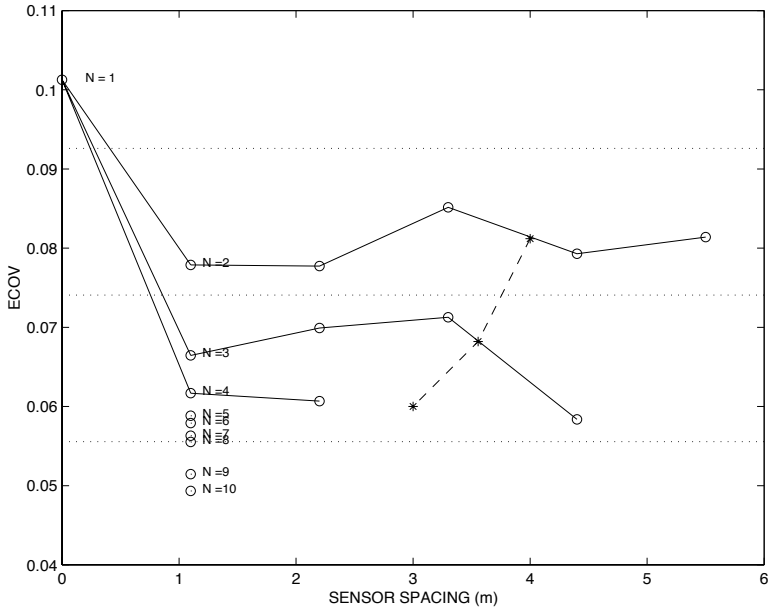

Fig. 37 WIM estimation errors as a function of sensor spacing Δ, for varying numbers of sensors in the array N, using the Sample Mean (SM) method. *Gross vehicle weight of the calibration vehicle* (all axles). Design spacings Δ_{d_1} (equation 19) are denoted by '*'.

Figure 35 presents the results for the *individual axle loads* of axle 3 of the calibration vehicle (The calibration axle was axle 2). Figure 36 shows the estimated total load for the *tandem axle group* of the trailer, calculated from the sum of the two estimated axle weights; and figure 37 shows the *gross vehicle weight*, calculated by adding together the estimated weights of all of the axles. Each figure shows the ECOV as a function of sensor spacing for 2, 3 and 4 sensor arrays; as well as the COST 323 class boundaries (COST 323, 1997b), and the design spacings Δ_{d_1}, calculated with equation 19, and denoted by a '*'.

With the ten sensor array, it was possible to perform two-sensor estimates with Δ = 1.1 to 5.5m; three-sensor estimates with Δ = 1.1 to 4.4m; and 4-sensor estimates with Δ = 1.1 and 2.2m. Arrays with 5 to 10 sensors could only be constructed using adjacent sensors – with spacings of Δ = 1.1m. In each case, as many different weight estimates as possible were calculated and averaged together to calculate the ECOV[3].

The following observations can be made:

(i) All of the curves display the characteristic 'U-shape' function which is predicted by theoretical models (eg figure 18 and (Cebon and Winkler, 1991a)).

(ii) The SM design spacings (denoted by '*') are often a little greater than might be desirable for this data set. It is believed that this is a consequence of the periodic surface roughness of the array, which generates large periodic tyre forces at an abnormally high frequency of about 20Hz.

(iii) For arrays with 3 sensors, typical reductions in ECOV (compared with the single–sensor systems, $\Delta = 0$) are up to 50% for optimal spacings, indicating an excellent improvement in accuracy for modest cost. For arrays with 5–10 sensors, a further 20% or so improvement in accuracy can be obtained.

(iv) The best accuracy (classes B and C) were obtained for the individual trailer axles (figure 35) and for the axle group (figure 36). The accuracy for the tractor axles was found to be less impressive (class D+). The gross vehicle weight was estimated in class C/D+.

Number of Sensors

Figures 38 to 40 show the effect of the number of sensors on the accuracy of the SM, ML1 and ML2 estimation approaches. Figures 38 is for Axle 3, figure 39 is for the trailer tandem, and figure 40 is for gross vehicle weight. The three lines on each graph show results for Δ = 1.1m, while the two points labelled '*' and 'o', (for 4 sensors), show the results for ML1 and SM respectively, with Δ = 2.2m. (Note that the ML1 method can only be used with 4 or more sensors, while ML2 needs at least 7 sensors.)

[3] Note that the number of runs used to calculate the confidence intervals for the weight classes was set to the 14 (the number of test runs) in every case.

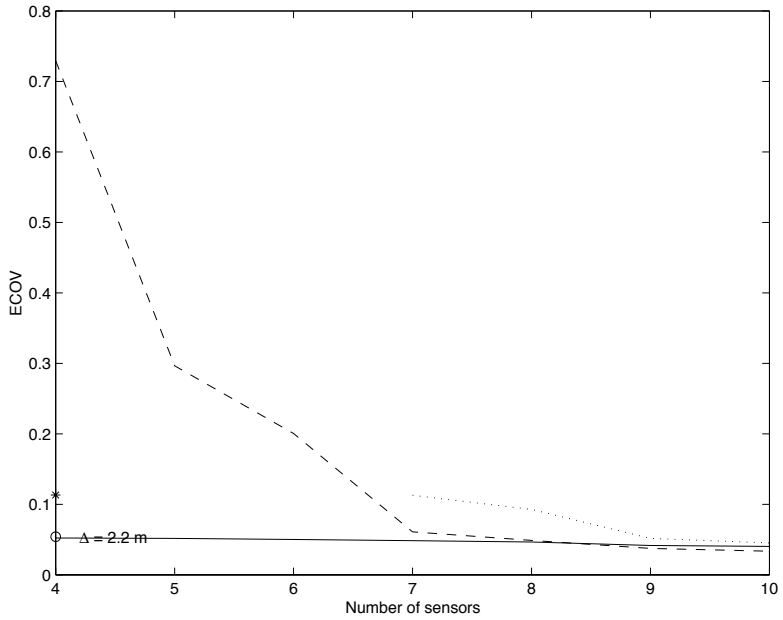

Fig. 38 WIM estimation errors for Axle 3 of calibration vehicle, as a function of the number of sensors *N,* for the three estimation methods.
———— = Sample Mean (SM) with Δ=1.1m; – – – – = ML1, with Δ=1.1m;
· · · · · · · = ML2, with Δ=1.1m; * = ML1 with Δ=2.2m; 'o' = SM with Δ=2.2m.

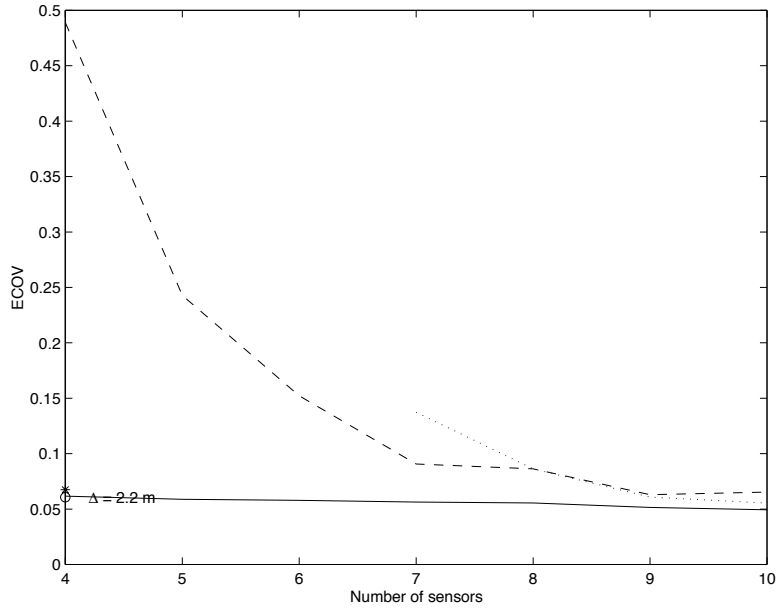

Fig. 39 WIM estimation errors for Axles 3 and 4 of calibration vehicle, as a function of the number of sensors *N,* for the three estimation methods.
———— = Sample Mean (SM) with Δ=1.1m; – – – – = ML1, with Δ=1.1m;
· · · · · · · = ML2, with Δ=1.1m; * = ML1 with Δ=2.2m; 'o' = SM with Δ=2.2m.

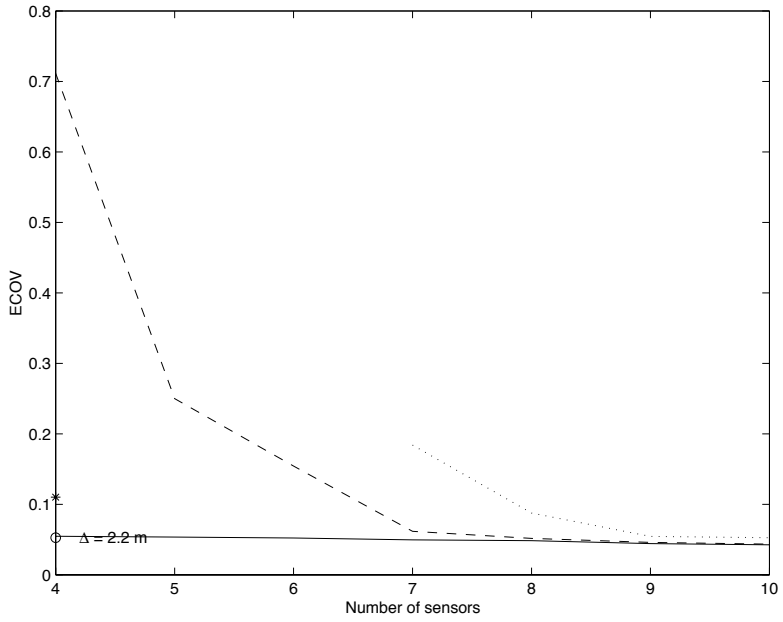

Fig. 40 WIM estimation errors for the gross vehicle weight of the calibration vehicle, as a function of the number of sensors *N,* for the three estimation methods.
———— = Sample Mean (SM) with Δ=1.1m; – – – – = ML1, with Δ=1.1m;
· · · · · · · = ML2, with Δ=1.1m; * = ML1 with Δ=2.2m; 'o' = SM with Δ=2.2m.

The following observations are made:

(i) The ML1 method with Δ = 1.1m (- - - - - curve) is very inaccurate for less than about 7 sensors, since the spacing is much smaller than required by equation 19, and the ML1 algorithm becomes ill-conditioned.

(ii) Changing from Δ = 1.1m to Δ = 2.2m for ML1 gives a dramatic performance improvement, since the larger spacing is much closer to the design spacing specified by equation 19. In fact, on most of the graphs, the improvement in accuracy due to the increased spacing (with 4 sensors) is as good as the gains obtained by increasing the number of sensors substantially, while keeping the 1.1m spacing.

(iii) For 10 sensors, the Maximum Likelihood methods ML1 and ML2 are generally little more accurate than the Sample Mean (SM). This is predicted by the theoretical analysis, which indicates only small benefit in the ML approach if the sensor noise is greater than about 4% RMS. (This is much less than the 8.8% measured for these sensors.)

5.5.5 Data Collection for Randomly-Selected Vehicles

Procedure

A survey of the weights of vehicles sampled at random from mixed traffic was also conducted. These survey was performed on six separate days over a period of approximately a month. Testing could only occur on days when the Vehicle Inspectorate's static weigh station at junction A415 was being used for weight enforcement purposes. The test conditions can best be characterised as 'full reproducibility' (R2) (COST 323, 1997b).

Test Vehicle Population

A number of unforeseen practical problems occurred which had a significant effect on the amount of data that was collected. See (Stergioulas and Cebon, 1999) for details. As a consequence, only 11 complete records were obtained out of six days of testing. Lack of resources prevented any further tests from being conducted.

Analysis of Test Vehicles

Figures 41 shows sample histograms of the relative error x_i, The cases shown are: Figure 41(a) SM with n=4 and Δ=2.2m; Figure 41(b), ML1 with n=4 and Δ=2.2m; Figure 41(c), ML2 with n=10 and Δ=2.2m.

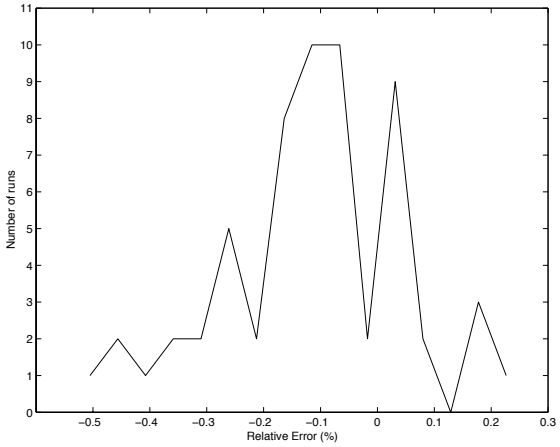

(a)

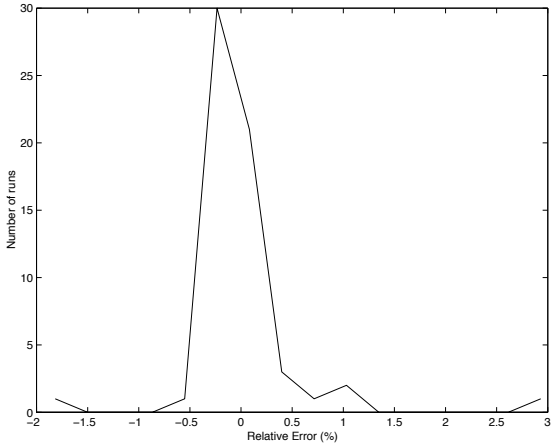

(b)

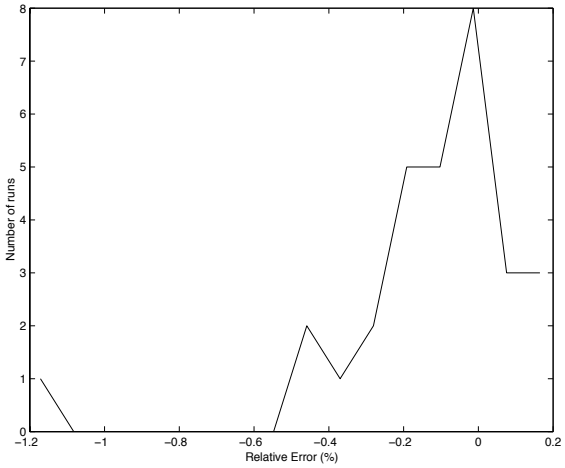

(c)

Fig. 41 Histogram of the relative errors x_i, for 22 *single axles*, of the 11 test vehicles, for the three estimation methods.
(a) Sample Mean (SM) with n = 4 and Δ=2.2m.
(b) Maximum Likelihood ML1 with n = 4 and Δ=2.2m.
(c) Maximum Likelihood ML2 with n=10 and Δ=1.1m.

In each case it can be seen that there the mean error is less than zero, indicating a negative bias. This is possibly due to calibration drift between the time of the calibration tests and the tests with mixed traffic. (During this period the temperature dropped significantly, and this may have reduced their sensitivity - see Chapter 8 of (Cebon, 1999).)

For the SM results (figure 41a), the errors are clustered between -0.5 and +0.2, whereas in both Maximum Likelihood cases (figures 41b and c), there are one or two outliers with very large errors. These are cases where the Maximum Likelihood algorithm has become ill-conditioned and has not converged correctly. This is a consequence of the sensor array not sampling the dynamic tyre forces adequately, because of their unusual frequency content (Stergioulas, Cebon et al.,

1999). It is likely that the abnormally high frequency surface roughness over the array contributed to this problem.

Figures 42 and 43 summarise the mean relative errors $\bar{x}$ for 22 *single axles*, and for 11 gross weights of the test vehicles. The following can be observed:

(i) The effects of the number of sensors on the mean errors are similar to those described above for the ECOV values for the calibration vehicle.

(ii) The three algorithms (SM, ML1 and ML2) have essentially the same accuracy for large numbers of sensors

(iii) The measurement bias is approximately 7–10% for all estimation methods – probably as a consequence of calibration drift due to temperature, as explained above.

(iv) On both plots, the most accurate estimates are obtained by ML1 with Δ=2.2m (ie the '*'). The reasons for this are not clear.

Unfortunately there were insufficient weight samples to obtain meaningful information from the COST 323 weight accuracy classes for this population.

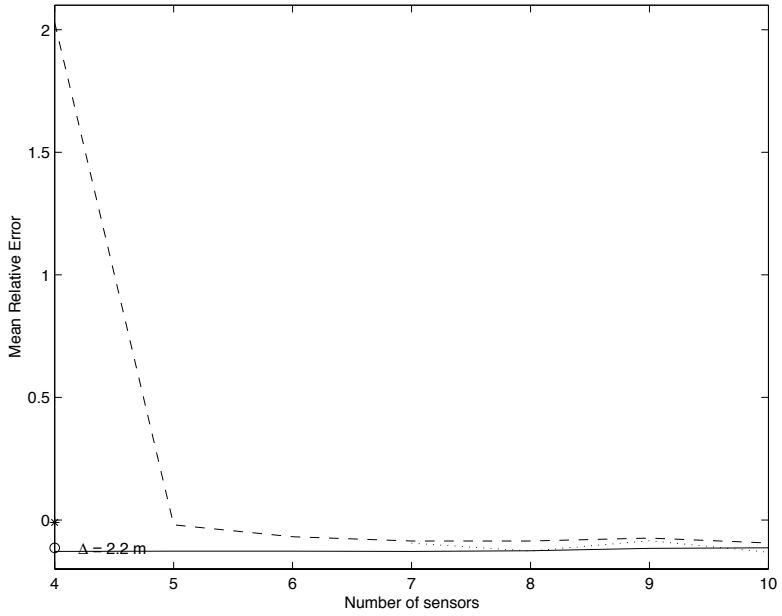

Fig. 44 *Mean* relative errors $\bar{x}$ for all 22 *single axles* on the 11 test vehicles, as a function of the number of sensors N, for the three estimation methods.
——— = Sample Mean (SM) with Δ=1.1m; – – – – = ML1, with Δ=1.1m;
· · · · · · · = ML2, with Δ=1.1m; * = ML1 with Δ=2.2m; 'o' = SM with Δ=2.2m.

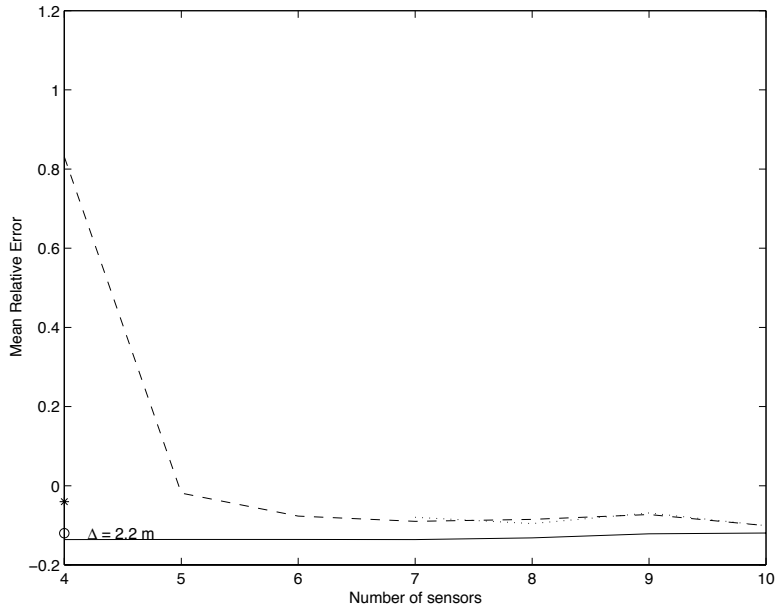

Fig. 45 *Mean* relative errors $\bar{x}$ for the *gross vehicle weights* of the 11 test vehicles, as a function of the number of sensors N, for the three estimation methods. ———— = Sample Mean (SM) with Δ=1.1m; – – – – = ML1, with Δ=1.1m; · · · · · · · = ML2, with Δ=1.1m; * = ML1 with Δ=2.2m; 'o' = SM with Δ=2.2m.

6 COMPARISON OF THE NEW ALGORITHMS USING THE TRAPPES MS-WIM ARRAY

This section compares the performance of the various algorithms developed by LCPC and CUED using data recorded on the MS-WIM array on highway RN10 at Trappes (see Section 5.2). The *Sample Mean* method is denoted 'SM', the *signal reconstruction and Kalman filtering method* 'SR' and the *Maximum Likelihood* algorithms are denoted 'ML1' and 'ML2' for one and two-tone fits respectively.

6.1 Vehicle Sample

Among the set of 100 pre–weighed vehicles, it was decided to compute the performance of each method using 20 vehicles with singles axles. This sub sample consists of:

(i) 12 two axle rigid vehicles (4x2) denoted T2,

(ii) 8 tractor units (4x2) with full trailers (two singles axles) denoted T2R2.

6.2 Computation Time

For the computation of one axle, and using a PC equipped with a Pentium II at 100 Mhz, the 'SM' method required 2 seconds, the SR method took 4 minutes, and the ML methods respectively 2 seconds (ML1) and 4 minutes (ML2). That means that the computation of all the axles of the considered sample took 2 minutes for the 'SM' and ML1 methods, and 4 hours for the SR and ML2 methods.

6.3 Outliers

The statistical outliers of the axle static load estimation for the 20 vehicles were detected by the Dixon test at the level of confidence of 95%. They were thought to be mainly due to some errors of the methods, sometime because of a poor convergence. In the whole sample, the SR method had no outliers, the 'SM' method had 0.5% of outliers, the ML1 method had 1.5% and the ML2: 19%.

The reasons for the large number of outliers for ML2 is that the sensor spacing used in the sub–arrays was unsuitable for this algorithm. Table 14 shows the three sub–arrays (MSA1, MSA2 and MSA3) used in the comparison study. In all cases the sensor spacings were 2.25m (see also Table 4 in Section 5.2.4). However the ML2 algorithm requires a spacing near to that given by Δ_{d2} Eq. (33), shown in the last column of the table. It can be seen that the 2.25m spacing is always considerably greater than the correct design spacing for this algorithm. Since the algorithm becomes ill-conditioned for incorrect spacings (see figure 13 and 20) many outliers are expected for this experiment.

Sub–array	No sensors n	Spacing	Δ_{d1} Eq. (19)	Δ_{d2} Eq. (33)
MSA1	16	2.25m	1.45	1.25
MSA2	13	2.25m	1.75	1.32
MSA3	7	2.25m	3.0	1.67

Table 14 Sensor spacings for the arrays used in the comparative tests.

6.4 Performance of Each Method

Figures 44 to 46 show the accuracy of each method for the 3 sub-arrays, MSA1, MSA2 and MSA3, expressed by the δ_{min} as proposed in the European Specification (COST 323, 1997b), after elimination of the outliers. Class A(5) is not obtained by any method. Class B+(7) is always obtained by the 'SM' method for single axle loads (figure 44). The other methods are more sensitive to the number of sensors. The accuracy of the SR and ML2 methods decrease with the number of sensor. However, figure 46, which compares the accuracy with the δ– class (standardised value of δ_{min} on the scale of the gross weights), shows that ML2 can achieve class A(5) if only the 2-axle rigid trucks are included.

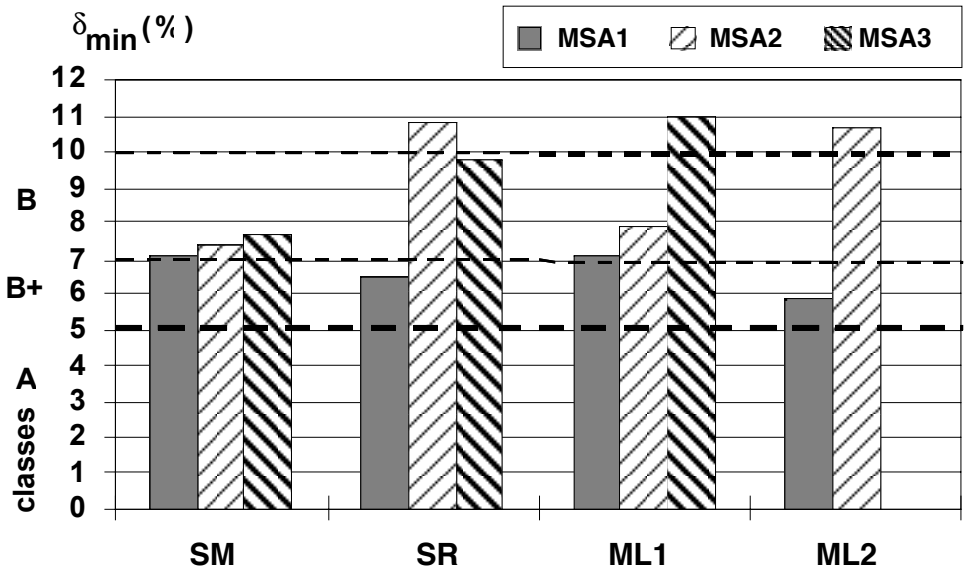

Fig. 44 Estimation of Gross Weights for T2 and T2R2 – Effects of sub–arrays

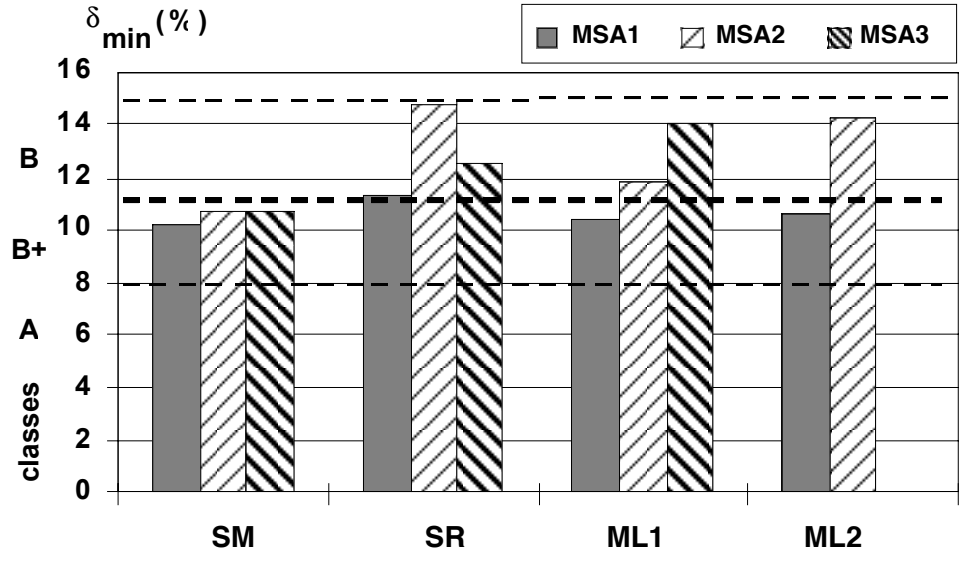

Fig. 45 Estimation of Single Axle loads for T2 and T2R2 – Effects of sub–arrays

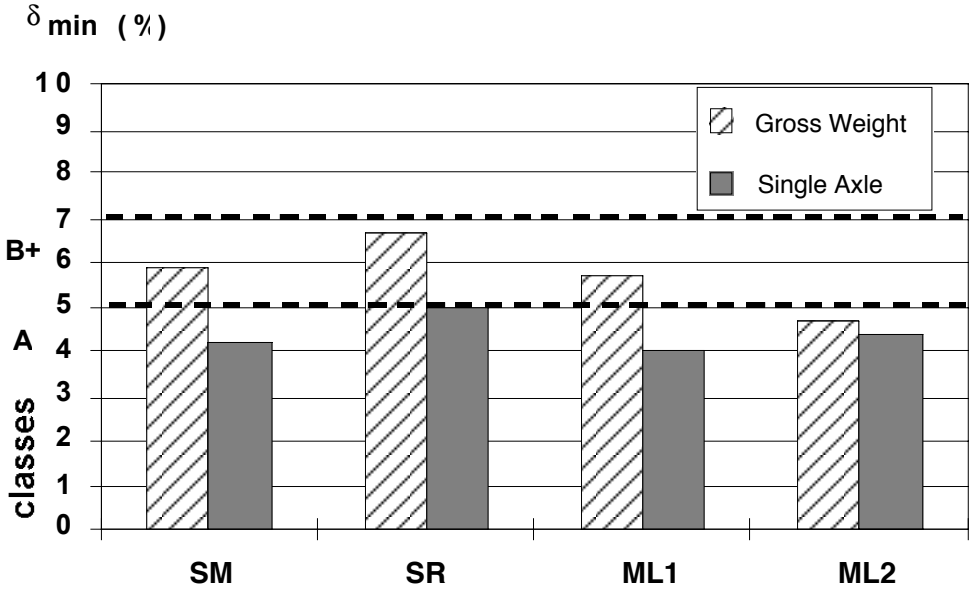

Fig. 46 Estimation Gross Weights and Single axle loads for T2 vehicles, sub–array MSA1

6.5 Influence of Calibration Method

Although SR, ML1 and ML2 methods were designed to work with sensors calibrated using dynamic tyre forces, it is interesting to examine the effect of a static calibration on the accuracy of static load estimation. For practical reasons, it is much easier to perform sensor calibration using measured static loads (which needs only passes of pre-weighed vehicles test vehicles), rather than using instrumented vehicles, which are expensive to operate.

Figures 47 to 50 show the accuracy of each method for both calibration procedures, for single axles and gross weights and for two MS arrays MSA1 and MSA2. For single axles, the accuracy of the SM and ML1 methods are similar whatever the calibration used. However, for the two other methods, the accuracy is better when sensors are calibrated using dynamic tyre forces, as expected. The accuracy of estimating gross weights decreases when the number of sensors decreases. For the SR method the accuracy is better when the sensor are calibrated statically.

The single axles are weighed in class B+(7) by all methods (Figure 47), when the sensors are calibrated using dynamic tyre forces. Methods SR and ML2 (Figure 48) give better results for single axles when the sensors are calibrated statically .

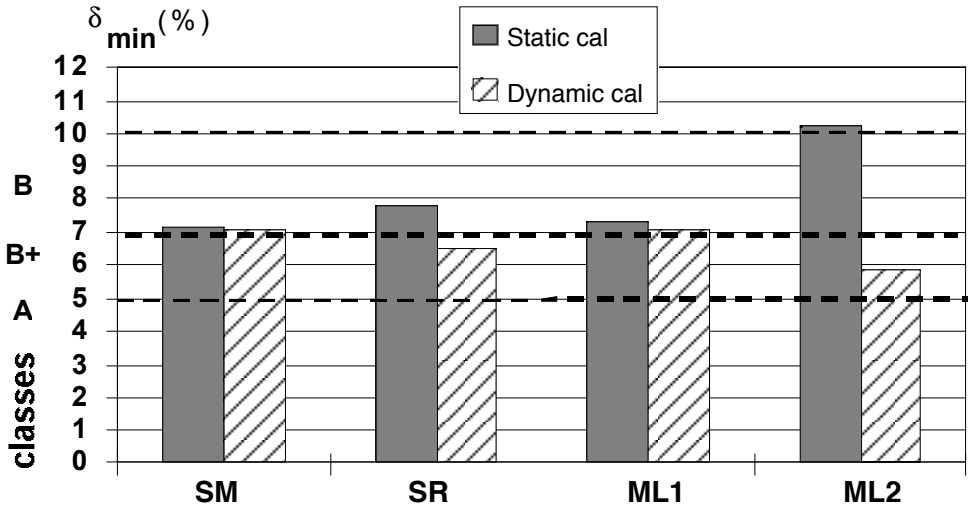

Fig. 47 Gross weights for T2 and T2R2,S1 sub-array MSA1

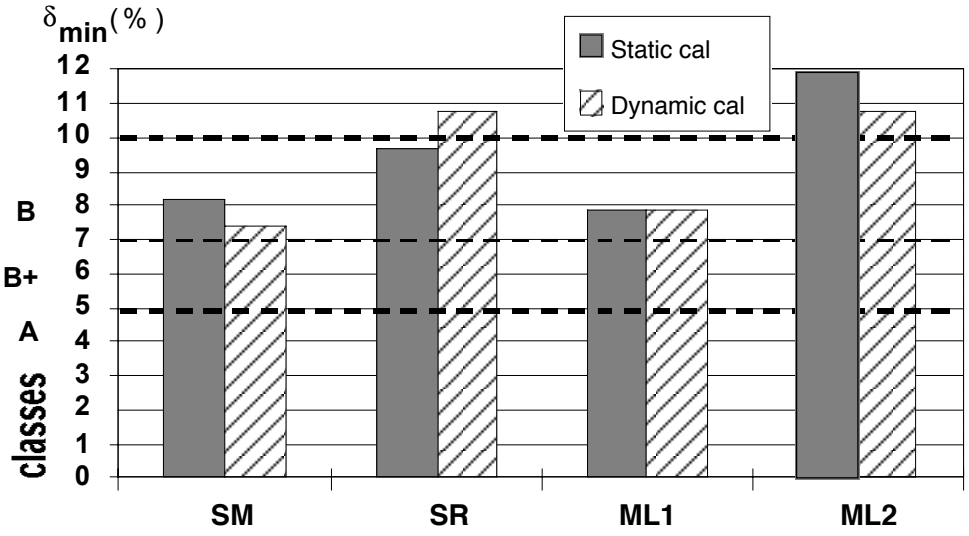

Fig. 48 Gross weights for T2 and T2R2, sub-array MSA2

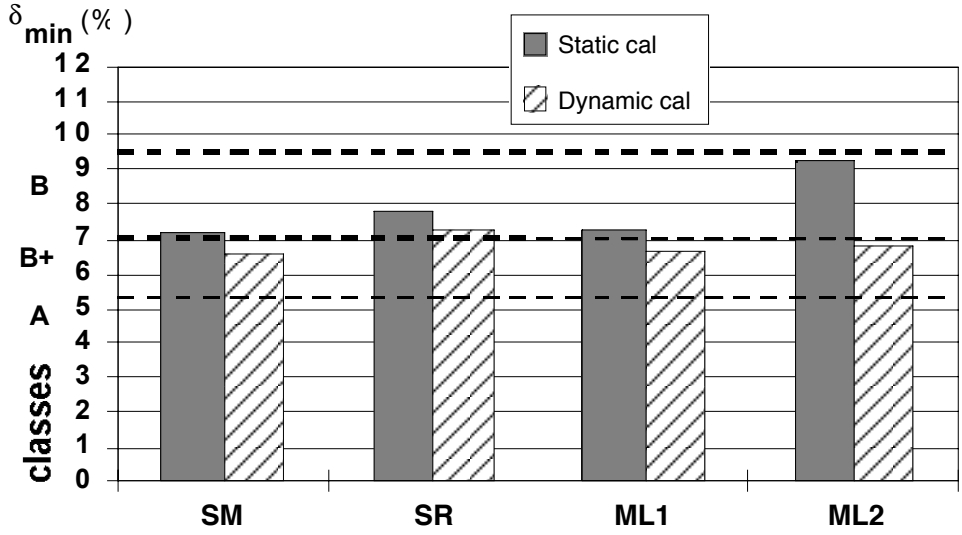

Fig. 49 Single axles for T2 and T2R2, sub-array MSA1

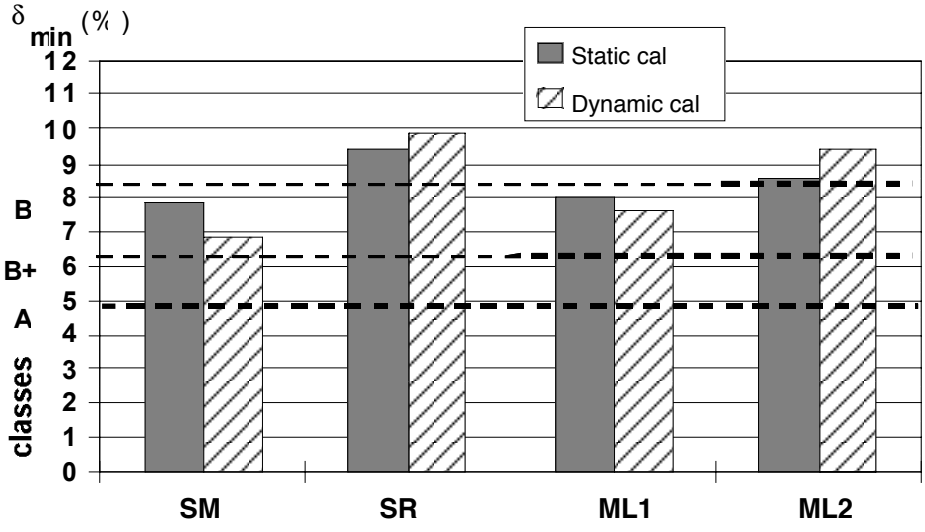

Fig. 50 Single axles for T2 and T2R2, sub-array MSA2

7 CONCLUSIONS

7.1 Theory of MS–WIM

(i) Two new processing methods for MS-WIM have been presented. The signal reconstruction method (SR) is based on interpolation and Kalman filtering. The Maximum Likelihood (ML) estimator uses one or two sine waves to model the dynamic forces.

(ii) The Maximum Likelihood (ML) estimator is more accurate for estimating the static load than the Sample Mean, provided the sensor noise is low. For a given level of accuracy, it requires less sensors, leading to more cost effective systems. Furthermore, the performance of the algorithm is not significantly affected by variations of parameters such as vehicle speed and type of suspension. If the sensor noise is larger than 4% RMS, the Maximum Likelihood approach is similar in accuracy to the Sample Mean.

(iii) The ML method can be used in conjunction with either a single sine wave model or a two-sine wave model. The two sine wave algorithm will be capable of measuring correctly nearly all classes of vehicles (including suspension types with two distinct frequencies). The two-sine wave approach will nevertheless require more sensors (a minimum of 7 sensors, compared to 4 sensors for the single-sine wave case).

(iv) Some validation of the SR method using measured tyre forces recorded with an instrumented vehicle showed that, *if the sensor error* is neglected, the reconstruction method can be very accurate. The static axle weight was estimated within ±3% with 9 sensors, and ±2% with 13 sensors.

(v) WIM sensor arrays can be designed using a new theory which predicts the success rate of the algorithms. The number and spacing of sensors can be determined to ensure accurate estimation of static weights for the range of vehicle types and speeds expected in the traffic stream. Depending on the distributions of vehicle speeds and resonant frequencies, the new design procedure will supply near optimal system configurations.

7.2 Tests in France

(i) Tests performed in France using the array at Trappes proved that with a Sample Mean algorithm and 5 to 7 piezo-ceramic strip sensors, the accuracy of an MS-WIM system installed on a class II site can reach class B+(10) of the European specification on WIM (COST-323). Accuracy class B+(7) is almost obtained with 13 sensors.

(ii) Tests performed on the array at Metz (Obrion) were inconclusive due to the poor performance of the sensors.

7.3 Tests in the UK

(i) It was found necessary to use a high speed, dynamic calibration method for the WIM array on the A34. This required an instrumented vehicle and careful attention synchronisation of the data collected on the vehicle with WIM data.

(ii) The RMS sensor errors were estimated to be approximately 8.8% RMS compared with a value of approximate 4% RMS determined in previous measurements using the same type of capacitative strip sensors in a 'load measuring mat' on a test track.

(iii) Using the Sample Mean (SM) method, the estimated axle loads for the axles of the calibration vehicle were found to follow a similar variation with sensor spacing as theoretical predictions.

(iv) Substantial improvements in static weight estimation accuracy were obtained using multiple sensors for the axles of the calibration vehicle, compared with single sensor systems. Errors as low as 4% RMS were obtained in some cases, for arrays of 10 sensors (compared with 11-12% errors for single-sensor systems). Accuracy classes of B and C were obtained for some single axles, although lower accuracy classes were obtained for axle groups and gross vehicle weights.

(v) Using a more suitable sensor spacing (2.2m instead of 1.1m) was found to have approximately the same influence on estimation accuracy as increasing the number of sensors in the array from 4 to 10.

(vi) All of the estimation methods (Sample Mean (SM) and Maximum Likelihood with one or two sine waves (ML1 and ML2)) gave essentially the same accuracy for large numbers of sensors. This confirmed the predictions of theoretical analyses for relatively high levels of sensor noise.

(vii) When performing tests with vehicles from mixed traffic, a measurement bias of approximately 7–10% was observed for all estimation methods. This was probably a consequence of calibration drift due to temperature.

(viii) Data from the load measuring mat indicated that systems with 8 or 9 sensors can achieve class B+(7) under some conditions. This corresponds to RMS measurement errors of less than 4%.

7.4 Comparison of WIM Algorithms

(i) ML2 is less reliable than the others, at least for a small number of sensors (10 to 15), because it provides a large proportion of outliers. However this is to be expected, because the sensor spacing used in the tests was not suitable for the method.

(ii) The Sample Mean and ML1 methods have a good robustness and are less sensitive to noisy sensors.

(iii) The accuracy of the Sample Mean and ML1 methods were found to give similar performance, except for array MSA3, which had 7 sensors.

(iv) the others methods need more sensors because they estimate more parameters; so, the performance of these methods are more sensitive to the number of sensors;

(v) The accuracy of the Sample Mean method is less sensitive to the calibration procedure, and may be calibrated using static axle loads. The other methods give generally better results when the sensors are calibrated using dynamic tyre forces.

(vi) Class A(5) was achieved for single axles of two axle rigid trucks and a sub-array with 13 sensors;

(vii) The accuracy and reliability of methods SR, ML1 and ML2 are expected to be better with less noisy sensors.

8 RECOMMENDATIONS AND FUTURE RESEARCH

8.1 Recommendations

(i) Multiple-sensor systems have the potential to improve the accuracy of high speed WIM significantly. In future, multiple-sensor systems using high quality sensors, installed in good quality pavement, are likely to provide sufficiently accurate weights to be used for enforcement purposes.

(ii) The conclusions in this report are based on measurements on a limited number of WIM sites, with relatively few vehicles. The results need to be confirmed with test data from more sites, with other types of sensor and a larger number of vehicles.

(iii) In future experiments on MS–WIM arrays, care should be taken to use the correct number and spacings of sensors, as specified in Section 4.5.2. Use of incorrect array designs will lead to spurious results - in the form of 'outliers', especially with the more sophisticated estimation algorithms (eg ML2).

8.2 Future Research

(i) Some work is needed to enhance the handling of 'outliers' by the more sophisticated methods (eg ML2). This would ensure that the calculations 'degrade gracefully' to simpler algorithms, (such as the Sample Mean) when the data lies outside prescribed ranges. Estimation accuracy would then always be at least as good as the Sample Mean.

(ii) The estimation algorithms need to be optimised and written in a lower-level language (eg 'C') so that they can be used for real-time processing in WIM data-loggers. This would simplify future experimentation and optimisation work.

(iii) There is a need to investigate MS–WIM signal processing methods which have better noise rejection characteristics than the Maximum Likelihood approach.

(iv) Sensor noise and measurement errors significantly degrade MS–WIM estimation accuracy. There is a need for more accurate WIM sensors to address this problem.

(v) The weight estimation algorithms need to be enhanced so that they output an indication of the level of confidence associated with each axle load estimate. This would facilitate their use as load limit enforcement tools.

(vi) As yet there has not been a convincing demonstration that MS-WIM systems can meet the accuracy requirements for enforcement purposes. A further measurement programme needs to be undertaken to achieve this. Great care will need to be taken over the performance of the sensors, the design of the array and the weight estimation algorithm.

9 IMPLEMENTATION AND DISSEMINATION

9.1 Pre–Selection, Enforcement and Monitoring

Automatic systems are used to enforce speed limits. In theory, similar devices using MS-WIM systems and cameras (or automatic vehicle identification systems) could be used to enforce weight limits. The research presented here shows that multiple-sensor WIM systems, with 12–15 sensors have the potential to measure static axle loads with less than 3% RMS error. This is thought to be approaching the accuracy needed for enforcement purposes.

High speed WIM (HS-WIM) systems can be used to:

(i) Select vehicles for enforcement weighing (pre-selection), thus improving the efficiency of enforcement. Such systems may use strip sensors, such as piezo or capacitive.

(ii) Monitor the level of overloading, allowing the authorities to make better decisions about the resources required for enforcement, the timing of enforcement checks, etc.

(iii) Automatic weight enforcement, using systems which record the weights and other details of vehicles. This would greatly improve the efficiency of enforcement and the probability of an individual overloaded vehicle being detected.

(iv) Identify vehicles for follow-up checks.

9.2 Pavement Design and Maintenance

There are significant financial benefits in having accurate vehicle loading data available for the purposes of pavement design and maintenance (Collop et al, 1998). In particular over-design can be avoided and maintenance requirements can be predicted more accurately. Thus significant cost savings can be achieved through implementation of high-accuracy WIM systems.

10 REFERENCES

Bennett, M. and Lawrence, C.M. (1991), Designing multiple-sensor arrays for weigh-in-motion, Department of Transport TRRL Report 281, Transport and Road Research Laboratory, Crowthorne UK.

Cebon, D (1989), 'Vehicle-generated road damage: A review', Vehicle System Dynamics, 18 (1-3), 107-150.

Cebon, D (1990), 'Design of multiple-sensor weigh-in-motion systems', Journal of Automobile Engineering, Proc. I.Mech.E., 204, 133-144.

Cebon, D (1993). 'Interaction between heavy vehicles and roads'. SAE SP–951 930001.

Cebon, D (1999). 'Handbook of Vehicle–Road Interaction'. Lisse, Swets and Zeitlinger.

Cebon, D and Winkler, CB (1991a) , 'Multiple-Sensor WIM: Theory and experiments', Transportation Research Record, TRB, 1311, 70-78.

Cebon, D and Winkler, CB (1991b), 'A study of road damage due to dynamic wheel loads using a load measuring mat.', Strategic Highway Research Program, National Research Council, Report, SHRP–ID/UFR–91–518.

Cole, DJ and Cebon, D (1989). 'A capacitative strip sensor for measuring dynamic tyre forces'. Proc. 2nd Int. Conf. on Road Traffic Monitoring., London, IEE.

Cole, DJ (1990), '*Measurement and analysis of dynamic tyre forces generated by lorries.*' PhD Thesis, Cambridge University Engineering Department.

Cole, DJ. and Cebon, D. (1992), 'Spatial repeatability of dynamic tyre forces generated by heavy vehicles', Proc. Inst. Mech. Eng., vol 206, 1992, pp.17-27.

Cole DJ and Cebon, D (1992), 'Validation of an articulated vehicle simulation', Vehicle System Dynamics, 21, 197-223.

Collop, AC, Al-Hakim, B, Thom, NH and Lloyd, WG (1998). 'The use of WIM data in traffic assessment'. Second European WIM conference, Lisbon, 14-16 September.

Corte, J.F (1998), 'Catalogue des dégradations de surface de chaussées - Méthode d'essai n°52', ed. Laboratoire Central des Pontes et Chaussées -Paris

COST 323 (1997a), Collection and analysis of needs and requirements of WIM systems, Final Report, EUCO-COST/323/1/1997, COST Transport, EC/DGVII, January.

COST 323 (1997b), European Specification on Weigh in Motion of Road Vehicles, Draft 2.2, EUCO-COST/323/6/1997, COST Transport, EC/DGVII, June.

COST 323 (1998), Test of four portable and one multiple-sensor WIM systems, EUCO-COST/323/1/1998, COST Transport, EC/DGVII, March.

Dolcemascolo, V., Jacob, B. (1998), 'Multiple Sensor Weigh In Motion: Optimal Design and Experimental Study ', in Pre-Proceedings of 2nd European Conference on Weigh-in-motion of road vehicles, Lisbon, eds. E.J. OBrien & B. Jacob, Sept 14 - 16, European Commission, Luxembourg, pp. 129-137.

Drouen, C.B.W. (1997), 'Enforcement using WIM', WAVE mid-term, Delft, ed. B. Jacob, LCPC, Paris, Sept. 16.

Fabre, P., Jacob, B., Stanczyk, D. (1995), 'Pesage multi-stations: intérêt et évaluation expérimentale', in Pre-proceedings of the first European conference on WIM, ed. B. Jacob, Zurich, March 8-10, ETH, pp. 307-314.

Fancher, PS., Ervin, R.D., Mac Adam, C.C and Winkler, C.B. (1980), 'Measurement and representation of the mechanical properties of truck leaf springs' technical report, Highway Safety Research Institute, Michigan University

Frith, B.A. and Barbour, I.A. (1992), 'Goods vehicle surveys at four WIM pre-selection sites (1990/1991)', TRL Report RR369, Transport Research Laboratory, Crowthorne. Berkshire, United Kingdom.

Gillespie, T.D (1992), 'Truck factors affecting dynamic loads and road damage', Proceedings of the third International Symposium on Heavy Vehicle and Dimensions, Heavy vehicles and roads - Technology, safety and policy, T. Telford, London, pp. 102-108

Glover, MH (1988), 'Weighing axles in motion with a multiple sensor system', TRRL, Working paper, WP VED/88/50.

Glover, MH and Newton, WH (1989), 'Evaluation of a multiple-sensor weigh-in-motion system', TRRL, Working paper, WP VED/90/69.

Glover, M.H. and Newton, W.H. (1991), Evaluation of a multiple-sensor weigh-in-motion system, Department of Transport TRRL Report RR307, Transport and Road Research Laboratory, Crowthorne UK.

Glover, M.H. and Newton, W. (1991), Evaluation of a multiple-sensor WIM system, Research Report 307, Transport Research Laboratory.

Hallström, B., Jehaes , S. (1998), 'European Test Program, Cold Environment Test (CET)', in Proceedings of the 2nd European conference on WIM, Lisbonne, Sept 14-16, COST 323

Henny, R.J. (1998), 'Experimental Use of WIM with Video for Control of Overloading', in Pre-Proceedings of 2nd European Conference on Weigh-in-motion of road vehicles, Lisbon, eds. E.J. OBrien & B. Jacob, Sept 14 - 16, European Commission, Luxembourg, pp. 335-363.

Jacob, B. (1995), 'Spatial repeatability of impact forces and multiple sensor WIM', Proceedings of the First european WIM conference, Zurich, ed. B. Jacob, 147-156.

Jacob, B. : The newsletter of the European WAVE Project, Issue 2: October 1998

Jacob, B. and Dolcemascolo, V. (1998), Dynamic interaction between instrumented vehicles and pavements, proc. 5th Int. Symp. on Heavy Vehicle Weights and Dimensions, Brisbane, March/April.

Jacob, B (1995), 'Répétabilité spatiale des forces d'impact sur une chaussée et pesage multicapteur (projet OCDE/DIVINE Element 5)', in Pre-proceedings of the first European conference on WIM, Zurich, March 8-10, Ed. B. Jacob, pp 147-156.

Jacob, B. (1997), "Presentation of the project WAVE", in Proceedings of the mid-term seminar WAVE, Delft, Sept. 16, LCPC, Paris, pp. 9-15.

Jacob, B. and Dolcemascolo, V. (1997), Spatial repeatability of axle loads on a pavement, Final report of the Element 5, OECD/DIVINE, Paris, LCPC.

Kay, SM (1988). 'Modern spectral estimation'. Englewood Cliffs, NJ, USA, Prentice-Hall.

LeBlanc, P.A., Woodrooffe, J.H.F and Papagiannakis, A.T (1992), 'A comparison of the accuracy of two types of instrumentation for measuring vertical wheel load', Proceedings of the third International Symposium on Heavy Vehicle and Dimensions, Heavy vehicles and roads - Technology, safety and policy, T. Telford, London, pp. 86-94

Macleod, MD (1998). 'Fast nearly ML estimation of the parameters of real or complex single tones or resolved multiple tones'. *IEEE Transactions on Signal Processing* 46(1): 141-148.

Marchadour, Y. (1998), 'Weighing of Road Vehcles in France for Enforcement', in Pre-Proceedings of 2nd European Conference on Weigh-in-motion of road vehicles, Lisbon, eds. E.J. OBrien & B. Jacob, Sept 14 - 16, European Commission, Luxembourg, pp. 339-344.

Mitchell, CGB and Gyenes, L (1989). 'Dynamic pavement loads measured for a variety of truck suspensions'. 2nd Int. Conf. on Heavy Vehicle Weights and Dimensions, Kelowna, British Columbia.

Newton, W.H. (1989), 'Methods of monitoring the overloading of goods vehicles', TRL Report RR193, Transport Research Laboratory, Crowthorne, Berkshire, United Kingdom.

Newton, W.H. (1998), 'Enforcement Applications of weigh-In-Motion', in Pre-Proceedings of 2nd European Conference on Weigh-in-motion of road vehicles, Lisbon, eds. E.J. OBrien & B. Jacob, Sept 14 - 16, European Commission, Luxembourg, pp. 331-338.

OECD, IR6 (1997), DIVINE: Dynamic Interaction Vehicle - Infrastructure Experiment, final report, Proceedings of the American, European and Asian-Pacific conferences, Ottawa (June 23-25), Rotterdam (September 17-19), Melbourne (November 5-7), OECD, Paris.

Rife, DC and Boorstyn, RR (1974). 'Single-tone parameter estimation from discrete-time observations'. IEEE Transactions on Information Theory 20(5): 591-598.

Rife, DC and Boorstyn, RR (1976). 'Multiple tone parameter estimation from discrete-time observations'. The Bell System Technical Journal 55(9): 1389-1410.

Robson, JD (1979). 'Road surface description and vehicle response'. Int. J. of Vehicle Design 1(1): 25–35.

Sainte-Marie, J., Argoul, P., Jacob, B., Dolcemascolo, V. (1998), 'Multiple Sensors WIM using Reconstruction Algorithms of The Dynamic Axles Loads', in Pre-Proceedings of 2nd European Conference on Weigh-in-motion of road vehicles, Lisbon, eds. E.J. OBrien & B. Jacob, Sept 14 - 16, European Commission, Luxembourg, pp. 109-117.

Sainte-Marie, J. (1999), 'Multiple Sensor WIM and Vehicle-Pavement Interaction', Weigh-in-motion of Road Vehicles - Proceedings of the Final Symposium WAVE, ed. B. Jacob, Hermes, Paris, 169-176.

Sainte-Marie, J., Argoul, P., Baumgärtner,W. (1995), 'Estimation of the traffic load on bridges by the extended Kalman filter procedure', in Proceedings of the International Conference MV2 – L.Jezequel Ed.,Balkema, 169-180.

Sainte-Marie, J., Argoul, P., Baumgärtner,W. (1997), 'Estimation of the traffic load on bridges by the extended Kalman filter procedure', in Proceedings of the International Conference MV2 – L.Jezequel Ed.,Balkema, 169-180.

Sainte-Marie, J. (1999), 'Echantillonage des signaux à bande limitée - Application à l'étude de l'intération vehicule-chaussée', Ph.D. thesis, Ecole Nationale des Ponts et Chaussées, Paris

Siffert, M. (1995), "Collection of data on heavy traffic and assessment of its aggressivity", in Post-proceedings of the 1st European Conference on WIM, ed. B. Jacob, Zurich, March 8-10, pp 299-307.

Siffert, M., Dolcemascolo, V., Jacob, B., Sainte-Marie, J. (1997), 'Multiple sensor WIM', in Proceedings of the WAVE mid-term seminar, Delft, Sept. 16, LCPC, Paris, pp. 91-100.

Siffert, M., V.Dolcemascolo, V :WAVE Project - WP1.1 MS-WIM Progress Reports n°1, 2, 3, 4, 5, 6 CCT-Trappes 11/96, 02/97, 05/97, 09/97, 11/97, 05/98.

Siffert, M., Dolcemascolo, V., Jacob, B., Sainte-Marie, J. (1997), 'Multiple-sensor WIM', in Proceedings of the WAVE mid-term seminar, Delft 16/9, ed. B. Jacob, LCPC, pp 91-100.

Stanczyk, D. and Jacob, B. (1998), 'European Test Program, Continental Motorway Test (CMT)', in Proceedings of the second European conference on WIM, Lisbonne, Sept 14-16, COST 323.

Stergioulas, L.K., Cebon, D., and Macleod, M.D. (1997), WIM Data Analysis Using the Maximum Likelihood Method, Proceedings of the WAVE Mid-term Seminar, Delft.

Stergioulas, L.K., Cebon, D., Macleod, M.D. (1998), 'Enhancing Multiple-Sensor WIM Systems', in Pre-Proceedings of 2nd European Conference on Weigh-in-motion of Road Vehicles, eds. E.J. OBrien & B. Jacob, Lisbon, Sept 14-16, European Commission, Luxembourg, 119-127.

Stergioulas, LK and Cebon, D (1999), 'An experimental trial of multiple-sensor weigh-in-motion', Cambridge University Engineering Department, Technical Report, CUED/C–MECH/TR 79, 28pp.

Stergioulas, LK, Cebon, D and Macleod, MD (1999). 'Static weight estimation and system design for multiple-sensor weigh-in-motion'. J Mech Eng Sci, IMechE (in press).

Sweatman, P.F. (1983), A study of dynamic wheel forces in axle group suspensions of heavy vehicles, Australian Road Research Board Special Report SR27.

Van Trees, HL (1968). 'Detection, Estimation and Modulation Theory'. New York, Wiley.